

MASTER

Design of a short stroke actuator for the ATLAS reticle stage

de Klerk, A.

Award date:
1997

[Link to publication](#)

Disclaimer

This document contains a student thesis (bachelor's or master's), as authored by a student at Eindhoven University of Technology. Student theses are made available in the TU/e repository upon obtaining the required degree. The grade received is not published on the document as presented in the repository. The required complexity or quality of research of student theses may vary by program, and the required minimum study period may vary in duration.

General rights

Copyright and moral rights for the publications made accessible in the public portal are retained by the authors and/or other copyright owners and it is a condition of accessing publications that users recognise and abide by the legal requirements associated with these rights.

- Users may download and print one copy of any publication from the public portal for the purpose of private study or research.
- You may not further distribute the material or use it for any profit-making activity or commercial gain



Afstudeerverslag

DESIGN OF A SHORT STROKE ACTUATOR
FOR THE ATLAS RETICLE STAGE

EMV 97-12

Angelo de Klerk

Hoogleraar: Prof.dr.ir. E.M.H. Kamerbeek

Mentor(en): Dr.ir. J.C. Compter
Ir. A.T.A. Peijnenburg

Eindhoven, augustus 1997

Summary

The department Mechatronics at Philips CFT is involved in the development of wafer steppers for ASM Lithography (ASML). A prototype of the first machine of a new generation of wafer steppers, which has to be on the market in the year 1999, is developed at Philips CFT in co-operation with ASML.

A wafer stepper exists of a number of modules, namely the wafer stage, the reticle stage, the lens and the illumination unit. The wafer stage positions the wafer beneath the lens. The reticle stage is mounted between the lens and the illumination unit and positions the reticle. A part of the prototype being developed at Philips CFT is the short stroke actuator for the reticle stage. This actuator is based on the Lorentz principle and is used for extreme accurate positioning in three degrees of freedom. The development together with the theoretical background of the short stroke actuator are described in this report.

Chapter 1 gives an introduction with the background information about the operation of wafer steppers (of ASML) and a brief description of the graduation project.

The actuator which has to be designed must satisfy requirements which are based on specifications given by ASML and the mechanical layout of the reticle stage. In a first design phase, the actuator is optimised with respect to the available space for the actuator. A figure of merit is introduced to compare different designs. The optimisation has been done using numerical simulation tools and analytical calculations. This design phase is described in chapter 2.

The actuator designed in the first design phase had insufficient dynamical performance, looking to the mechanical behaviour. Therefore the layout of the actuator is changed during a second design phase. The new design is optimised like the first, but with the dynamical behaviour as an extra boundary condition. The actuator also has effects which are not wanted but occur due to mechanical tolerances. These include for example disturbance forces and damping which need to be quantified and minimised. The second design phase is described in chapter 3.

To verify the design of the actuator, experiments are carried out. These show that the simulation models give a good prediction of the performance of the actuator. On the other hand, not all of the unwanted effects are checked by experiments. Therefore, additional experimental configurations need to be build to further investigate the actuator. The results obtained by the experiments are described in chapter 4.

Conclusions based on the graduation project as well as points of attention for the final design (given by the recommendations) are described in chapter 5.

Preface

This report has been written during my final phase of the study Electrical Engineering at the Eindhoven University of Technology. My graduation project was carried out at Philips CFT within the Drive Systems group of the department of Mechatronics and concerned the design of a linear Lorentz actuator for extreme accurate positioning in three degrees of freedom. The whole graduation project has been done under the supervision of the department MBS, section EMV, of the Eindhoven University of Technology.

During the 8 months I worked on my graduation project at Philips CFT, I learned a lot about the way electro mechanics is carried out in practice and I improved my skills concerning electro-mechanics. I also learned a lot about working together in a team of experts to achieve certain goals. This gives my graduation project an extra dimension.

First of all I would like to thank Philips CFT for giving me the opportunity to carry out my graduation project within the ATLAS project. I realise that this is an unique situation and I am very glad I got this opportunity. I would also like to thank my Philips colleagues in the department of Mechatronics for their help, especially Kees van Tiel for making the prototype and changing the measurement set-up, without this I would not have been able to carry out my experiments.

Finally I would like to thank my supervisor at the Eindhoven University of Technology, Prof.dr.ir. E.M.H. Kamerbeek, who always had constructive criticism on this report and work and was always willing to spend time. And I also want to thank my company supervisors Ton Peijnenburg and John Compter for their help, support and enthusiasm during my graduation project.

Angelo de Klerk

Eindhoven, august 1997

List of symbols

ω	:	angular frequency	[rads ⁻¹]
Φ	:	magnetic flux	[Wb]
ρ_{Cu}	:	copper specific resistance	[Ωm]
Φ_G	:	magnetic flux in airgap	[Wb]
μ_o	:	permeability of vacuum	[Hm ⁻¹]
μ_o	:	relative permeability	[-]
a	:	acceleration	[ms ⁻²]
a_{av}	:	average acceleration	[ms ⁻²]
B	:	magnetic flux density	[T]
b_c	:	coil width	[mm]
B_m	:	magnetic flux density in magnet	[T]
b_o	:	coil core width	[mm]
d	:	copper diameter	[mm]
E	:	sum of magnetic energy present in magnetic field	[J]
E_{ind}	:	induced voltage in coil	[V]
F	:	force	[N]
f	:	frequency	[Hz]
f_{Cu}	:	copper filling factor	[-]
F_{ED}	:	electrodynamic disturbance force	[N]
F_{REL}	:	reluctance force	[N]
F_X	:	force in X-direction	[N]
F_y	:	force in Y-direction	[N]
$F_{Y,max}$:	maximum force in Y-direction	[N]
F_Z	:	force in Z-direction	[N]
h	:	total actuator height	[mm]
h_c	:	coil height	[mm]
H_{cB}	:	coercivity permanent magnet	[Am ⁻¹]
H_{Fe}	:	magnetic field strength in iron	[Am ⁻¹]
h_g	:	physical air gap	[mm]
h_m	:	magnet height	[mm]
H_m	:	magnetic field strength in permanent magnet	[Am ⁻¹]
h_y	:	iron height	[mm]
I_s	:	current in amplifier due to disturbance voltage	[A]
I_X	:	X-coil current	[A]
I_Y	:	Y-coil current	[A]
J	:	current density	[A/mm ²]
j_k	:	jerk	[ms ⁻³]
K	:	motor constant	[NA ⁻¹]
K_0	:	motor constant for one turn	[NA ⁻¹]
KF_{CAL}	:	calculated correction factor	[-]
l_c	:	coil length	[mm]
l_o	:	length of strait parts of coil	[mm]
L_o	:	self inductance if coil has turn	[H]
l_y	:	effective iron length	[mm]
m	:	mass	[kg]
M_o	:	mutual inductance if coil has one turn	[H]

N	:	number of turns	[-]
N_X	:	number of turns X-coil	[-]
N_Y	:	number of turns Y-coil	[-]
P	:	dissipated power	[W]
$P_{Y,av}$:	average power dissipation in Y-coil	[W]
R_G	:	magnetic leakage resistance	[H ⁻¹ m]
R_1	:	inner radius coil	[mm]
R_2	:	outer radius coil	[mm]
R_{cable}	:	cable resistance	[Ω]
R_{Fe}	:	magnetic resistance iron	[H ⁻¹ m]
R_G	:	magnetic resistance airgap	[H ⁻¹ m]
R_o	:	resistance coil if coil has one turn	[Ω]
R_r	:	magnetic replacement resistance	[H ⁻¹ m]
S	:	steepness	[N ² W ⁻¹]
U_m	:	magnetic voltage permanent magnet	[A]
v_d	:	speed difference between coil carrier and iron yoke	[ms ⁻¹]
W_m	:	magnetic energy	[J]

Contents

SUMMARY	ii
PREFACE.....	iii
LIST OF SYMBOLS.....	iv
CONTENTS.....	vi
1. ATLAS PROJECT.....	1
1.1 WAFER STEPPER.....	1
1.1.1 Step and scan	1
1.1.2 Reticle stage.....	2
1.2 GRADUATION DESCRIPTION.....	2
1.3 PLANNING	3
2. SPECIFICATIONS AND DESIGN.....	5
2.1 SPECIFICATIONS.....	6
2.2 FIGURE OF MERIT	6
2.3 INFLUENCE OF THE GEOMETRY ON THE FIGURE OF MERIT	7
2.3.1 Iron height vs. magnet height	7
2.3.2 Magnet with vs. coil width.....	8
2.3.3 Coil length	8
2.3.4 Coil core width.....	9
2.3.5 Coil width.....	9
2.4 DESIGN RULES	10
2.5 ANALYTICAL MODEL	10
2.6 DESIGN.....	14
2.6.1 Disturbance forces.....	15
2.6.2 Disturbance forces obtained from 2D simulations.....	16
2.6.3 Disturbance forces obtained from 3D simulations.....	17
2.6.4 Comparison between 3D- and 2D-simulations	18
2.7 MOTOR CONSTANT	18
2.7.1 Motor constant obtained from 2D simulations.....	19
2.7.2 Motor constant obtained from 3D simulations.....	19
2.8 THERMAL CALCULATIONS	20
3. PROTO TYPE DESIGN.....	21
3.1 NEW DESIGN	21
3.2 DISTURBANCE FORCES	23
3.2.1 Disturbance forces obtained from 2D simulations.....	23
3.2.2 Disturbance forces obtained from 3D simulations.....	24
3.2.3 Comparison between 3D- and 2D-simulations	24
3.3 MOTOR CONSTANT	25
3.4 AMPLIFIER MATCHING	26
3.5 COILS AND COIL CARRIER.....	28
3.6 DAMPING	28

3.6.1 Eddy current	29
3.6.2 Damping due to control loop of amplifier	29
3.6.3 Total damping	30
4. EXPERIMENTAL RESULTS.....	31
4.1 DISTURBANCE FORCES	31
4.1.1 Reluctance force.....	33
4.1.2 Electrodynamic disturbance force.....	34
4.2 COMPARISON EXPERIMENTAL RESULTS WITH SIMULATION RESULTS	35
4.3 MOTOR CONSTANT	35
4.4 MEASURED COIL PROPERTIES.	36
4.4.1 Transfer function of the coil.	36
4.4.2 Mutual induction	37
4.5 FIGURE OF MERIT.....	37
4.6 MEASURING INSTRUMENTS	38
5. CONCLUSIONS AND RECOMMENDATIONS.....	39
5.1. CONCLUSIONS.....	39
5.2. RECOMMENDATIONS.....	39
REFERENCES.....	40
APPENDIX A ACTUATOR CONFIGURATION.....	41
APPENDIX B CALCULATION FIGURE OF MERIT.....	42
APPENDIX C OPERA2D SIMULATION DATA.....	44
APPENDIX D ANALYTICAL MODEL.....	47
APPENDIX E EXAMPLE APPLICATION OF ANALYTICAL MODEL.....	49
APPENDIX F OPERA 3D SIMULATION DATA.....	50
APPENDIX G EFFECT OF THE MAGNET LENGTH.....	52
APPENDIX H OPERA 3D SIMULATION DATA, NEW DESIGN FOR FUMQ.....	54
APPENDIX I AMPLIFIER SPECIFICATION.....	56
APPENDIX J EDDY CURRENT.....	59
APPENDIX K DAMPING DUE TO CONTROL LOOP OF AMPLIFIER.....	62
APPENDIX L PROTOTYPE.....	64
APPENDIX M MEASURED DATA.....	65
APPENDIX N TRANSFER FUNCTIONS.....	68

1. ATLAS project

ASM Lithography (ASML) develops and produces wafer steppers for the production of integrated circuits. ASML expects in the future an increase in the demands on the wafer steppers which can not be fulfilled with the current assortment of products. A new range of machines has to be defined and developed, the first machine of this range must be ready for production (at the customers) in the year 1999. Philips CFT is participating in the definition and development of this range of machines and is providing the project with knowledge and resources on the dynamics, the control technology, mechanical construction, thermal behaviour and electro-mechanics.

The main purpose of the new wafer steppers is to illuminate large wafers, due to these large wafers the following name is invented within ASML: Advanced Technology for Large Area Substrates (ATLAS).

Paragraph 1.1 describes the basics of the functioning of a wafer stepper (the step and scan principle) in order to give the reader a short introduction in the world of wafer steppers.

The graduation project description is mentioned in paragraph 1.2. From this description a planning has been made, which is given in paragraph 1.3.

1.1 WAFER STEPPER

The wafer stepper has only one function and that is transferring a defined pattern on a silicon wafer. The wafer has a photosensitive layer which is exposed to a light source. The light changes the properties of the photosensitive layer. The defined pattern can be transferred to the wafer by placing a mask or reticle between the light source and the wafer. The parts of the photosensitive layer which have not been exposed to the light can not be removed in the next process step. The defined pattern is now present on the wafer.

An important aspect on the wafer stepper is the handling of the wafer and the reticle. The wafers are in most cases processed at more than one wafer stepper. Each wafer stepper generates a different pattern layer on the wafer. Because the wafers will be processed on different wafer steppers, high accuracy is needed in positioning the wafer and the reticle to ensure the layers will "overlay".

1.1.1 Step and scan

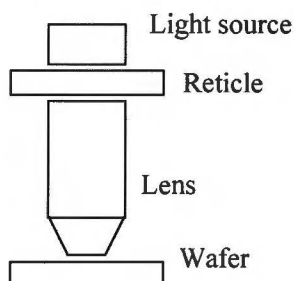


Figure 1.1 Principal layout.

A few years ago, a new exposure method was invented. This new method can shorten the process time and increase the size of the areas that can be exposed. But the biggest advantage is that the lens does not have to increase in size. The price of the lens is about 25 % of the total costs of a wafer stepper, this means that the cost of the wafer stepper does not have to increase that much.

Figure 1.1 displays a schematic side view of the wafer stepper. It shows that the reticle is placed between the light source and the lens. The wafer is positioned under the lens. In the conventional exposure process, one area of the wafer (called die) is illuminated at a time.

Then the wafer is displaced (stepped) and a new area is illuminated. This process will continue until the whole wafer is illuminated.

The new method, called step and scan, has a different illumination process. The big difference is at constant speed both the reticle and the wafer move during illumination. In the scan operation the wafer and the reticle move in opposite directions and the wafer is illuminated. After the full length of a wafer die is illuminated, the wafer is displaced in the transverse direction, which is called the step operation. The next step is another scan operation. This process will continue until the whole wafer is illuminated. The challenge in developing this concept is the moving reticle stage and the synchronisation of the wafer stage and the reticle stage.

1.1.2 Reticle stage

The main function of the reticle stage is to position the reticle during scan operation. During scan operation the reticle has to move about 650 mm with an accuracy of 1 nm. Because it is very difficult to obtain such an accuracy over a long distance with one motor, a two stage drive is developed. This two stage drive is based on a master slave principle. This master slave principle is shown in figure 1.2 [4].

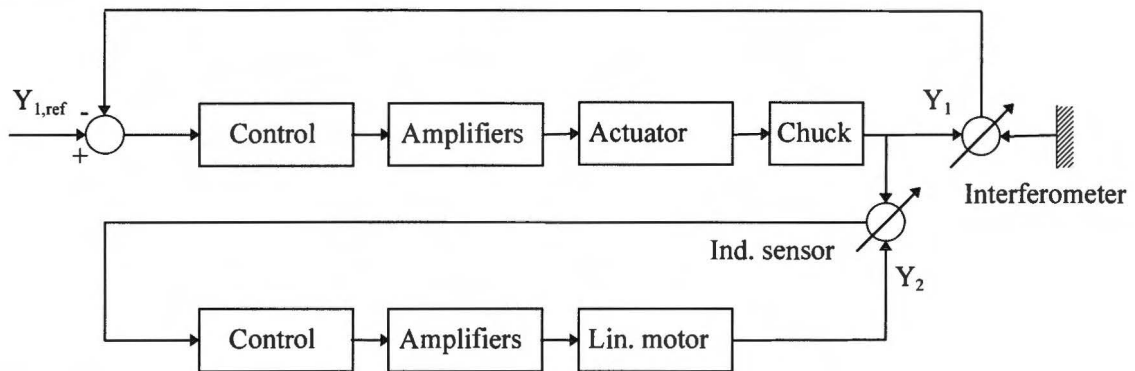


Figure 1.2 Master slave control diagram

There are two motors present in the master slave concept. First a long stroke linear motor with a stroke of about 650 mm and an accuracy of at least 1 mm and second a short stroke actuator which can deliver the required accuracy. The short stroke actuator is the master, this means the long stroke follows the short stroke. The desired position is called $Y_{1,ref}$. Due to the master slave principle the long stroke ensures that the short stroke stays within its limited stroke. The short stroke positions the reticle stage with the desired accuracy.

The reticle stage has the following important parts:

- chuck, a part made of zerodur (thermal expansion coefficient of nearly zero) on which the reticle is placed as well as mirrors for the interferometers;
- short stroke actuator, actuating the X- and Y- co-ordinate and rotation about the Z axis;
- long stroke motor, actuating the Y- co-ordinate of the short stroke actuator;
- laser interferometer measuring system, measuring the X-, Y- and Z- co-ordinates.

1.2 GRADUATION PROJECT DESCRIPTION

The present generations of short stroke actuators are not suited for the ATLAS machine. Therefore a new short stroke actuator has to be designed. Optimisation of this design must take place to get the required force using the lowest power dissipation possible.

The graduation project contains the design of a short stroke actuator and optimise the design. The end result of the graduation project is a written report which contains the optimisation, simulation of and measurements on a prototype of the linear actuator.

The following describes the graduation project in a more extensive manner:

The subject of the graduation project is to design a linear actuator for the reticle stage of the ATLAS wafer scanner, which drives the reticle stage in three degrees of freedom (X,Y and ϕ_z) with limited stroke of 1 mm in X-, Y- and Z- direction. The driving force in the Y-direction has a value of about 1000 N. The actuator has to fulfil very high demands on the temperature rise at the outer side, disturbance forces in the directions other than the drive direction and variation in the motor constant. The demands on the available space for the actuator depend on other disciplines within the ATLAS project.

The following points have to be carried out during the graduation project:

- make a planning [1];
- define the specifications of the linear actuator;
- make models of the actuators electromechanical properties (analytical as well as using finite the element method [4,5];
- optimisation using the developed models with respect to thermal behaviour and disturbance forces, within the available volume;
- measurements on the prototype using a test plan, for verification of the specifications and the models used;
- a written English report of the graduation project.

The title of the graduation project is: **“Design of a linear Lorentz actuator for extreme accurate positioning in three degrees of freedom.”**

1.3 PLANNING

To guide the graduation project in a well organised way a planning has been made. The basis for this planning are a the following important dates:

- June / July 1997; physical actuator has to be ready;
- August 21, 1997; last date for presentation of the graduation project at the university;
- August 31, 1997; end of graduation period;

The planning made in the beginning of the graduation period is displayed in table 1.1.

Table 1.1 Planning for the graduation.

Week	2	3	4	5	6	7	8	9	10	11	12	13	14	15	16	17	18
1. Settling in																	
2. Optimising																	
3. Physical dimensions																	
4. Order and supply																	
5. 3D simulations																	
6. Develop test plan																	
7. Documentation																	
8. Build experimental set up																	
9. Execute test plan																	
10. Processing test data																	

Table 1.1 Continuation planning for the graduation.

Week	19	20	21	22	23	24	25	26	27	28	29	30	31	32	33	34	35
1. Settling in																	
2. Optimising																	
3. Physical dimensions																	
4. Order and supply																	
5. 3D simulations																	
6. Develop test plan																	
7. Documentation																	
8. Build experimental set up																	
9. Execute test plan																	
10. Processing test data																	

There are 10 points of action:

1. Settling in means to know the colleagues, learning about the social infrastructure within Philips CFT, reading of the collected documentation on the subject [4,5,7,8], installing the PC and learning to use the finite element package Opera2D;
2. Choosing the dimensions of the actuator in such a way that the actuator has the best performance possible given the dimension limitations;
3. Defining the real dimensions of the actuator in co-operating with a mechanical engineer, this process has to be iterative with the optimising process;
4. Ordering of the magnets and other parts of the actuator;
5. After the 2D simulations and the optimisation of the actuator, 3D simulations have to be carried out. For these simulations a great amount of time is spend, because it takes time to get familiar with the tool;
6. Make a test plan in such a way that it is easy to execute the tests;
7. Writing the obtained data in a report and analyse it;
8. When the actuator is physically present, the experimental set up has to be build, may be done in parallel;
9. Execute the tests which has been written in the test plan;
10. Processing the test data and analyse it.

2. Specifications and design

In the first design phase, the objective is to understand the electrodynamics of the actuator. This means to know the possibilities and the limitations of the actuator as a function of the given parameters. This knowledge leads to a optimised design.

The function of the actuator is to move the reticle chuck both in X- and Y-direction and to rotate about the Z-axis. The Y-direction corresponds with the scanning direction of the reticle stage. Movement of the reticle stage in X- and Z-direction and rotation about the Z-axis are due to disturbing forces and torques. With this in mind, the concept of the actuator can be developed. The total actuator consists of two Y-actuators and one X-actuator. The Y-actuators produce the required force in the scan direction. If the two forces generated by the Y-actuators differ, a resulting torque about the Z-axis is generated. This torque is not desired.

In paragraph 2.1 the specifications of the actuator are mentioned. The designed actuator has to fulfil all these requirements. To be able to compare the different designs with each other, a figure of merit is introduced. This figure of merit is independent of the current but dependant on the coil geometry. The deviation of the figure of merit is described in paragraph 2.2.

The influence of the geometry on the figure of merit is described in paragraph 2.3. The purpose of this is to get an idea of the performance of the actuator with respect to the geometry of the actuator. From the results of paragraph 2.3, design rules can be derived. These rules are described in paragraph 2.4 and can be used to design an actuator with the highest performance within the given dimensions.

At this moment, there is not an analytical model available at Philips CFT for this kind of actuators. The purpose of an analytical model is to predict values for the figure of merit and the generated force with an accuracy within 10 %. Using an analytical model would reduce time to design an actuator, because otherwise all calculations have to be done using finite element packages. The method used to develop an analytical model is explained in paragraph 2.5.

Paragraph 2.6 describes the actual design of the actuator. The actuator has its limitations with respect to the given dimensions. With these dimensions in mind the "best possible" actuator has to be designed. This design is modelled with the finite element packages Opera2D and Opera3D. Disturbance forces are obtained from the simulation results. Another important design parameter is the motor constant, the deviation of the motor constant is done in paragraph 2.7. The motor constant obtained from the simulations are also displayed in this paragraph. Figure A.1 and A.2 in appendix A show the actuator configuration.

Thermal calculations are done by a specialist from another department. The results of these calculations are shown in paragraph 2.8.

2.1 SPECIFICATIONS

The performance of the reticle stage is characterised by the preferred production capacity of the scanner and the results of these calculations are:

- speed of the reticle stage during scan is 2 m/s, this is the maximum speed of the reticle stage;
- maximum acceleration is 48 m/s²;
- maximum jerk is 6000 m/s³ (the jerk being the derivative of the acceleration).

Based on the above specifications, the proposed mechanical design of the reticle stage and the know how present within the CFT, the specifications for the short stroke actuator are determined. These specifications are:

- maximum actuator height is 45 mm;
- maximum required force in Y-direction ($F_{Y,max}$) is equal to the mass times the maximum acceleration of 48 m/s²;
- maximum required force in X-direction is 10 % of the maximum force in Y-direction;
- a displacement of ± 1 mm with respect to the magnet body in each direction of the coil body must be possible. This is called the high performance operating area;
- maximum of ± 1 % K-factor variation within ± 0.5 mm displacement in X-, Y- and Z-direction;
- maximum of ± 5 % K-factor variation within ± 1.0 mm displacement in X-, Y- and Z-direction;
- maximum parasitic force in Z-direction of 1 % of the force in Y-direction;
- maximum temperature rise at the outside of the actuator is 0.4 °C.

The K-factor or the motor constant is defined as the quotient of the force generated by the actuator and the current through the actuator coil. Due to variation in the K-factor a variation in the gain of the control loop is introduced. This leads to feed forward control errors.

2.2 FIGURE OF MERIT

There is a relationship between the generated force and the dissipated power of the actuator coils. This relationship can be written as a figure of merit and is defined as the square of the force divided by the dissipated power. The figure of merit is totally independent of the current and is determined by the geometry of the coil of the actuator. The geometry is shown in figure 2.1.

The derivation of the equation of the figure of merit can be found in appendix B and the boundary conditions for using this equation are also found in this appendix. Equation 2.1 displays the figure of merit and the variables used. When using the figure of merit, different actuator designs can be compared. An other name for the figure of merit is “steepness”, S [3].

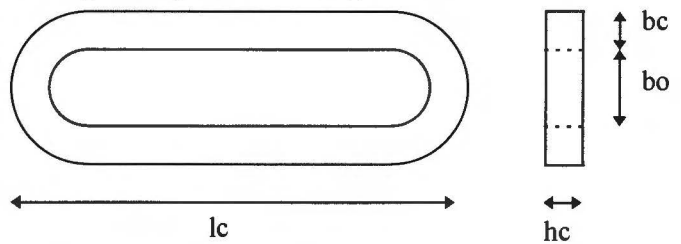


Figure 2.1 Coil geometry.

The steepness can be written as:

$$S = \frac{F^2}{P} = \frac{4(h_c b_c B)^2 (l_c - b_c)^2 f_{Cu}}{\rho_{Cu} h_c [2(l_c - 2b_c - b_o) b_c + \pi b_c b_o + \pi b_c^2]} \tag{2.1}$$

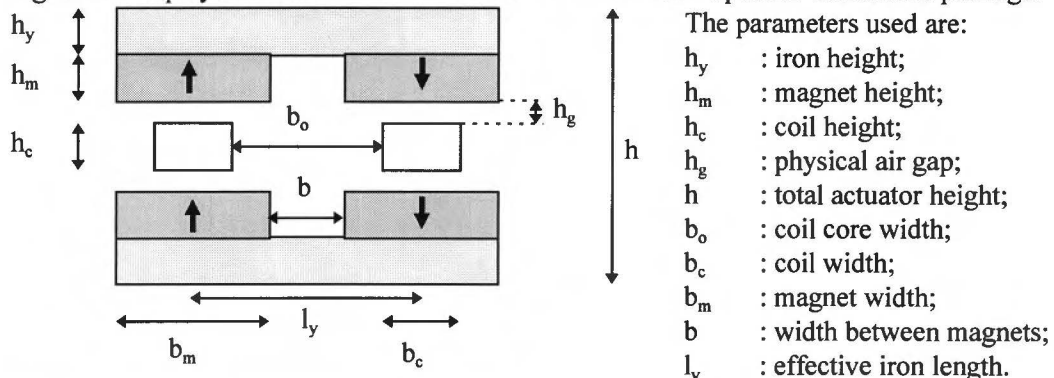
Where F is the generated force [Newton] and P is the dissipated power in the coil [Watt].

2.3 INFLUENCE OF THE GEOMETRY ON THE FIGURE OF MERIT

Before designing an actuator, the influence of the geometry has to be known, in order to make the performance of the design as good as possible (maximise the figure of merit). To get an idea of the influence of the geometry on the figure of merit the following investigations are made:

- the relation of the iron height vs. the magnet height with fixed total actuator height;
- the relation of the magnet width and the coil width;
- the influence of the coil length;
- the influence of the coil core width;
- the influence of the coil width.

Figure 2.2 displays a cross section of the actuator used in the Opera2D simulation package.



The parameters used are:
 h_y : iron height;
 h_m : magnet height;
 h_c : coil height;
 h_g : physical air gap;
 h : total actuator height;
 b_o : coil core width;
 b_c : coil width;
 b_m : magnet width;
 b : width between magnets;
 l_y : effective iron length.

Figure 2.2 Configuration used in Opera-2D.

The coil is symmetric with respect to the middle position of the magnet.

2.3.1 Iron height vs. magnet height

The total height of the actuator is fixed and has a value of 45 mm. The physical air gap is 2.5 mm and is present above and beneath the coil. In this space, 45 mm minus 5 mm, the magnet height, iron height and the coil height have to be divided. The following values are used in the simulation:

$$h_g = 2,5 \text{ mm} \quad b_c = 14 \text{ mm} \quad b_o = 14 \text{ mm} \quad b_m = 20 \text{ mm} \quad l_c = 112 \text{ mm}$$

$$f_{Cu} = 0,7 \quad \rho_{Cu} = 17,5 \cdot 10^{-9} \Omega \text{m at } 20^\circ \text{C}$$

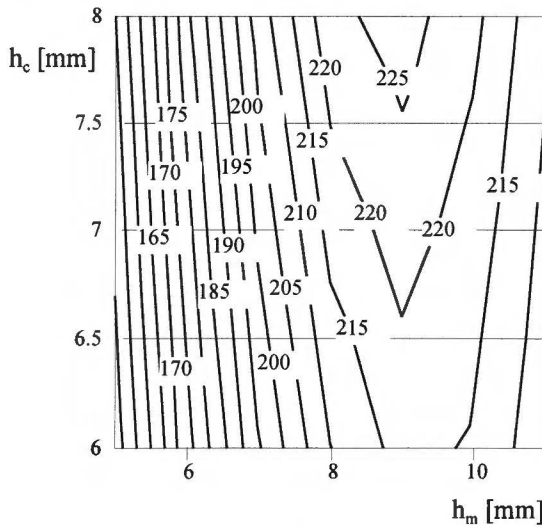


Figure 2.3 Contour plot of S , $h = 45$ mm.

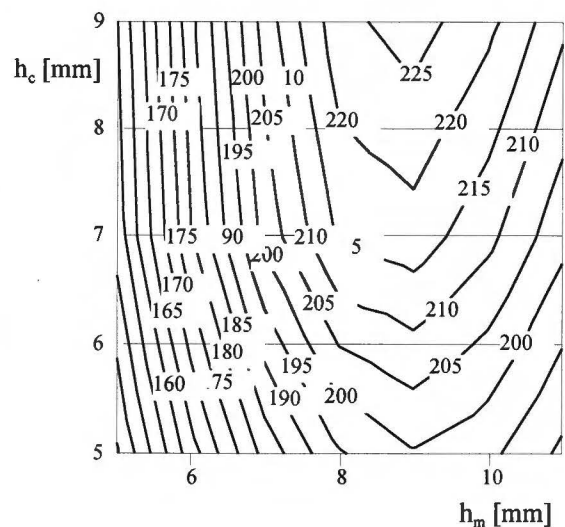


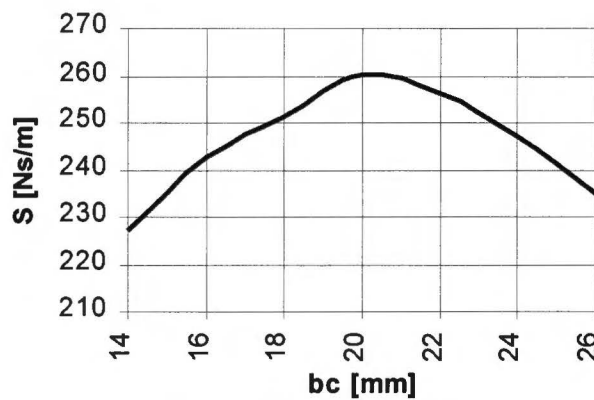
Figure 2.4 Contour plot of S , $h = 44$ mm.

The simulation data can be found in table C.1, appendix C. This data has been drawn as contour plots and are displayed in figures 2.3 and 2.4. Figure 2.3 displays the contour plot for a total actuator height of 45 mm and in figure 2.4 for a total actuator height of 44 mm. The values of the figure of merit for intermediate points are interpolated values.

The height of the iron can be calculated using this contour plot, because the magnet height, coil height and the airgap are known. The figure of merit in both cases has the highest value if the magnet height, the iron height and the coil height are about the same size.

2.3.2 Magnet with vs. coil width

The next step is to look at the effect on the figure of merit when changing the ratio between the magnet width (b_m) and the coil width (b_c). The following values are used in the simulation:



$h_g = 2,5 \text{ mm}$ $b_o = 14 \text{ mm}$
 $h_c = 8 \text{ mm}$ $b_m = 20 \text{ mm}$
 $l_c = 112 \text{ mm}$ $h_m = 9 \text{ mm}$
 $h_y = 7 \text{ mm}$ $f_{Cu} = 0,7$
 $\rho_{Cu} = 17,5 * 10^{-9} \Omega\text{m}$ at $20 \text{ }^\circ\text{C}$

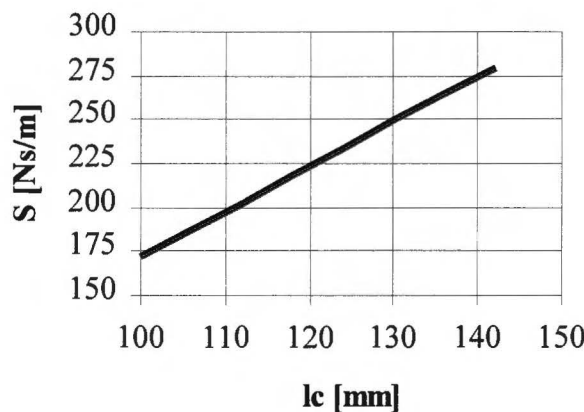
In table C.2, appendix C, the simulation results are displayed. Figure 2.5 shows a plot of the figure of merit as a function of the coil width. The figure of merit has been calculated using equation B.5. Figure 2.5 shows that the figure of merit has a peak value if the coil width equals the magnet width.

Figure 2.5 Figure of merit vs. coil width

2.3.3 Coil length

The influence of the coil length on the figure of merit can be found in table 2.1. The following values are used in the simulation:

$h_g = 2,5 \text{ mm}$ $b_o = 14 \text{ mm}$ $h_c = 8 \text{ mm}$ $b_m = 20 \text{ mm}$ $b_c = 14 \text{ mm}$
 $h_m = 9 \text{ mm}$ $h_y = 7 \text{ mm}$ $f_{Cu} = 0,7$ $\rho_{Cu} = 17,5 * 10^{-9} \Omega\text{m}$ at $20 \text{ }^\circ\text{C}$



$$\iint B_z \, dA = 122.91 \text{ Tmm}^2$$

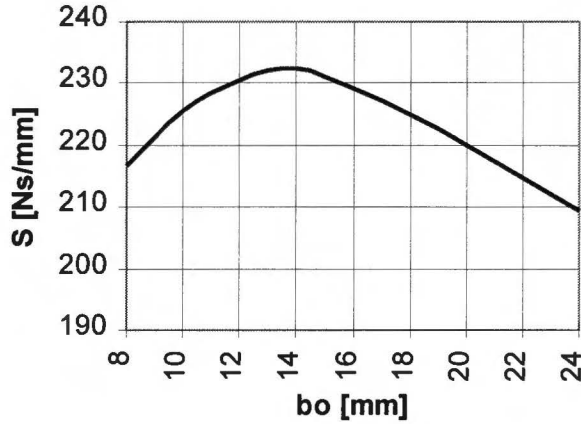
The last expression is necessary for the calculation of the figure of merit, see equation B.5.

The figure of merit becomes larger when the coil length increases. What can be seen in figure 2.6 is that there is a linear relation between the figure of merit and the coil length (in the applied region).

Figure 2.6 Figure of merit vs. coil length.

2.3.4 Coil core width

What the influence on the figure of merit is when the coil core width varies is unknown. The next step is varying the coil core width, the coil width in all the cases being positioned symmetrically under the magnet. The following values are used in the simulation:



are used in the simulation:
 $h_g = 2,5 \text{ mm}$ $b_c = 14 \text{ mm}$
 $h_c = 8 \text{ mm}$ $b_m = 20 \text{ mm}$
 $l_c = 112 \text{ mm}$ $h_m = 9 \text{ mm}$
 $h_y = 7 \text{ mm}$ $f_{Cu} = 0,7$
 $\rho_{Cu} = 17,5 * 10^{-9} \Omega\text{m}$ at 20°C

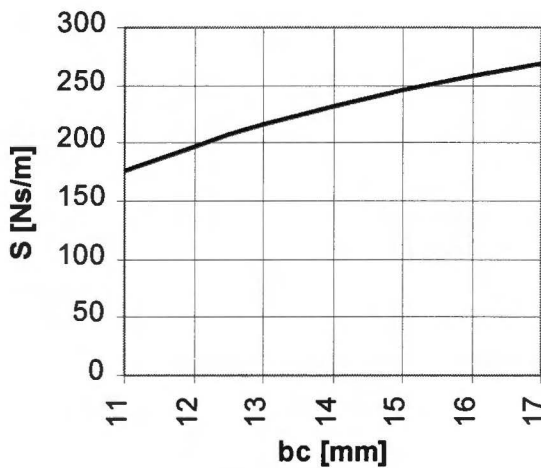
Figure 2.7 Figure of merit vs. coil core width.

In table C.3, appendix C, the simulation results are displayed. Figure 2.7 shows a plot of the figure of merit as a function of the coil core width. There is no unambiguous result of the effect of varying the coil core width on the figure of merit. The result of the simulations are that the figure of merit has it's highest value if the coil core width is almost equal or equal to the coil width. A

disadvantage of this method is the increase in motor volume, in most cases there is a limitation on the space which can be used.

2.3.5 Coil width

In this step, a few assumptions are made for the simulation. These assumptions are that the coil core width is equal to the coil width and the magnet width is always 6 mm bigger than the coil. This means that the magnet has a 3 mm overlap on each coil side. The following values are used in the simulation:



$h_g = 2,5 \text{ mm}$ $h_c = 8 \text{ mm}$
 $h_m = 9 \text{ mm}$ $h_y = 7 \text{ mm}$
 $f_{Cu} = 0,7$ $l_c = 112 \text{ mm}$
 $\rho_{Cu} = 17,5 * 10^{-9} \Omega\text{m}$ at 20°C

Figure 2.8 Figure of merit vs. coil with

In table C.3, appendix C, the simulation results are displayed. Figure 2.8 displays the simulation results in a graph. The figure of merit increases when the coil width increases. It looks like the line is going to an asymptote. This could be due to the saturation of the iron. The bigger the coil width, the larger the width of the magnets. This means that the iron becomes more saturated, see table C.4, and has a negative influence on the figure of merit.

2.4 DESIGN RULES

With the results of paragraph 2.3 in mind, the following design rules can be made up. Obeying these rules for the geometry of the actuator yields approximately the optimum design, that is the highest value of the figure of merit. The design rules are:

- given a total height of the actuator the subdivision of the magnet height, the iron height and the coil height should be in such a way that these heights are approximately equal;
- the length of the coil should be as long as possible given the dimensions of the actuator;
- make the coil core width equal or almost equal to the coil width;
- the coil width should be as large as possible given the dimensions of the actuator;

Remark: in previous designs of linear actuators the magnet width used was larger then the coil width. This to reduce the electrodynamic disturbance force.

2.5 ANALYTICAL MODEL

The purpose of making an analytical model is to get an idea of the values of the figure of merit without using finite element packages. This reduces time for making a good initial design. From this initial design an optimum can be found using finite elements calculations.

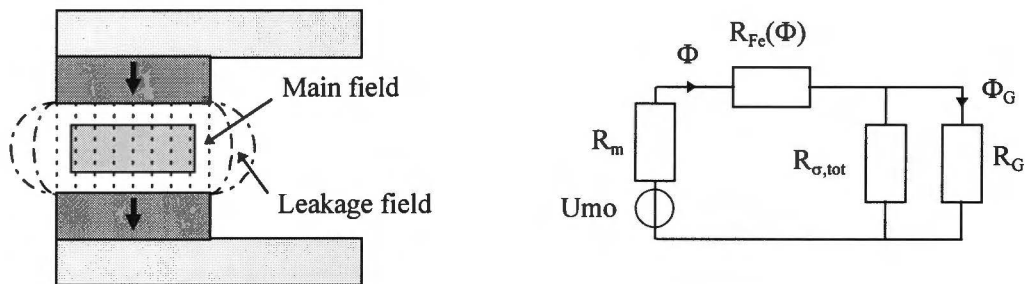


Figure 2.9 Analytical model

The assumptions used for the analytical model are displayed on the left of figure 2.9. These assumptions are that the main field is homogenous distributed over the magnet area and the leakage field is only present in an area which is bound by the circular field line having a diameter equal to the distance between the magnets. Per definition this assumption is only valid for soft magnetic materials. Because it is difficult to describe the leakage of hard magnetic material parts, this assumption should be regarded as a first order approximation. The layout on the left of figure 2.9 can be transformed to an equivalent electrical network [5]. Notable in this network is the magnetic resistance of the iron, which is non linear related to the magnetic flux. The following definitions for the voltage and current are used:

- $U = H \cdot l$; magnetic voltage is equal to strength of field times length;
- $\Phi = B \cdot A$; magnetic flux is equal to flux density times surface.

This model is based on 2 dimensional layouts and the magnetic flux is redefined by:

- $\Phi = B \cdot b$; magnetic flux is equal to flux density times width.

The flux density in the magnet is equal to [6]:

$$B_m = \mu_0 \cdot \mu_r \cdot (H_m - H_{cB})$$

H_{cB} is the absolute value of the coercive strength of field. This is the point in the second quadrant of the BH curve of the permanent magnet where the flux density is zero.

This can be written as:

$$H_m = \frac{B_m}{\mu_0 \cdot \mu_r} + H_{CB} \quad (2.2)$$

Equation 2.2 has to be rewritten in a form where a magnetic voltage and magnetic flux are present. This is done by multiplying equation 2.2 by b_m and 2 times h_m , this is due to the fact that there are 2 magnets in series. The result is:

$$b_m \cdot 2 \cdot h_m \cdot H_m = b_m \cdot 2 \cdot h_m \cdot \left(\frac{B_m}{\mu_0 \cdot \mu_r} + H_{CB} \right) \quad (2.3)$$

The magnetic voltage and flux in the magnet are defined as:

$$U_m = -H_m \cdot 2 \cdot h_m$$

$$\Phi_m = b_m \cdot B_m$$

Substituting these expressions in equation 2.3 leads to:

$$U_m = 2 \cdot h_m \cdot \left(\frac{-\Phi_m}{\mu_0 \cdot \mu_r \cdot b_m} - H_{CB} \right) \quad (2.4)$$

Saturation of the iron means the relative permeability of the iron decreases. In figure 2.10 the BH-curve of the iron used is shown. For the model a first order approximation is used and this can be written as:

$$\begin{cases} H_{Fe} = 0 & \text{if } B_{Fe} \leq 2.13 \\ H_{Fe} = \frac{B_{Fe} - 2.13}{1.2 \cdot 10^{-6}} & \text{else} \end{cases}$$

The above equation has also to be rewritten in a form where a magnetic voltage and magnetic flux are present. This is done by multiplying the equation by h_y and l_y . The result is:

$$\begin{cases} l_y \cdot h_y \cdot H_{Fe} = 0 & \text{if } B_{Fe} \cdot h_y \leq 2.13 \cdot h_y \\ l_y \cdot h_y \cdot H_{Fe} = l_y \cdot h_y \cdot \frac{B_{Fe} - 2.13}{1.2 \cdot 10^{-6}} & \text{else} \end{cases} \quad (2.5)$$

The meaning of the geometrical parameters can be found in figure 2.2. The magnetic voltage and flux in the iron are defined as:

$$U_{Fe} = H_{Fe} \cdot l_y$$

$$\Phi_{Fe} = h_y \cdot B_{Fe}$$

Inserting these expressions in equation 2.5 leads to:

$$\begin{cases} U_{Fe} = 0 & \text{if } \Phi_{Fe} \leq 2.13 \cdot h_y \\ U_{Fe} = \frac{(\Phi_{Fe} - 2.13 \cdot h_y) \cdot l_y}{1.2 \cdot 10^{-6} \cdot h_y} & \text{else} \end{cases} \quad (2.6)$$

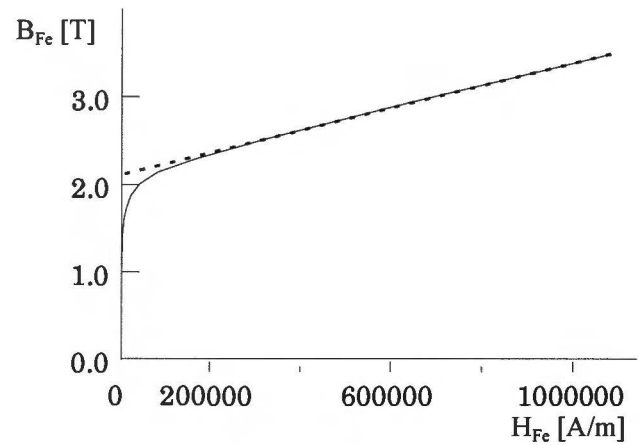


Figure 2.10 BH-curve of iron n041.

The magnetic voltage across the total airgap (which is the sum of the coil height and twice the physical airgap) is equation 2.4 minus equation 2.6. This magnetic voltage has to be equal to the product of the magnetic flux and the magnetic replacement resistor of the total airgap and the total leakage (R_G parallel with R_σ). The magnetic resistance of parts with a uniform flux is defined as the length of the material divided by the product of the permeability of air, the relative permeability of the material and the surface of the material. Because the model is based on two dimensions the surface of the material can be replaced by the width of the material. This is our definition of the magnetic resistance. For the airgap the resistance is:

$$R_G = \frac{2 \cdot h_g + h_c}{\mu_0 \cdot b_m}$$

The leakage magnetic resistance is difficult to determine and is assumed to be equal to:

$$R_\sigma = \frac{l}{\mu_0 \cdot A} \quad (2.7)$$

Where l and A are average length and surface where the leakage flux is present. There is leakage at the left and right side of the magnet and this leakage is approximately symmetric. So only one side has to be calculated. The average length of one side is equal to:

$$l = \frac{\left(\frac{\pi}{2} + 1\right) \cdot g}{2} \quad (2.8)$$

The volume of the area where the leak field is present is equal to the average length times the average area. The volume of the leakage area is equal to the volume of a half cylinder and so:

$$\frac{1}{8} \cdot \pi \cdot g^2 \cdot L = A \cdot l$$

The constant L is the third dimension and the average surface is:

$$A = \frac{\pi \cdot g^2 \cdot L}{8 \cdot l} \quad (2.9)$$

Substituting equations 2.8 and 2.9 in equation 2.7 leads to:

$$R_\sigma = \frac{4 \cdot \left(\frac{\pi}{2} + 1\right)^2}{\mu_0 \cdot \pi \cdot L} \quad (2.10)$$

The expression for the total leakage magnetic resistance in two dimensions is equal to two resistance's of R_σ parallel. The following expression is valid for the total leakage resistance:

$$R_{\sigma, \text{tot}} = \frac{2 \cdot \left(\frac{\pi}{2} + 1\right)^2}{\mu_0 \cdot \pi} \quad (2.11)$$

The replacement magnetic resistance is called R_r and is equal to the magnetic resistance R_G and $R_{\sigma, \text{tot}}$ parallel. Because the magnetic flux in the magnet, the iron and the magnetic resistance R_r is the same, the following equation holds for the magnetic flux:

$$\left| \begin{array}{l} \left(\frac{-\Phi}{\mu_0 \cdot \mu_r \cdot b_m} - H_{CB} \right) \cdot 2 \cdot h_m = R_r \cdot \Phi \quad \text{if } \Phi \leq 2.13 \cdot h_y \\ \left(\frac{-\Phi}{\mu_0 \cdot \mu_r \cdot b_m} - H_{CB} \right) \cdot 2 \cdot h_m - \frac{(\Phi - 2.13 \cdot h_y) \cdot l_y}{1.2 \cdot 10^{-6} \cdot h_y} = R_r \cdot \Phi \quad \text{else} \end{array} \right.$$

Solving this set of equations leads to a value of the magnetic flux.

Solving the equations described in the previous pages can also be done graphically. This is shown in figure 2.11 [6]. The start is to draw the U_m, Φ line. Subtracting R_{Fe} times Φ from this line, creates the U_g, Φ line. The U_g, Φ_g line arises by subtracting $U_g/R_{\sigma,tot}$ from Φ .

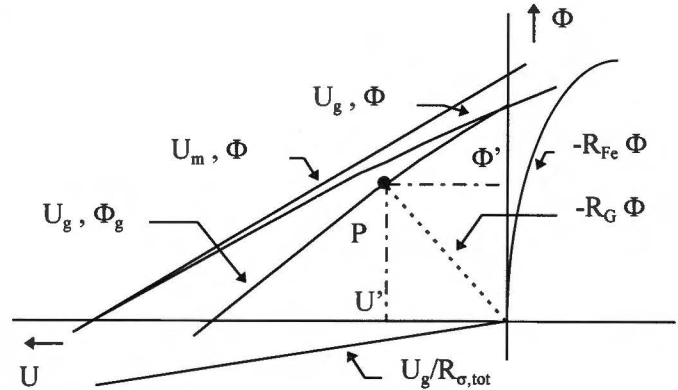


Figure 2.11 Construction of magnetic flux in airgap.

The working point P is the point of intersection of the work line $U = R_G \Phi$ and the U_g, Φ_g line. The co-ordinates of this working point are the values of the magnetic voltage across and the magnetic flux in the airgap.

The magnetic flux has been calculated by solving the set of equations from the previous page. The magnetic flux in the airgap can be determined with the value of the magnetic flux and is equal to:

$$\Phi_G = \frac{R_G}{R_G + R_G} \cdot \Phi$$

The magnetic flux density in the airgap is the magnetic flux divided by the magnet width, so:

$$B_G = \frac{R_G}{R_G + R_G} \cdot \frac{\Phi}{b_m} \tag{2.12}$$

When substituting equation 2.12 in equation B.3 the figure of merit can be calculated. In appendix D, table D.1 column 4, the results of the surface integral $\iint B_z \, dA$ over the cross section of the coil are displayed. This is done by using the model for the geometry of table C.1, appendix C. When this data is compared with column 3 (the data of the simulation), it can be concluded that there is a difference. In column 5 this difference is calculated and called KF. To make the model more accurate a correction factor is introduced. This factor depends on the geometry, because:

- the greater the ratio between magnet width and coil width, the more homogeneous the magnetic field and the less there should be corrected;
- the smaller the distance between the magnets the more homogeneous the magnetic field and the less correction is necessary.

With this in mind we can define two surfaces, those are:

- cross section coil surface, called active surface;
- air surface, called passive surface.

The ratio between the active and passive surface is a variable for the correction factor. This can be written down as:

$$x = \frac{b_c \cdot h_c}{b_m \cdot (2 \cdot h_g + h_c)} \tag{2.13}$$

The ratio displayed in equation 2.13 is independent of the magnet and iron height. For each configuration in table D.1 an average correction factor can be found by taking the 6 middle values in table D.1 (column 5) and calculating the average value. A graphic can be drawn with the variable x and the average correction factor. This graphic is displayed in figure 2.12.

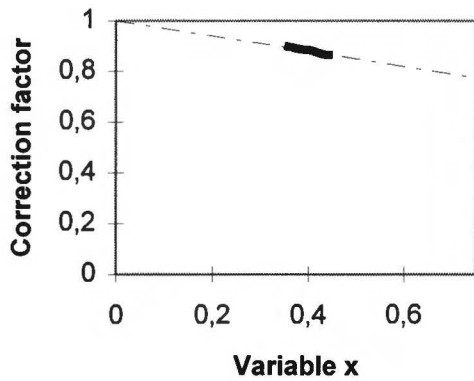


Figure 2.12 Correction factor.

the analytical model can be calculated. This figure of merit is displayed in table D.1, column 8. A comparison with the figure of merit calculated using simulation data is displayed in column 9 of table D.1. This column displays the error of the figure of merit of the analytical model with respect to the figure of merit of the simulation data of table C.1. The conclusion is that in most cases the analytically calculated figure of merit is a good approximation of the figure of merit obtained by the simulation results of table C.1. Because the model is not valid for all geometries the next restrictions have to be kept in mind:

- the total width of the coil should not exceed 54 mm and should not be less then 39 mm, this means that: $39\text{ mm} \leq (2 \cdot b_c + b_o) \leq 54\text{ mm}$;
- the coil width should not be greater than the magnet width, meaning $b_m > b_c$;
- the ratio between the magnet height and the iron height should not exceed 2.4 and should not be less than 0.4 ; meaning: $0.4 \leq \frac{h_m}{h_y} \leq 2.4$;

When obeying these rules the analytical model gives a good approximation of the value of the figure of merit to within 10 % of finite element calculated figures.

2.6 DESIGN

Before the actuator can be designed the outer dimensions has to be known (other dimensions result from the design process). Figure 2.13 displays the dimensions of the actuator in the XY-plane.

The total actuator height is 45 mm and the physical airgap is 4 mm. Resulting in a total height of 37 mm for the coil, the iron and the magnets. Obeying the design rules of paragraph 2.4, a subdivision of the magnet-, iron- and coil height can be made.

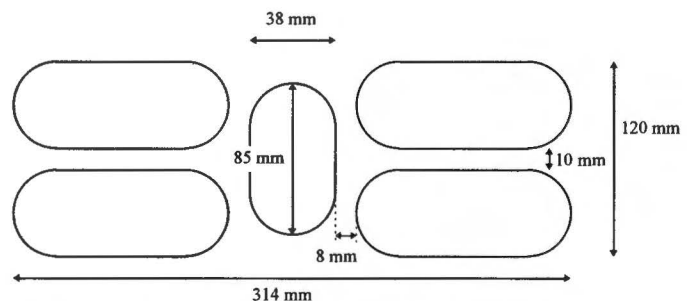


Figure 2.13 Actuator dimensions in the X-Y plane.

The subdivision for the actuator is:

- iron height: 6 mm (this is a standard size and is chosen because of the easiness of ordering);
- magnet height: 8 mm;
- coil height: 9 mm

Next step is trying to fit the coils in the given dimensions of the XY-plane. The Y-actuator will fit if the total coil width is 55 mm maximum and the coil length is 130 mm maximum. The X-actuator will fit if it has the maximal dimensions of 38 mm by 85 mm. Figure 2.13 displays these dimensions. The magnets overlap the coil width (b_c) by 4 mm, see figure 2.2. The magnet width (b_m) is therefore 8 mm larger than the coil width. This is valid for the X- and Y-coil.

Table 2.2 shows a number of possible coils which will fit within the given dimensions.

Table 2.2 Coil dimensions

Y-coil						
Case	b_c [mm]	b_o [mm]	$\iint B_z$ [Tmm ²]	S [Ns/m]	$B_{y_{max}}$ [T]	F [N/mm]
1	18	15	139.80	231.33	2.34	0.1398
2	17	17	133.02	223.05	2.29	0.1330
X-coil						
Case	b_c [mm]	b_o [mm]	$\iint B_z$ [Tmm ²]	S [Ns/m]	$B_{y_{max}}$ [T]	F [N/mm]
3	13	10	95.87	95.68	2.33	0.0856
4	12	12	92.47	97.33	2.16	0.0855

Case 1 is chosen for the initial design of the Y-coil. Because there is not much difference in the figure of merit for case 3 and case 4 the choice has to be made on an other argument. This argument is the value of the magnetic field in the iron. The iron in case 4 is less saturated than the iron in case 3, this is a good reason to choose for case 4 as the initial design of the X-coil.

The analytical model is applied on case 1 and the results of this application can be found in appendix E. The values of the figure of merit, the magnetic field in the iron and the generated force are compared with the values of the simulation results of case 1. The conclusion is that the analytical model is accurate within 3 % (for this particular case).

2.6.1 Disturbance forces

When the coils are not in their nominal position, that is completely symmetric with respect to the magnets, disturbance forces are generated. These forces have a direction that differ from the direction of the driving force. Because of this, the forces are called disturbance forces. They don't contribute to the driving force and are therefore not wanted. Two types of disturbance forces are considered, those are:

- Electrodynamic disturbance force: due to a current in a non homogeneous permanent magnetic field. The generated force can be resolved in two parts (for 2 dimensional configurations), one in the drive direction and one perpendicular to the drive direction. The latter one is not wanted and is therefore regarded as a disturbance force. This electrodynamic disturbance force is proportional to the current.
- Reluctance force: due to the attraction of current carrying coil towards the iron. When the coil is in the symmetric position there is no net reluctance force on the coil. The reluctance force can be calculated via the energy balance. This balance is represented in figure 2.14.

From this figure there can be concluded that the sum of the stored magnetic- and delivered mechanical energy is equal to the supplied electric energy. The equation is:

$$i \cdot d\phi = dW_m + F \cdot dz \tag{2.14}$$

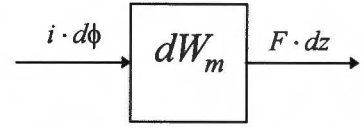


Figure 2.14 Energy balance

The flux ϕ and the magnetic energy W_m are functions of the current i and the position z . The current I and the position z are independent from each other. There can be written:

$$\begin{aligned} \phi &= \phi(i, z) \\ W_m &= W_m(i, z) \end{aligned}$$

Equation 2.14 can be rewritten with respect to the force and is equal to:

$$F = i \cdot \frac{\partial \phi(i, z)}{\partial z} - \frac{\partial W_m(i, z)}{\partial z} \tag{2.15}$$

Assuming that the system is linear, the following expressions can be written for the flux and the magnetic energy:

$$\begin{aligned} \phi &= L(z) \cdot i \\ W_m &= \frac{1}{2} \cdot L(z) \cdot i^2 \end{aligned}$$

Substituting the above expressions in equation 2.15 leads to the reluctance force:

$$F = i \cdot \frac{\partial}{\partial z} \cdot (L \cdot i) - \frac{\partial}{\partial z} \cdot \left(\frac{1}{2} \cdot L \cdot i^2 \right) = \frac{1}{2} \cdot i^2 \cdot \frac{dL}{dz} \text{ ,for} \tag{2.16}$$

When the position derivative of the inductance is constant, then the reluctance force is a proportional to the square of the current.

2.6.2 Disturbance forces obtained from 2D simulations

The 2D simulation package can not distinguish the disturbance force between the two mentioned parts. Because it is known that the reluctance force is a function of the square of the current and the electrodynamic disturbance force is linear to the current the two forces can be resolved easily by changing the direction of the current. When doing this in a certain position the reluctance force has the same direction, but the electro dynamic force has not. Subtracting the results of the two different current directions and divided it by two leads to the electro dynamic disturbance force. Adding the results and dividing it by two leads to the reluctance force. In other words:

- Positive current: $F^+ = F_{ED} + F_{REL} \ ;$
- Negative current: $F^- = -F_{ED} + F_{REL} \ ;$
- F_{ED} = electro dynamic force and F_{REL} = reluctance force.

In this case the assumption is made that a positive current leads to a positive electrodynamic disturbance force and vice versa for a negative current.

The reluctance force is equal to:
$$F_{REL} = \frac{F^+ + F^-}{2}$$

And the electro dynamic disturbance force is equal to:
$$F_{ED} = \frac{F^+ - F^-}{2}$$

The results of the generated forces obtained by the 2D simulation data are used to calculate the disturbance forces. The electrodynamic force and the reluctance force are calculated by using the

expressions of the previous page. In table 2.3 the results are displayed for the total Y actuator. The simulation is carried out in 2 dimensions, so the influence of the third dimension on the disturbance force can not be concluded from the simulation results.

Table 2.3 Disturbance forces total Y actuator.

Sign J	dy [mm]	dz [mm]	F _y [N]	F _z [N]	F _{ED} [N]	F _{REL} [N]
+1	0	0	1139.04	0	0	0
+1	1	1	1136.58	13.06	7.28	5.78
-1	1	1	-1141.50	-1.5	-7.28	5.78
+1	-1	1	1141.50	1.22	-4.56	5.78
-1	-1	1	-1136.58	10.36	4.56	5.78
+1	-1	-1	1141.50	1.5	7.28	-5.78
-1	-1	-1	-1136.58	-13.06	-7.28	-5.78
+1	1	-1	1136.58	-10.36	-4.56	-5.78
-1	1	-1	-1141.50	-1.22	4.56	-5.78

The forces in table 2.3 are calculated with a value of the current density of 17.56 A/mm², this value is used to get the maximum required force in Y-direction if the mass is 25 kg. In this particular case the maximal disturbance force in Z-direction is about 13.1 N.

The same calculations are done for the X-actuator and can be found in table 2.4 (the third dimension is neglected). The current density is 16.30 A/mm², this value is used to get a force in X-direction of about 10 % of the maximum force in Y-direction.

Table 2.4 Disturbance forces X actuator.

Sign J	dx [mm]	dz [mm]	F _x [N]	F _z [N]	F _{ED} [N]	F _{REL} [N]
+1	0	0	-107.35	0	0	0
+1	1	1	-107.41	-1.32	-1.49	0.26
-1	1	1	107.30	1.65	1.49	0.26
+1	-1	1	-107.30	1.11	0.95	0.26
-1	-1	1	107.41	-0.79	-0.95	0.26
+1	-1	-1	-107.30	-1.75	-1.49	-0.26
-1	-1	-1	107.41	1.23	1.49	-0.26
+1	1	-1	-107.41	0.69	0.95	-0.26
-1	1	-1	107.30	-1.21	-0.95	-0.26

In this particular case the maximal disturbance force in Z-direction is about 1.8 N. The contribution of the reluctance force is minimal and therefore it can be said that the disturbance force is mainly due to the electrodynamic disturbance force at the current density level used.

2.6.3 Disturbance forces obtained from 3D simulations

To get an idea of the influence of the third dimension on the disturbance forces, simulations with a 3D finite element package have been carried out. In particular coil end effects are now also considered. The electrodynamic disturbance force and the reluctance force can be calculated in the same way as done by the 2D simulations. That is by changing the direction of the current. Because this will cost a lot of calculation time, an other method is applied. The other method is to calculate the magnetic field in the airgap between the magnets. With this magnetic field known, a conductor is placed in the airgap. Then the cross product of the current density vector and the magnetic field

vector is calculated, resulting in a force vector. This force vector has an element which is equal to the drive force and elements for the disturbance forces. Because the coil field is not present in the magnetic field, the disturbance force has only an electrodynamic component. The reluctance force can be calculated by removing the magnets and then calculated the force on the coils. All the calculations are done by the simulation package. The actuator is symmetric in three directions, therefore only one octant has been looked at. All the simulations are carried out with a current density of 1 A/mm² and displacements in X-, Y- and Z-direction of 1.0 mm. The results of the simulations are:

- Y actuator: electrodynamic disturbance force is less than 400·10⁻³ N;
reluctance disturbance force is less than 18·10⁻³ N.
- X actuator: electrodynamic disturbance force is less than 20·10⁻³ N;
reluctance disturbance force is less than 0.848·10⁻³ N.

The values for the disturbance forces can be easily calculated for other current densities. The electrodynamic disturbance force is proportional to the current density, while the reluctance force is quadratic related to the current density. The results of the 3D simulations are displayed in appendix F, table F.1 for the Y actuator and table F.2 for the X-actuator. The reluctance force is simulated at one XY-position and different Z-positions. Because of the large iron yokes, the X- and Y-position do not have any influence on the reluctance force.

2.6.4 Comparison between 3D- and 2D-simulations

The current density of the 3D simulation differs from the current density of the 2D simulation. To compare the 3D results with the 2D results they are calculated for the current densities of the 2D simulations. Table 2.5 displays the results.

Table 2.5 Comparison between 3D- and 2D-simulations.

Y-actuator $j=17.56 \text{ A/mm}^2$			
2D-results		3D-results	
$F_{ED} \text{ [N]}$	$F_{REL} \text{ [N]}$	$F_{ED} \text{ [N]}$	$F_{REL} \text{ [N]}$
7.3	5.8	7.0	5.6
X-actuator $j=16.30 \text{ A/mm}^2$			
2D-results		3D-results	
$F_{ED} \text{ [N]}$	$F_{REL} \text{ [N]}$	$F_{ED} \text{ [N]}$	$F_{REL} \text{ [N]}$
1.5	0.3	0.4	0.2

It can be seen that the values obtained by the 2D and 3D simulations are comparable. The difference between the electrodynamic disturbance of the X-actuator can be due to a reduced mesh density in the 3D calculations.

2.7 MOTOR CONSTANT

The motor constant can also be calculated from the simulation results. The motor constant describes the relation between the applied current and the generated force. Both the force and the current are known, therefore it is easy to determine the motor constant. If the coil has one turn, the motor constant can be written as:

$$K_0 = \frac{F}{I_0}$$

If the coil has N turns, then the initial current (I_0) can be reduced by one over N , thus:

$$K = N \cdot K_0 = \frac{F}{I}$$

The left term is called the motor constant. The larger the number of windings the larger the motor constant. The motor constant can be calculated using the opera 2D and opera 3D simulation results and will be calculated for one turn.

2.7.1 Motor constant obtained from 2D simulations

When the current density is multiplied with the area where the current is present the total current can be calculated. The total current of a single Y-coil is 2845 A and for the X-coil 1760 A. The results of the 2D simulation concerning the motor constant are displayed in table 2.6. This table displays the motor constant for the total Y-actuator and the X-actuator. The variation in the motor constant is compared with the value in the nominal position.

Table 2.6 Motor constants.

total Y actuator					X actuator				
	dy [mm]	dz [mm]	K_y [N/A]	ΔK [%]		dx [mm]	dz [mm]	K_x [N/A]	ΔK [%]
+j	0	0	0.4002		+j	0	0	0.0609	
+j	1	1	0.3994	-0.1999	+j	1	1	0.0610	0.0559
-j	1	1	0.4012	0.2499	-j	1	1	0.0609	-0.0466
+j	-1	1	0.4012	0.2499	+j	-1	-1	0.0609	-0.0466
-j	-1	1	0.3994	-0.1999	-j	-1	-1	0.0610	0.0559
+j	-1	-1	0.4012	0.2499	+j	-1	-1	0.0609	-0.0466
-j	-1	-1	0.3994	-0.1999	-j	-1	-1	0.0610	0.0559
+j	1	-1	0.3994	-0.1999	+j	1	1	0.0610	0.0559
-j	1	-1	0.4012	0.2499	-j	1	1	0.0609	-0.0466

Table 2.6 shows that the variation in K-factor for the Y-actuator is small, a maximum of 0.25 % variation in the largest displacement. The X-actuator has an accurate K-factor, almost no variation.

2.7.2 Motor constant obtained from 3D simulations

The calculations of paragraph 2.7.1 can also be done for the opera 3D simulation data, these calculations can be found in appendix F, table F.1 and F.2. A displacement of 1.0 mm is used in X-, Y- and Z-direction. The results of these calculations are:

- total Y actuator: motor constant in nominal position is 0.4096 N/A;
variation in motor constant is less than 0.6 %.
- X actuator: motor constant in nominal position is 0.0593 N/A;
variation in motor constant is less than 1.15 %.

The above results are compared with the results of table 2.6. What can be seen is that for both the X- and Y-actuator the variation in motor constant is larger in the 3D simulation results than the 2D simulation results. The reason for this difference can be the influence of the coil end effects, also a reduced mesh density present in the 3D simulations can influence the motor constant.

2.8 THERMAL CALCULATIONS

One of the most critical specifications is the temperature specification. The allowed temperature difference at the outside of the actuator is ± 0.4 °C. The actuator is enclosed by two heat shields and the temperature is measured at the outside of these shields. The reason for the severe critical temperature specifications is that in the area of the actuator a laser interferometer measuring system is present. The function of the laser interferometer measuring system is to determine the position of the reticle chuck. The chuck has to be positioned with an accuracy of 1 nano meter. The air in the machine is conditioned by air showers and the temperature of the air floating into the machine is measured at the showers. This measured temperature is used to correct the laser interferometer measuring system. The mean temperature along the laser beam path effects the value measured for the position. This mean temperature should not vary more than ± 0.004 °C. If this mean temperature differs from the temperature measured at the air shower, an offset in the position of the reticle stage will occur which is not wanted. The temperature rise at the heat shields of the actuator is set on 22 °C ± 0.4 °C.

The calculations effecting the actuator on temperature are done by Ir. Sonja de Vrieze-Voorn. The actuator is simulated using a finite element package and the results of the simulations are written in [11].

The effect of the actuator size on the temperature rise was unknown. To obtain results in a short time the actuator size has been varied in one dimension, that is the length of the Y-coils. Table 2.7 displays the dissipated power and temperature rise of the actuator for the different Y-coil dimensions. The base for these calculations was a moving mass of 30 kg and a length of the Y-coil equal to 130 mm. The power is the average power and can be calculated by using equation 2.1. This means that the average dissipation for one Y-coil with a coil length of 130 mm is equal to:

$$P_{Y,av} = \frac{F^2}{S} = \frac{\left(\frac{m \cdot a_{av}}{4}\right)^2}{S} = \frac{\left(\frac{30 \cdot 24}{4}\right)^2}{231} = 140 \text{ W}$$

The average dissipation can be calculated for the different coil lengths. Reducing the coil length results in a lower mass but also the steepness decreases. The values obtained by the simulations are summarised in table 2.7.

Table 2.7 Dissipation and temperature rise of actuator

Y coil [mm]	Dissip. Y coil [W]	Dissip X coil [W]	Total dissip. [W]	ΔT [°C]
80	237	45	993	2.2
110	164	50	706	1.6
130	140	53	613	1.3

The result is that a smaller Y-coil does not lead to a lower temperature rise. The temperature rise has the lowest value if the Y-coil has a length of 130 mm (this is the maximum coil length in this configuration), but still about a factor 3 higher then the specification. The solution decreasing the temperature rise further has to be found in another way. In [11] the possible solutions are mentioned, the most important are:

- investigate the possibilities of a cooling system with different water temperatures, the cooler the water the lower the temperature rise of the actuator. A negative effect is that if the actuator is not dissipating, the temperature difference of the actuator can bigger than -0.4 °C;
- applying a cooling system to the heat shields.

3. Proto type design

The objective in the second design phase is to design an actuator which will perform optimal in the Functional Model. The FUMO is a pre-prototype of the machine as it will be build within ASML. The objective of the FUMO is to research the dynamic performance and to prove the feasibility of the technologies used.

In paragraph 3.1 a new design is described. This design is significantly different from the first design. The dimensions are different and the layout of the coils is different. Also the effect of shorter magnets on the generated force has been looked at. This is done in order to reduce the mass of the actuator.

The new design has also been simulated with the finite element packages Opera2D and Opera3D. From these simulations disturbance forces, that is the electrodynamic disturbance force and the reluctance force, are calculated. In paragraph 3.2, the results obtained by the Opera2D and Opera3D simulations are compared with each other.

The motor constant can also be derived by using the Opera2D and the Opera3D simulation results, this is done in paragraph 3.3. The motor constant is compared with the motor constant in nominal position. The variation in the motor constant can be obtained from the Opera2D and Opera3D simulation results, this is also done in paragraph 3.3. The variation in the motor constant is an important design parameter and it has to meet the specifications mentioned in paragraph 2.1.

The actuator is powered by standard current amplifiers. In paragraph 3.4 the calculation of the maximum current which these standard amplifiers have to deliver has been carried out. For a good calculation of the maximum current the motor parameters like self inductance, resistance and motor constant need to be known. The self inductance and the resistance are calculated from results obtained by the Opera2D simulation. When all these parameters are known the motor current and the number of turns can be calculated.

The generated forces in the coils have to be transferred to the coil carrier. Therefore, the coils and the coil carrier have to form one solid block. Which material has to be chosen for the coil carrier is described in paragraph 3.5. Also, the types of wires and the wire copper diameter are described in this paragraph.

The coil carrier moves between the yokes, due to this movement an unwanted damping effect occurs. In paragraph 3.6 this unwanted damping is examined. The damping can be split in two parts, a part due to eddy currents and a part due to the control loop of the amplifier. The total damping is the sum of both parts.

3.1 NEW DESIGN

The FUMO design is different from the design described in chapter 2. The reason for this is the bad dynamical behaviour of the total actuator when using this first design. The total actuator is connected to the reticle chuck through an interface. The span of the total actuator is too large to obtain a first modal frequency of 500 Hz. The dynamical behaviour of the FUMO is very important so the layout of the first design had to be changed. To decrease the span of the actuator, the X-coil is

placed outside the Y-coils and split into two for reasons of symmetry. Dynamical simulations of the new design showed that the first modal frequency still was not as high as desired. The next step was to decrease the length of the Y-coils to decrease the span of the total actuator. Simulations show that if the coil length of the Y-actuator is equal to 99 mm the obtained first modal frequency is about 500 Hz. Figure 3.1 shows the new layout and the new dimensions.

The total height for the Y-actuator stayed 45 mm and the subdivision of the total height can be found in paragraph 2.6. Due to constraints posed by the mechanical construction, the total height of the X-actuator is reduced to 32 mm. The following division has been made for the X-actuator:

- magnet height and iron height are 5 mm;
- physical airgap: 2,5 mm;
- coil height: 7 mm.

To reduce the mass of the X-actuator the coil core width has been decreased from 15 mm in the previous design to 10 mm in the new design.

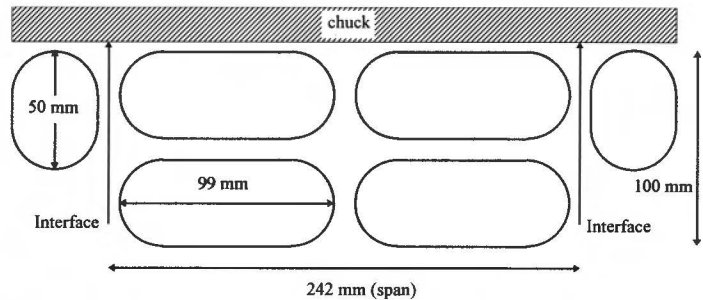


Figure 3.1 New actuator dimensions in X-Y plane.

An important issue for reducing the mass of the total actuator is the length of the magnets. Is it really important that the magnets “cover” the coils fully to generate the required force? This issue has been analysed analytically and by 3D finite element simulations. Equation 3.1 displays an analytical expression to calculate the force generated by the total Y-actuator in the scan direction. The derivation of this equation can be found in appendix G. The assumptions, that has been done in deriving this equation, can also be found in this appendix.

$$F_y = \begin{cases} 8 \cdot h_c \cdot J \cdot B \cdot \left(2 \cdot \left(R_2 \cdot A - \frac{1}{2} \cdot (A^2 + R_1^2) \right) + l_o \cdot b_c \right) & \text{if } R_1 \leq A \leq R_2 \\ 8 \cdot h_c \cdot J \cdot B \cdot \left(2 \cdot (R_2 - R_1) \cdot A + l_o \cdot b_c \right) & \text{if } A < R_1 \end{cases} \quad (3.1)$$

Figure 3.2 displays the force generated by the total Y-actuator using expression 3.1, where A is used to represent the border of the magnet. The parameters used are:

- coil length $l_c = 99$ mm;
- coil height $h_c = 9$ mm;
- coil width $b_c = 18$ mm;
- coil core width $b_0 = 10$ mm.

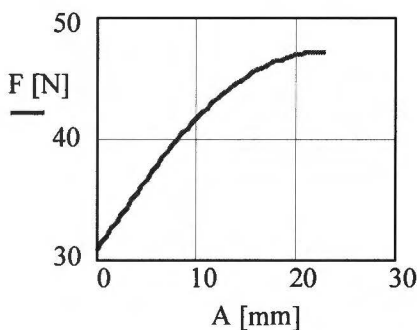


Figure 3.2 Generated force.

The parameter A has been varied between zero and radius R_2 , which is equal to 23 mm. The figure displays thus the force generated by the Y-actuator where the magnets cover the coil from only the straight parts to the whole coil. What can be seen from this figure is that the curvature of the force has a flat trend. When the coils are fully covered by the magnets, meaning $A = 23$ mm, the generated force is 47.2 N. When the coils are covered for 90 % by the magnets, meaning $A = 18$ mm, the generated force is still 46.6 N. Decreasing the magnet length to 90 % of the coil length only has a minor effect on the generated force.

To verify the analytical expression, the whole Y-actuator has been simulated using the Opera3D package. This has been done for 2 cases, that is:

- magnets covering the whole coil;
- magnets covering the coil for 90 %.

The results of these simulations can be found in appendix G, table G.1. The performances, with a displacement of ± 1.0 mm, of the two cases are:

- a) magnets covering the whole coil:
- $K = 46.00$ N/A;
 - $|\Delta K| \leq 0.45$ %;
 - $F_z \leq 0.34$ N.
- b) magnets covering 90 % of the coil:
- $K = 45.80$ N/A;
 - $|\Delta K| \leq 0.46$ %;
 - $F_z \leq 0.38$ N.

The conclusion is that there is almost no difference in the two cases, so it is allowed to cover the coils for 90 % with magnets. With this in mind the performance of the new actuators can be calculated. For the Y-coils the magnet length is equal to 90 mm and for the X-coils the magnet length is equal to 44 mm. The new dimensions and the performances are displayed in table 3.1.

Table 3.1 Dimensions and performances new coils.

Coil	b_c [mm]	b_o [mm]	l_c [mm]	$\iint B_z$ [Tmm ²]	S [Ns/m]	F [N/mm]
Y	18	10	99	136.2	154.93	0.136
X	10	10	50	61.7	33.85	0.062

3.2 DISTURBANCE FORCES

The same disturbance forces as described in chapter 2 are considered in the new design. The X- and Y-actuator are simulated using the Opera2D and Opera3D finite element packages, this to get an idea of the values of the disturbance forces,

3.2.1 Disturbance forces obtained from 2D simulations

The results of the generated forces obtained by the Opera2D simulation are displayed in table 3.2 for the total Y-actuator.

Table 3.2 Disturbance forces total Y-actuator.

Sign J	dy [mm]	dz [mm]	Fy [N]	Fz [N]	F _{ED} [10 ⁻³ N]	F _{REL} [10 ⁻³ N]
+1	0	0	45.648	0.0	0.0	0.0
+1	1	1	45.645	0.417	404.838	12.620
-1	1	1	-45.655	-0.392	-405.0	12.620
+1	-1	1	45.653	-0.238	-250.776	12.620
-1	-1	1	-45.644	0.263	250.776	12.620
+1	-1	-1	45.655	0.392	404.838	-12.620
-1	-1	-1	45.645	-0.417	-404.838	-12.620
+1	1	-1	45.644	-0.263	-250.776	-12.620
-1	1	-1	45.653	0.238	250.776	-12.620

The current density used to calculate the forces in table 3.2 is equal to 1 A/mm². In this particular case the maximum disturbance force in Z-direction is 0.42 N.

The same calculations are done for the X-actuator and can be found in table 3.3. The current density is 1 A/mm².

Table 3.2 Disturbance forces X-actuator.

Sign J	dx [mm]	dz [mm]	F _x [N]	F _z [10 ⁻³ N]	F _{ED} [10 ⁻³ N]	F _{REL} [10 ⁻³ N]
+1	0	0	4.990	0.0	0.0	0.0
+1	1	1	4.992	87.574	86.240	1.322
-1	1	1	-4.993	-84.931	-86.240	1.322
+1	-1	1	4.991	-51.233	-52.552	1.322
-1	-1	1	-4.990	53.872	52.552	1.322
+1	-1	-1	4.993	84.931	86.240	-1.322
-1	-1	-1	-4.992	-87.574	-86.240	-1.322
+1	1	-1	4.990	-53.872	-52.552	-1.322
-1	1	-1	-4.991	51.233	52.552	-1.322

In this particular case the maximal disturbance force is 87.6 mN.

3.2.2 Disturbance forces obtained from 3D simulations

The total Y-actuator and the X-actuator are simulated using the Opera3D simulation package. Because the actuator is symmetric in three axes it is only necessary to look at one octant. The applied current density in the simulations was 1 A/mm². The results of the simulations can be found in appendix H, table H.1 and H.2 and summarised:

- total Y-actuator: electrodynamic disturbance force is less than 375·10⁻³ N;
reluctance disturbance force is less than 12·10⁻³ N.
- X-actuator: electrodynamic disturbance force is less than 105·10⁻³ N;
reluctance disturbance force is less than 1.2·10⁻³ N.

3.2.3 Comparison between 3D- and 2D-simulations

To get an idea of the reliability of the simulation results, the 3D- and 2D-simulations are compared with each other. Table 3.3 displays the results.

Table 3.3 Comparison between 3D- and 2D-simulations.

total Y-actuator			
2D-results		3D-results	
F _{ED} [N]	F _{REL} [N]	F _{ED} [N]	F _{REL} [N]
405·10 ⁻³	12.6·10 ⁻³	375·10 ⁻³	12.0·10 ⁻³
X-actuator			
2D-results		3D-results	
F _{ED} [N]	F _{REL} [N]	F _{ED} [N]	F _{REL} [N]
86·10 ⁻³	1.3·10 ⁻³	105·10 ⁻³	1.2·10 ⁻³

It can be seen that the values obtained by the 2D and 3D simulations are comparable. There is a slight but acceptable difference between the 2D and the 3D electrodynamic disturbance force of the X- and total Y-actuator. This is due to the fact that in 3D simulations the end effects of the magnets are modelled and a reduced mesh density is present.

The total disturbance force is the sum of the reluctance force and the electrodynamic force. Obtained from paragraph 2.6.1 is that the reluctance force is proportional to the square of the current density and the electrodynamic disturbance force is proportional to the current density. The total disturbance force is equal to the sum of both components and can be written as:

$$F_z = \alpha \cdot j + \beta \cdot j^2$$

The factor β is about 30 times smaller than the factor α . The current density during acceleration is about 20 times larger than the current density during constant speed. This means that during acceleration the value of the second term is almost as large as the first term. During constant speed the second term can be neglected.

3.3 MOTOR CONSTANT

The motor constant can be calculated with the results of the Opera2D and Opera3D simulation results. The motor constant is a parameter which gives the relation between the generated force and the applied current. The results of the 2D simulations concerning the motor constant are displayed in table 3.4. The motor constant in other positions than the nominal position is compared with the value of the motor constant in nominal position. This comparison is called the variation in the motor constant, ΔK .

Table 3.4 Motor constants for new design.

total Y actuator					X actuator				
	dy [mm]	dz [mm]	K_y [N/A]	ΔK [%]		dx [mm]	dz [mm]	K_x [N/A]	ΔK [%]
+j	0	0	0.28178	0	+j	0	0	0.07129	0
+j	1	1	0.28176	-0.0064	+j	1	1	0.07132	0.0352
-j	1	1	0.28182	0.0152	-j	1	1	0.07133	0.0492
+j	-1	1	0.28181	0.0110	+j	-1	-1	0.07130	0.0115
-j	-1	1	0.28175	-0.0100	-j	-1	-1	0.07129	-0.0022
+j	-1	-1	0.28182	0.0152	+j	-1	-1	0.07130	-0.0492
-j	-1	-1	0.28176	-0.0064	-j	-1	-1	0.07132	0.0352
+j	1	-1	0.28175	-0.0100	+j	1	1	0.07129	-0.0224
-j	1	-1	0.28181	0.0110	-j	1	1	0.07130	0.0138

The motor constant calculated with the data acquired from the 3D simulations results are displayed in table H.1 and H.2 in appendix H. This has been done for the total Y- and X-actuator. The results of these calculations are:

- total Y-actuator: motor constant in nominal position is 0.2828 N/A;
variation in motor constant less than 0.46 %.
- X-actuator: motor constant in nominal position is 0.0670 N/A;
variation in motor constant less than 1.0 %.

If the results of the 2D simulations are compared with the results of the 3D simulation, it can be seen that there is a large difference, up to a factor 20, between the variation in motor constant calculated with the 2D simulations and the variation in motor constant calculated with the 3D simulations ($K_{2D} \ll K_{3D}$). A contributing factor is the shorter magnets. In the 2D simulations the end effects of the magnetic field are not taken into account. The end effects can have an influence on the variation of the motor constant.

3.4 AMPLIFIER MATCHING

The current which has to run through the coils depends on the force which has to be generated by those coils and the number of turns. The force that must be generated depends on the moving mass and the maximum acceleration. In figure 3.3 the acceleration and velocity profile is displayed. The force is equal to the mass times the acceleration, therefore the force profile has the same shape as the acceleration profile.

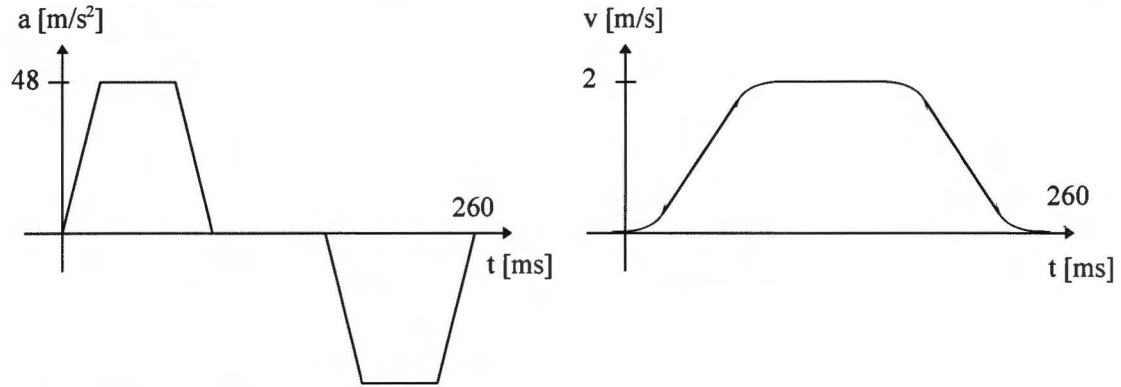


Figure 3.3 Acceleration and speed profile.

The amplifier must be able to deliver the power to generate the force. An important component in the short stroke actuator design is the current amplifier. There is a standard amplifier available, which can deliver a current of 10 A maximum. The actual amplifier output voltage is 45 V and from this voltage 10 % has to be reserved for the servo margin. For the actuator and the cable to the actuator a voltage of 40.5 V then remains. The amplifier can deliver about $40 \text{ V} \times 10 \text{ A} = 400 \text{ W}$. When the chuck of 22.5 kg is almost a constant speed the power needed is equal to $48 \text{ m/s}^2 \times 22.5 \text{ kg} \times 2 \text{ m/s} = 2160 \text{ W}$. This means more than 5 amplifiers for the total Y-actuator. The X-actuator needs approximate 10 % of the power of the total Y-actuator, so one amplifier is enough for the X-actuator.

The amplifier voltage is equal to [3]:

$$U = R_{cable} \cdot \frac{m \cdot a}{K_0 \cdot N} + R_0 \cdot N \cdot \frac{m \cdot a}{K_0} + (L_0 + M_0) \cdot N \cdot \frac{m \cdot j_k}{K} + K_0 \cdot N \cdot v_d \quad (3.2)$$

The derivation of this equation can be found in appendix I. Rewriting of this equation to the expression for N:

$$\left(R_0 \cdot m \cdot a + (L_0 + M_0) \cdot m \cdot j_k + K_0^2 \cdot v_d \right) \cdot N^2 - U \cdot K_0 \cdot N + R_{cable} \cdot m \cdot a = 0 \quad (3.3)$$

Equation 3.3 is a quadratic expression in the number of turns and can be solved with the mass as variable. The mass is the variable because it is the only unknown term. The term R_0 can be easily calculated, because the coil dimensions are known (that is the coil volume and coil cross section). For a single Y-coil is R_0 equal to $30.4 \mu\Omega$ and for the X-coil $37.3 \mu\Omega$, at a temperature of $20 \text{ }^\circ\text{C}$. These values of the resistance are temperature dependent and a temperature rise up to $80 \text{ }^\circ\text{C}$ is expected.

The self inductance L_0 can be determined using the simulation package. One Y-actuator has 2 coils and has therefore a self inductance and a mutual inductance. The X-actuator has two coils which are not coupled with each other and has only a self inductance. Assumed is that the Y-coils don't effect the X-coil and vice versa.

The simulation package also calculates the magnetic energy in the system. Due to the magnets, the iron is saturated and therefore the system is not linear anymore. To get a first approximation of the values of the self inductance's, the system is considered to be linear. This means that the magnets have to be removed. Using the linear system, the energy in one Y-actuator is equal to:

$$E_y = \frac{1}{2} \cdot L_1 \cdot i_1^2 + \frac{1}{2} \cdot L_2 \cdot i_2^2 + M \cdot i_1 \cdot i_2 \quad (3.4)$$

And for the X-coil the energy is:

$$E_x = \frac{1}{2} \cdot L \cdot i^2 \quad (3.5)$$

Calculation of the self induction of the X-coil is easy, there is only one unknown. The simulation has been done using a value of the current of 2 A. The stored energy was 0.345 nJ/mm and the value of the self inductance of the X-coil can be calculated. The dimension of the self inductance is H/mm. To get a value of the self inductance it has to be multiplied by a length. As a first order approximation the effective length has been taken. The definition of the effective length is the coil length (l_c) minus the coil width (b_c) and is equal to 40 mm for the X-coil. The value of the X-coil self inductance per turn is:

$$L_{x_0} = 27.6 \text{ nH}$$

The calculation of one Y-actuator self inductance is different. There are 3 unknown variables, see equation 3.4. This problem can be solved by 3 equations. The current i_1 is kept constant at 2 A and the current i_2 is 1, 2 or 3 A. Substituting these values in equation 3.4 leads to a set of 3 equations. They can be written as a matrix and a vector and are:

$$\begin{pmatrix} 2 & 0.5 & 2 \\ 2 & 2 & 4 \\ 2 & 4.5 & 6 \end{pmatrix} \cdot \begin{pmatrix} L_1 \\ L_2 \\ M \end{pmatrix} = \begin{pmatrix} 2.339 \\ 3.932 \\ 6.271 \end{pmatrix} \cdot 10^{-9}$$

Solving this set of equations and multiplying the values with the effective length (that is 81 mm for a Y-coil) leads to the following values for the Y-coil self inductance per turn:

$$L_{y1_0} = 61.1 \text{ nH}$$

$$L_{y2_0} = 61.1 \text{ nH}$$

$$M_0 = 19.5 \text{ nH}$$

The only unknown in equation 3.3 is the speed difference. This difference is assumed to be equal to 0.1 m/s. The total mass which needs to be accelerated is about 22.5 kg. Everything except the number of turns is known and this number can be calculated as function of the mass. The current of the coil can be calculated when the number of turns is known. The Y-actuator has 8 amplifiers, i.e. two amplifiers per Y-coil, the X-actuator has one amplifier for two coils which are in series. Another important parameter is the resistance of the cable from the amplifiers to the coils, the cable length can be up to 10 m and there are a number of contacts as well. An assumption for the value of this resistance is 0.5 Ω . The calculations have been done in MathCad and are for one Y-coil shown in appendix I.

The results of the amplifier matching are:

- One Y-coil: number of windings $N_y = 403$;
motor constant $K_y = 28.5 \text{ N/A}$;
current $I_y = 9.5 \text{ A}$.
- X-actuator: number of windings one X-coil $N_x = 495$;
motor constant $K_x = 34.9 \text{ N/A}$;
current $I_x = 1.7 \text{ A}$.

3.5 COILS AND COIL CARRIER

The coils conduct the electric current, therefore the actuator force acts on the coils. The coils are placed in a coil carrier and this carrier is connected to the long stroke assembly. Therefore the force generated by the coils must be transferred to the coil carrier. It is important that the coils and the coil carrier become one solid block. This is achieved by connecting the coils to the coil carrier using an epoxy casting resin.

The copper filling factor gives a relation between the area used by the copper and the area available for the copper, that is the coil cross section. This copper filling factor depends on the shape of the wire, the thickness of the isolation and the method of winding the coil. From a theoretical point of view a square wire would be ideal. However this type of wire gives problems when the wire goes from one layer to the next layer. In practice a serious risk on short circuited turns exists here. When the wire type used is cylindrical, the best method for winding the coils is applying orthocyclic winding, resulting in the maximum value for the filling factor. Figure 3.4 displays the method of orthocyclic winding, where the diameter d is the diameter of the copper including the insulation. The wires used for the Y-coils have a copper diameter of 0.63 mm and the X-coils have a copper diameter of 0.45 mm.

The coil carrier has multiple functions: it transfers the force from the coils to the long stroke assembly, it is used to fix the relative locations of the coils and it provides means to remove heat [3]. The coil body is made of non-ferromagnetic material which has to have a high E-module and a low electrical conductivity. The high E-modules gives the coil carrier a smaller displacement for a given force which is good for the dynamical performance of the actuator. A low electrical conductivity will reduce the amount of eddy currents which will flow in the coil carrier due to movement with respect to the magnets. As a result of all these considerations the material for the coil carrier is stainless non-ferromagnetic steel, however for direct water cooling ceramic material is a better choice.

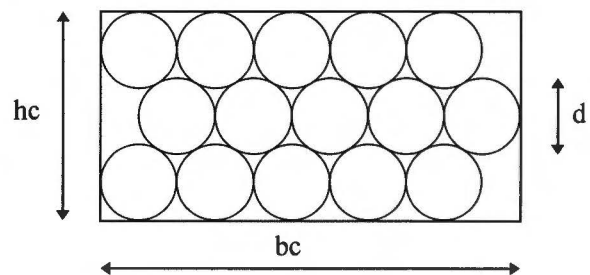


Figure 3.4 Orthocyclic winding.

During motion the coil carrier and the magnet yoke behave as a viscous damper. This damping is the result of two effects:

3.6 DAMPING

During motion the coil carrier and the magnet yoke behave as a viscous damper. This damping is the result of two effects:

Eddy current: Due to the movement of the stainless steel coil carrier with respect to the magnet yokes, eddy current are generated in the coil carrier. This current will produce a force on the coil carrier trying to cancel the movement.

Amplifier: Because of the movement of the coil carrier a voltage is induced in the coils. This voltage disturbs the control loop of the current controlled amplifier. The loop amplification is not finite and therefore a current will flows through the coil resistance and inductance. Again a current is present in a magnetic field and will produce a force on the coil carrier trying to cancel the movement.

These effects can be regarded as viscous damping, dependent on and proportional to relative speed of actuator parts.

3.6.1 Eddy current

There is an analytical method to approximate the force produced by the eddy currents. The value of this method can be used to compare it with the results obtained by the Opera2D finite element calculations. The effects have been studied for the Y-coils.

The eddy current density vector can be written as:

$$\vec{J} = \sigma \cdot \vec{v} \times \vec{B} \quad (3.6)$$

The deviation of this equation can be found in appendix J. The force generated by a velocity in Y-direction is equal to:

$$F_y = \int_V -\sigma \cdot v_y \cdot B_z^2 dV$$

And in Z-direction:

$$F_z = \int_V -\sigma \cdot v_z \cdot B_y^2 dV$$

The derivation of these equations can be found in appendix J. Assuming that the velocity is equal to 0.1 m/s, the conductivity σ is $1.1 \cdot 10^6$ S/m (N1198) and integrating leads to a force in Y- and Z-direction. The applied volume is equal to an area times the length in the third dimension. When using these parameters, the modulus of the generated force is equal to:

- 1.10 N in Y-direction;
- 0.12 N in Z-direction.

The force divided by the velocity is called the damping, using the above forces and the velocity of 0.1 m/s leads to the damping in Y- and Z-direction. The values are:

- 11 Ns/m in Y-direction;
- 1.2 Ns/m in Z-direction.

The results obtained by the Opera2D simulations are:

- Y-direction, 1.38 N at a velocity of 0.1 m/s leads to a damping of 13.8 Ns/m;
- Z-direction, 0.19 N at the same velocity leads to a damping of 1.9 Ns/m.

3.6.2 Damping due to control loop of amplifier

Due to the induced voltage a current is present in the amplifier. The transfer function of the current with respect to the induced voltage is displayed in equation 3.7. The derivation of this transfer function can be found in appendix K.

$$\frac{I_s(\omega)}{E_{ind}(\omega)} = \frac{3.16 \cdot 10^{-4} \cdot \frac{j \cdot \omega}{100} + 1}{\left(\frac{j \cdot \omega}{1005} + 1\right) \cdot \left(\frac{j \cdot \omega}{45886} + 1\right)} \quad (3.7)$$

The force due to the disturbance current I_s is equal to this current times the motor constant. The induced voltage is equal to minus the motor constant times the velocity, when using the generator orientation. Dividing the force by the velocity leads to:

$$\frac{F}{v} = \frac{-K \cdot I_s}{v} = \frac{-K^2 \cdot I_s}{E_{ind}} \quad (3.8)$$

Substituting equation 3.7 in equation 3.8 leads to the transfer function of the force over the velocity and is displayed in figure 3.5 for the total Y-actuator. The transfer function is displayed for frequencies from 1 Hz to 10 kHz, because the bandwidth of the current control loop is 10 kHz. The coil inductance becomes for frequencies higher than 1 kHz dominant and therefore the amplitude plot of figure 3.5 goes to zero for very high frequencies and the phase plot to -270° .

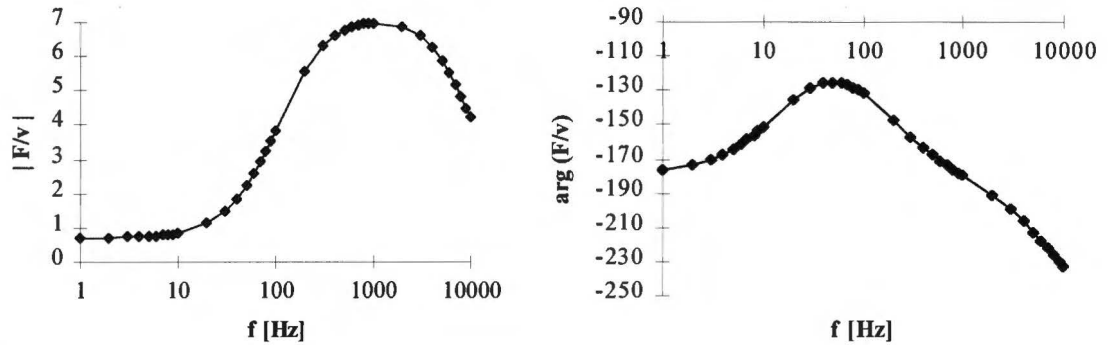


Figure 3.5 Amplitude and phase plot of transfer function.

What can be seen from figure 3.5 is that there are more effects than damping alone. The real part of the transfer function, that is equation 3.7, is a representation for the damping.

3.6.3 Total damping

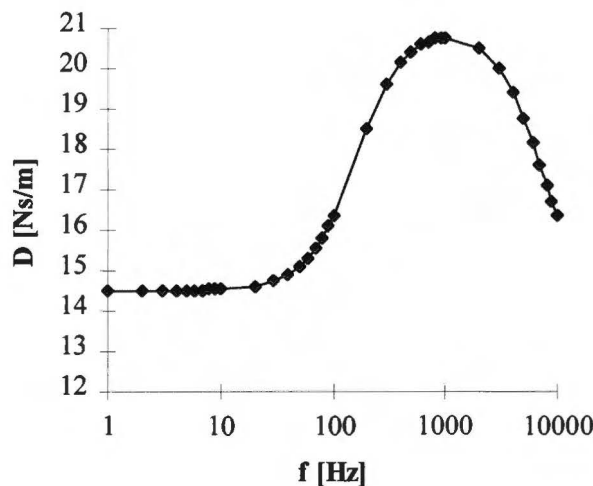


Figure 3.6 Total damping.

What can be seen is that the damping due to eddy currents is the main part of the total damping for low frequencies. For higher frequencies the damping due to the amplifiers has the same order as the damping due to the control loop of the current amplifier.

The total damping is the sum of the damping due to the eddy currents and the damping due to the amplifier.

A graphic can be drawn for the total damping. This graphic is the sum of the real part of the transfer function displayed in figure 3.5 and the damping due to the eddy currents. Assumption is that the damping due to eddy currents has the same phase as the damping due to the amplifier and has a constant value in the frequency range. The damping for the total Y-actuator, for a velocity in Y-direction, is displayed in figure 3.6.

4. Experimental results

To verify the simulation results, experiments have to be carried out at the real actuator. Due to the late time of delivery of the real actuator a fast prototype has been made. This prototype consists of one Y actuator, meaning two coils and their magnets. The coil carrier has been made of aluminium instead of N1198. Two slots have been made into the aluminium coil carrier. The two Y coils have been glued into the slots and then covered with a kind of epoxy resin to fix the coils in the coil carrier and to make one solid block. Figure L.1 to L.3, in appendix L, displays the prototype.

Paragraph 4.1 describes the way the force experiments are carried out. Also the conditions to reproduce the experiments are described in this paragraph. The reluctance force and the electrodynamic disturbance force can be calculated using the experimental results. The reluctance force has been calculated in paragraph 4.1.1 and the electrodynamic disturbance force has been calculated in paragraph 4.1.2.

The reluctance force and the electrodynamic disturbance forces obtained by the experimental results have to be compared with the simulation results to give a good judgement of the accuracy of the simulation models. This comparison has been made in paragraph 4.2.

Another important design parameter is the motor constant, which can be calculated using the experimental results. The variation in the motor constant with respect to the nominal position has to be less than 5 % within a displacement of ± 1.0 mm in X-, Y- and Z-direction. The motor constant has to be compared with the simulation results. The motor constant, the variation in the motor constant and the comparison with the simulation results are described in paragraph 4.3.

The transfer function of the coil and the mutual inductance between to Y-coils are of great importance for a good current amplifier controller design. The resistance and the self inductance can be calculated using the transfer function and they can be compared with the results obtained by the simulations. The mutual inductance can also be calculated using the experimental results and compared with the simulation results. This is done in paragraph 4.4.

Paragraph 4.4 lists the measuring instruments used, which is important for tracing possible errors and for the reproduction of the experiments.

4.1 DISTURBANCE FORCES

The force is measured by two force transducers. One transducer to measure the drive force, the Y-force transducer, and one to measure the disturbance force, the Z force transducer, which is perpendicular to the driving force. The right part of figure 4.1 displays a close up of the measuring configuration, in which the transducer to measure the disturbance force can be seen. The left part of figure 4.1 is an overall view of the measuring configuration.

To reproduce the experiments a X,Y,Z reference system has been introduced. The positive Z-axis is in the direction of the Z force transducer and the X- and Y-axis are perpendicular to the Z-axis. This reference system can be seen in figure 4.1.

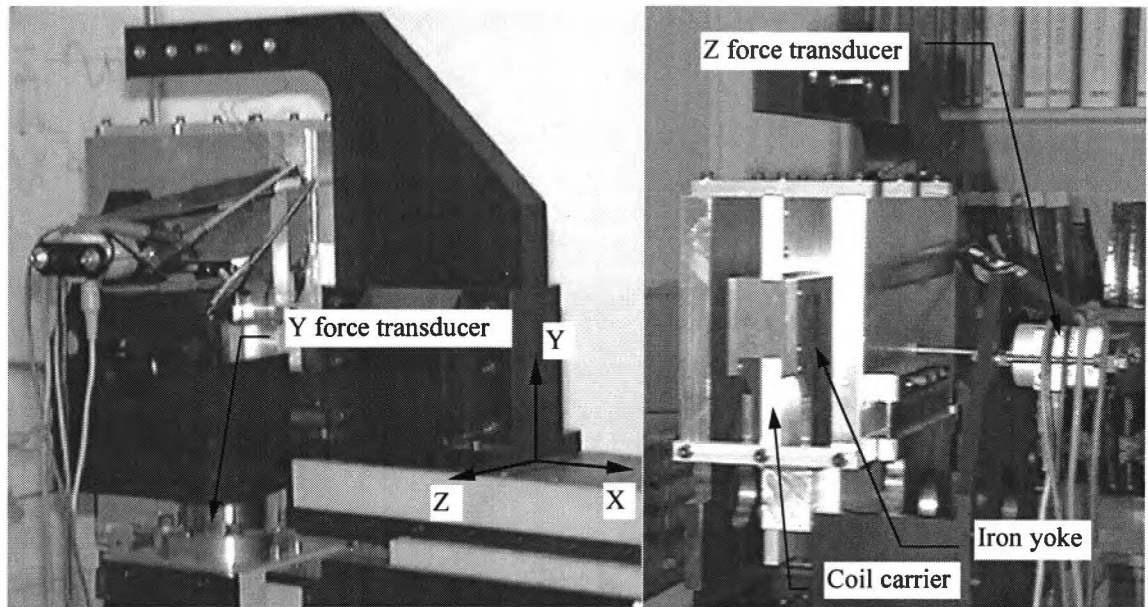


Figure 4.1 Experiment configuration.

The maximum displacements in the X-,Y- and Z-direction are limited by the mechanical construction. For the measurements the following displacements have been chosen:

- ± 1.0 mm in the X-direction;
- ± 1.0 mm in the Y-direction;
- ± 1.0 mm in the Z-direction.

The basis for the measurements are 9 defined points in the XY-plane, see figure 4.2. In each defined point in the XY-plane, 5 different Z-positions are taken into account. There are in total 45 points in the XYZ system where the drive force and the disturbance force have been measured.

The substitute coil carrier is made of aluminium and contains two coils instead of the four coils of the total Y-actuator. The values of the experimental results (that is F_y, F_z) have to be multiplied by 2 to get the results for the total Y-actuator.

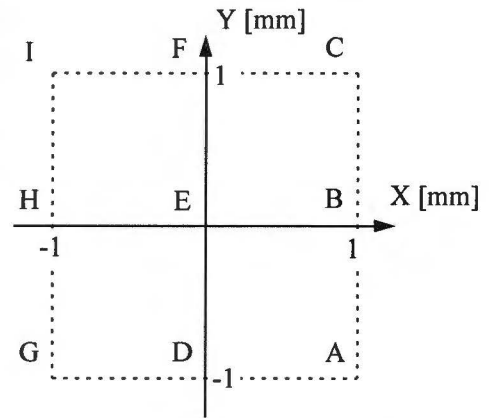


Figure 4.2 Measure points in XY plane.

The Z-force transducer measures the sum of the reluctance force and the electrodynamic disturbance force. These forces can be resolved when a positive and negative current are applied. The disturbance force due to the positive current is equal to:

$$F_{Z+} = I_+ \cdot K_{ED} + I_+^2 \cdot K_{REL}$$

And due to the negative current:

$$F_{Z-} = I_- \cdot K_{ED} + I_-^2 \cdot K_{REL}$$

These two equations can be used to solve K_{ED} and K_{REL} . They are equal to:

$$K_{REL} = \frac{I_- \cdot F_{Z+} - I_+ \cdot F_{Z-}}{I_+ \cdot I_- \cdot (I_+ - I_-)} \tag{4.1}$$

$$K_{ED} = \frac{I_-^2 \cdot F_{Z+} - I_+^2 \cdot F_{Z-}}{I_+ \cdot I_- \cdot (I_+ - I_-)} \tag{4.2}$$

With these parameters known, the electrodynamic disturbance force and reluctance force can be calculated. Table M.1, appendix M, displays the results obtained by the experiments. Graphical representations can be found in the next two paragraphs.

4.1.1 Reluctance force

In table M.1, appendix M, the reluctance force has been calculated using equation 4.1 and a current of 1 A. Figure 4.3 displays the graphics of the reluctance force as function of the Z position. This is done for the 9 different points in the XY-plane.

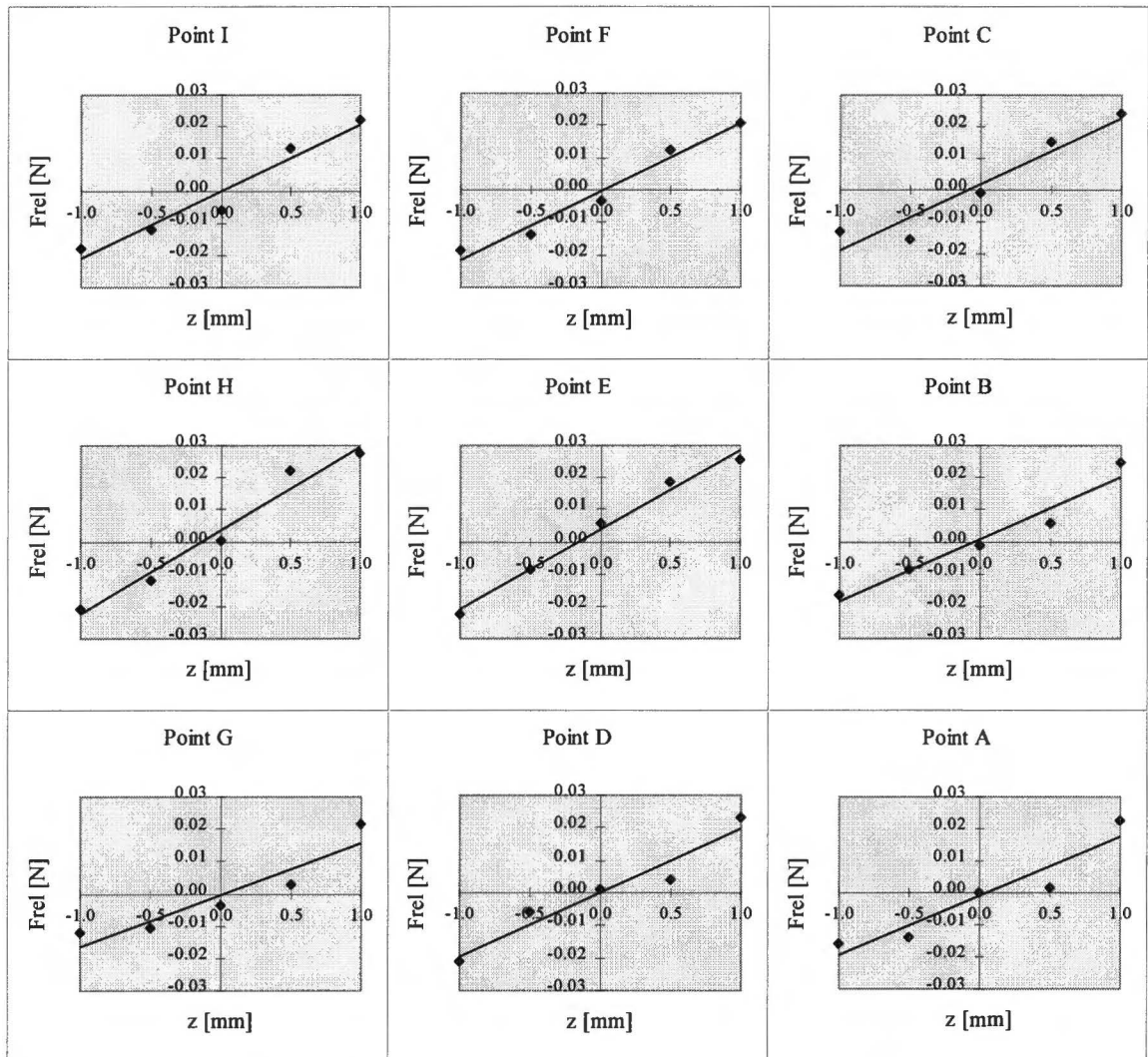


Figure 4.3 Reluctance force.

What can be seen is that the sign of the reluctance force is equal to the Z-position, meaning a positive Z-position leads to a positive reluctance force. The reluctance force becomes larger when the Z displacement increases.

4.1.2 Electrodynamic disturbance force

In table M.1, appendix M, the electrodynamic disturbance force has been calculated using equation 4.2 and a current of 1 A. Figure 4.4 displays the graphics of the electrodynamic disturbance force as function of the Z-position. This is done for the 9 different points in the XY-plane.

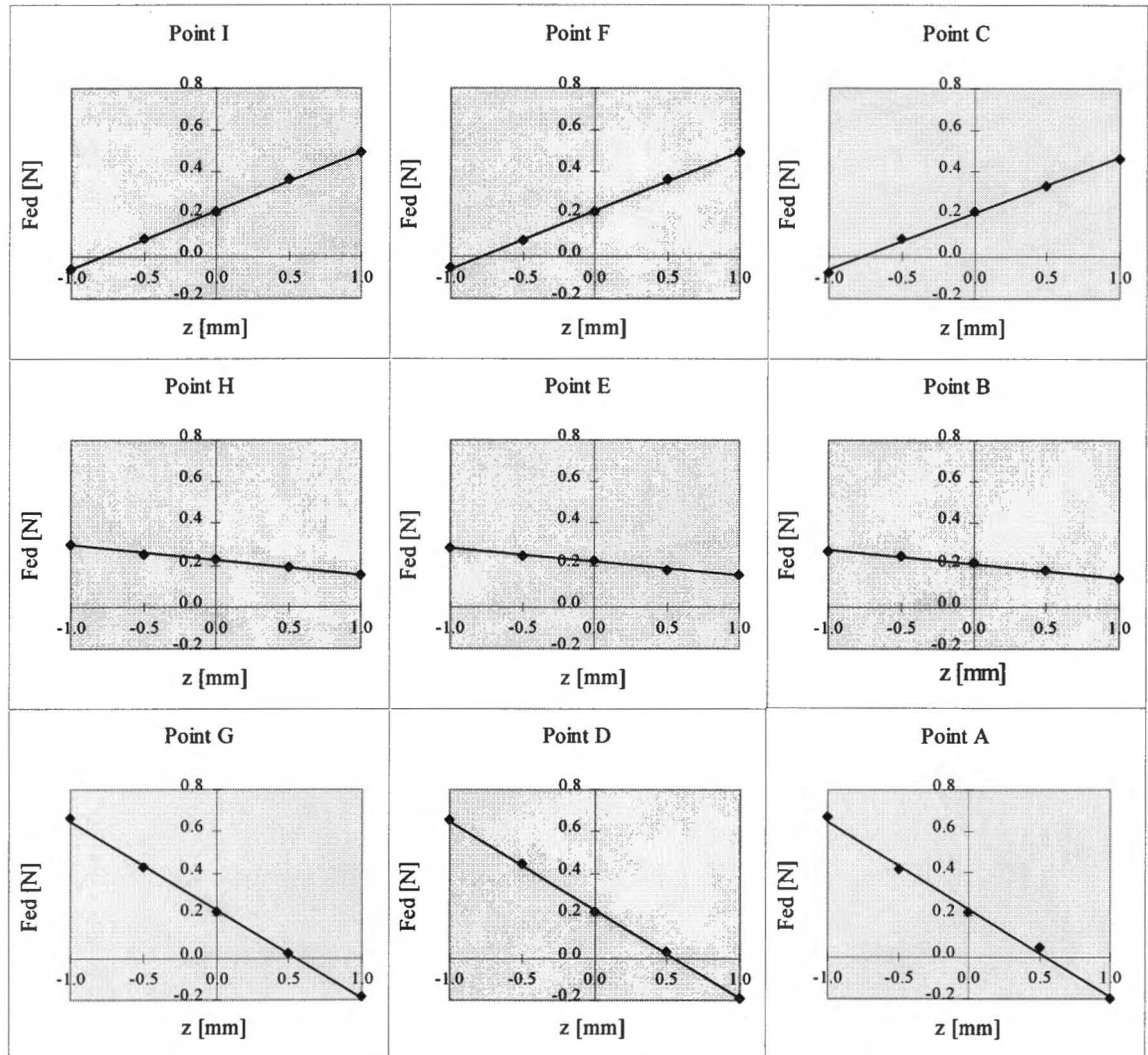


Figure 4.4 Electro dynamic disturbance force.

An important conclusion from figure 4.4 is that there is an offset in the electrodynamic disturbance force. An offset can only occur when the magnet field is not perpendicular to the coils or to the Z-force transducer. This could be caused by the mechanical layout or the magnetisation vector of the magnets or by misalignment. The offset is about 0.2 N at a current of 1 A. What also can be seen is that the slope of the graphics does not change when the X-position is changed (from the left column to the right column in figure 4.4), but the slope turns from a positive value into a negative value when the Y-position is changed (from the top row to the bottom row in figure 4.4).

4.2 COMPARISON EXPERIMENTAL RESULTS WITH SIMULATION RESULTS

To get an idea whether the values of the disturbance forces obtained by the simulation results are comparable to the experimental results, a comparison between the experimental results and the simulation results have to be made.

The reluctance force obtained by the simulations is equal to $12 \cdot 10^{-3}$ N. This value is valid for a current density of 1 A/mm^2 . The total ampere turns is in this case equal to 162. The maximum value for the reluctance force obtained by the experiments is 0.02 N for one Y-actuator, meaning for the total Y-actuator a reluctance force of 0.04 N. The number of ampere turns is equal to 335. The reluctance force obtained by the simulation has to be calculated to the same number of ampere turns as the experiment. The reluctance force is equal to:

$$F_{REL} = \left(\frac{335}{162} \right)^2 \cdot 12 \cdot 10^{-3} = 0.05 \text{ N}$$

Comparing this with the 0.04 N for the experimental results the conclusion can be made that the experimental results fulfil the expectations.

The electrodynamic disturbance force obtained by the simulations has a maximum value of $400 \cdot 10^{-3}$ N at a current density of 1 A/mm^2 . In the experiments the maximum electrodynamic disturbance force with respect to the offset is equal to 0.4 N for one Y-actuator, meaning an electrodynamic disturbance force of 0.8 N for the total Y-actuator. Also in this case the electrodynamic disturbance force obtained by the simulations has to be calculated for the same number of ampere turns as the experiment. The simulated electro dynamic disturbance force is equal to:

$$F_{ED} = \frac{335}{162} \cdot 400 \cdot 10^{-3} = 0.83 \text{ N}$$

When this result of the simulations is compared with the results obtained by the experiments the conclusion can be made that the actuator fulfils the expectations.

4.3 MOTOR CONSTANT

The motor constant in the nominal position for the total actuator obtained by the simulations is equal to 0.2828 N/A for one turn. The real Y-coils have 335 turns so the expected simulated motor constant is equal to:

$$K = 335 \cdot 0.2828 = 94.7 \frac{\text{N}}{\text{A}}$$

In the case of the experiment the motor constant in nominal position is equal to 45.5 N/A, for the total Y-actuator the motor constant is equal to 91.0 N/A. Compared with the simulation result the conclusion is that the motor constant is within 5 % of the expected value.

An other important design parameter is the variation in the motor constant. This variation has been calculated and is displayed in figure M.1 in appendix M. The figure shows the variation in the motor constant in the XY-plane at the 5 different Z-positions. In the total range the variation is within the specification of 5 %. However the variation of the motor constant is not within the specification of 1 % for the XY range of $\pm 0.5 \text{ mm}$ at $Z=0.5 \text{ mm}$ and $Z=-0.5 \text{ mm}$. What must be kept in mind is that the force measurements have only been carried out at the borders of the defined XY-plane and the middle position of the XY-plane. The contour plots of figure M.1 have been drawn with these points as input data, meaning that there could be an error in the contour plots due to the limited points in the XY-plane.

The differences between the simulation results and the experimental results could be due to:

- mechanical tolerances of the coil geometry;
- positioning of the coil;
- tolerances on the magnet positioning;
- tolerances on the magnet vector.

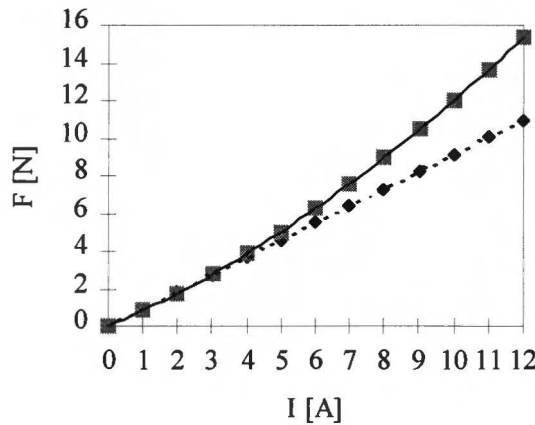


Figure 4.5 Maximum parasitic Z-force.

As mentioned in paragraph 2.1, the maximum parasitic force in Z-direction is 1 % of the force in Y-direction. With the motor constant, the electro dynamic disturbance force and the reluctance force known a comparison between the parasitic Z-force and 1 % of the force in Y-direction can be made. This comparison is displayed in figure 4.5, where the solid line is the force in Z-direction (worst case) using the following expression:

$$F_z = 0.04 \cdot I^2 + 0.8 \cdot I$$

and the dashed line represents 1 % of the force in Y-direction.

What can be seen is that for currents lower than 3 A the parasitic force in Z-direction is within 1 % of the force in Y-direction. If the

4.4 MEASURED COIL PROPERTIES.

current is larger than 3 A the parasitic force in Z-direction becomes larger than 1 % of the force in Y-direction. At a current of 11 A the force in Y-direction has its maximum value (1001 N), the parasitic force in Z-direction is then 1.4 % of the force in Y-direction.

To control the current in the coil the transfer function of the coil need to be known. The transfer function displays the resistance and the inductance of the coil as function of the frequency. An other important parameter which need to be known is the mutual inductance. This can also be displayed as function of the frequency. The coils are placed in an aluminium carrier.

4.4.1 Transfer function of the coil.

The following expression is valid for the voltage across the coil:

$$U = (R + j \cdot \omega \cdot L) \cdot I$$

When the voltage across the coil and the current through the coil are measured, then the impedance can be calculated. The used frequency analyser has the possibility to calculated the impedance. This is displayed as a gain and a phase angle. The transfer function has been measured in three different cases: the coil in air, the coil between the yoke without the magnets and the coil between the yoke with the magnets. This is displayed in figure N.1 to N.3.

What can be seen is that the difference between the three different cases is negligible small. For low frequencies the $\omega \cdot L$ term is very small and the value of the DC resistance can be calculated. The gain for low frequencies is 11.5 dB, so the resistance is:

$$11.5 \approx 20 \log R \quad \Rightarrow \quad R = 3.8 \Omega$$

This is the resistance of the coil and the wires from the analyser to the coils. The resistance of the wires is equal to 0.2 Ω . So the measured DC resistance of the coil is equal to 3.6 Ω .

The expected DC resistance is equal to:

$$R = R_0 \cdot N_y^2 \cdot \frac{h_c}{h_{cc}} = 3.04 \cdot 10^{-5} \cdot 335^2 \cdot \frac{8.8}{9.0} = 3.4 \Omega$$

Where R_0 is the resistance when the coil has one turn, N_y is the number of turns of the coil, h_c the real height of the coil and h_{cc} the used height in the calculations. The difference between the expected and the measured resistance could be due to wire tolerances or a stretched wire.

In the ideal situation the phase should be 90° for high frequencies. But in the three cases can be seen that the phase is less than 90°. This is due to eddy currents which will try to reduce the magnetic field induced by the coils and therefore reduce the self inductance. At 100 Hz the gain is equal to 15 dB, using this and the value of the DC resistance the value of the self inductance can be calculated and is equal to 6.6 mH. The expected value for the self inductance is equal to:

$$L = 61.1 \cdot 10^{-9} \cdot 335^2 = 6.8 \text{ mH}$$

4.4.2 Mutual induction

The two Y-coils are coupled to each other by a magnetic field. When one coil is fed by a current, the next expression is valid for the voltage across the second coil:

$$U_2 = (R_2 + j \cdot \omega \cdot L_2) \cdot I_2 + j \cdot \omega \cdot M \cdot I_1$$

When the current I_2 is equal to zero, then the following expression is valid for the voltage across the second coil:

$$U_2 = j \cdot \omega \cdot M \cdot I_1$$

So when the open terminal voltage of the second coil and the current of the first coil are measured, the mutual inductance can be calculated. This is also done using the frequency analyser. The mutual induction has been measured in three different cases, that is the coils in air, the coils between the yoke without the magnets and the coils between the yoke with the magnets. This is displayed in the figures N.4 to N.6. What can be seen is that there is a large difference between the three figures. Figure N.6 is disturbed by mechanical frequencies and eddy currents and is therefore not useful for determination of the mutual inductance. There is also a big difference between figure N.4 and N.5, that is the start point of the gain at 10 Hz. This is 5 dB larger in the case of the coil between the yokes without the magnets. This is due to the fact that the iron gives the flux a better guide path and therefore more gain. For higher frequencies the eddy currents have a negative effect and will reduce the value of the mutual induction. The value of the gain at 10 Hz is equal to -30 dB in the case of the coils between the yokes without the magnets. The value of the mutual induction is then equal to:

$$-30 = 20 \log(2 \cdot \pi \cdot f \cdot M) \quad \Rightarrow \quad M = 0.5 \text{ mH}$$

The value for the mutual inductance obtained by the simulations is equal to:

$$M = 19.5 \cdot 10^{-9} \cdot 335^2 = 2.2 \text{ mH}$$

There is a difference between the value obtained by the experiments and the value obtained by the simulations. The Opera2D program calculates an expression in the cross section of the actuator. To get the results for the total actuator these values are multiplied by an effective length. What can be concluded is that this method is valid for calculating the self inductance, but on the other hand for calculating the mutual induction it seems that this method is not accurate enough. What must be kept in mind is that the phase of figures N.4 to N.6 have a negative sign, which should be positive.

4.5 FIGURE OF MERIT

The calculated figure of merit of one Y-coil (with a coil height of 9 mm) is equal to 154.9 Ns/m, this value can be found in table 3.1. This means that for a coil height of 8.8 mm the figure of merit is equal to 151.4 Ns/m and for the total Y-actuator 605.8 Ns/m.

Substituting the value of the motor constant found in paragraph 4.3 and four times the value of the resistance found in paragraph 4.4.1 in the next equation leads to the figure of merit found by the experiments and is equal to:

$$S = \frac{K^2}{R} = \frac{91.0^2}{4 \cdot 3.6} = 575.1 \frac{Ns}{m}$$

Conclusion is that the calculated figure of merit is about 5 % larger than the actual figure of merit.

4.6 MEASURING INSTRUMENTS

The used measuring instruments are displayed in table 4.1.

Table 4.1 Used instruments.

Device	Manufacturer	Manufacture number	CFT number
Oscilloscope	Fluke	PM3384A	scope7
Function generator	Philips	PM5193	signaal gen. 8
Power supply	Kepeco	BOP 72-6M	amp 1
Current probe	Tektronix	AM503	meter 28
Power analyser	Infratek	104A	meter 8
Charge amplifier	Kistler	5007 415	-
Analyser	HP	HP35670A	Analyser 7
Loadcel	Kister	9272 A	-

5. Conclusions and recommendations

5.1. CONCLUSIONS

The purpose of the graduation project was the design of a short stroke actuator for the ATLAS reticle stage. In this report the design of this actuator is presented and the conclusions based on the graduation project are:

- The Opera2D and Opera3D models give a good prediction of the generated forces of the actuator;
- The variation in the motor constant is within 5 % for a displacement of ± 1.0 mm in X-, Y- and Z-direction;
- The maximum parasitic force in Z-direction is less than 1 % of the force in Y-direction if the current is lower than 3 A. If the current is between 3 A and the maximum current level (11 A), that is the level needed for the maximum force in Y-direction (1000 N), the maximum parasitic force is between 1 % and 1.4 %;
- The damping between the coil carrier and the iron yoke consists of two components: one due to eddy currents in the coil carrier and the other component due to the finite (frequency dependent) output impedance of the current controlled amplifier. The damping due to eddy currents is the major part of the damping, there is assumed that they are frequency independent. On the other hand the damping due to the current controlled amplifier is frequency dependent and has a maximum at 1 kHz;
- For the controller design the transfer function is important, the measured transfer function is like the one which was expected. For higher frequencies the eddy currents in the system reduce the gain and the phase of the transfer function;
- Mutual inductance is also present in the system, but the value of the mutual inductance is about four times smaller than the value expected. Conclusion is that the method used for calculating this mutual inductance is not valid due to neglecting the third dimension;
- Due to the higher masses and better performance, the current amplifiers of the previous machine are not capable for driving the new actuator.

5.2. RECOMMENDATIONS

During the design process of the short stroke actuator some unwanted effects are detected. These effects need to be investigated further to get an idea how they affect the performance of the actuator. Therefore the following is recommended:

- The damping due to the eddy currents in the coil carrier and also the damping due to the control loop of the current controlled amplifier should be checked by measurements to get an idea of the representation of the calculated results;
- The possibility to reduce the eddy currents in the coil carrier should be investigated by using other material for the coil carrier;
- Mass reduction would decrease the power dissipation, because the power dissipation is proportional to the mass squared;
- Because of the large number of current controlled amplifiers needed to drive the actuator, the question arises whether it is necessary to develop a new current controlled amplifier.

References

- [1] De Wilde, F.H.P.
STOEIEN MET ORGANISATIES: een inleiding organisatiekunde. Deel 2: vervolgboek.
Alphen aan de Rijn: Samson, 1987.
- [2] ELECTRA REFERENCE MANUAL.
Vector Fields Limited, Oxford (UK), 1994.
- [3] Compter, J.C.
Amplifier-specification and the mass of the reticle stage.
Philips CFT, division Mechatronics, Eindhoven (NL), 1995.
Internal Report CTB 595-95-4056.
- [4] Jansen, E.P.
DESIGN OF A SHORT STROKE ACTUATOR FOR A WAFER STEPPER.
Philips CFT, division Mechatronics, Eindhoven (NL), 1994.
Internal Report CTB 595-94-4034.
- [5] Jansen, E.P. and J. Compter
SHORT STROKE RETICLE STAGE MOTOR: pre prototype.
Philips CFT, division Mechatronics, Eindhoven (NL), 1994.
Internal Report CTB 595-94-4025.
- [6] Kamerbeek, E.M.H.
MINI-ELEKTROMECHANICA: Hoofdstuk 1 Permanente magneten.
Collegedictaat nr. 5741. Technische Universiteit Eindhoven, Electrotechniek, 1994.
- [7] Lequesne, B.
FAST ACTING, LONG STROKE BISTABLE SOLENOIDS WITH MOVING
PERMANENT MAGNETS.
IEEE Trans. Ind. Appl., Vol 26 (1990), No. 3, p. 401-407.
- [8] Lequesne, B.
FAST ACTING, LONG STROKE SOLENOIDS WITH TWO PRINGS.
In: Conference Record of the 1989 IEEE Industry Applications Conference. Annual Meeting.
New York: IEEE 1989. p. 195-202.
- [9] Lowther, D.A. and P.P. Silvester
COMPUTER AIDED DESIGN IN MAGNETICS.
New York: Springer, 1986.
- [10] Scharten, Th.
ELEKTROMAGNETISME 2: Aantekeningen bij het college.
Collegedictaat nr. 5757. Technische Universiteit Eindhoven, Electrotechniek, 1992.
- [11] Vrieze-Voorn, S.T. de
THERMISCHE BEREKENINGEN KORTE SLAG MOTOR RECTICLE STAGE ATLAS.
Philips CFT, division Development Support, Eindhoven (NL), 1997.
Internal Report CTB 598-97-6051.

Appendix A Actuator configuration

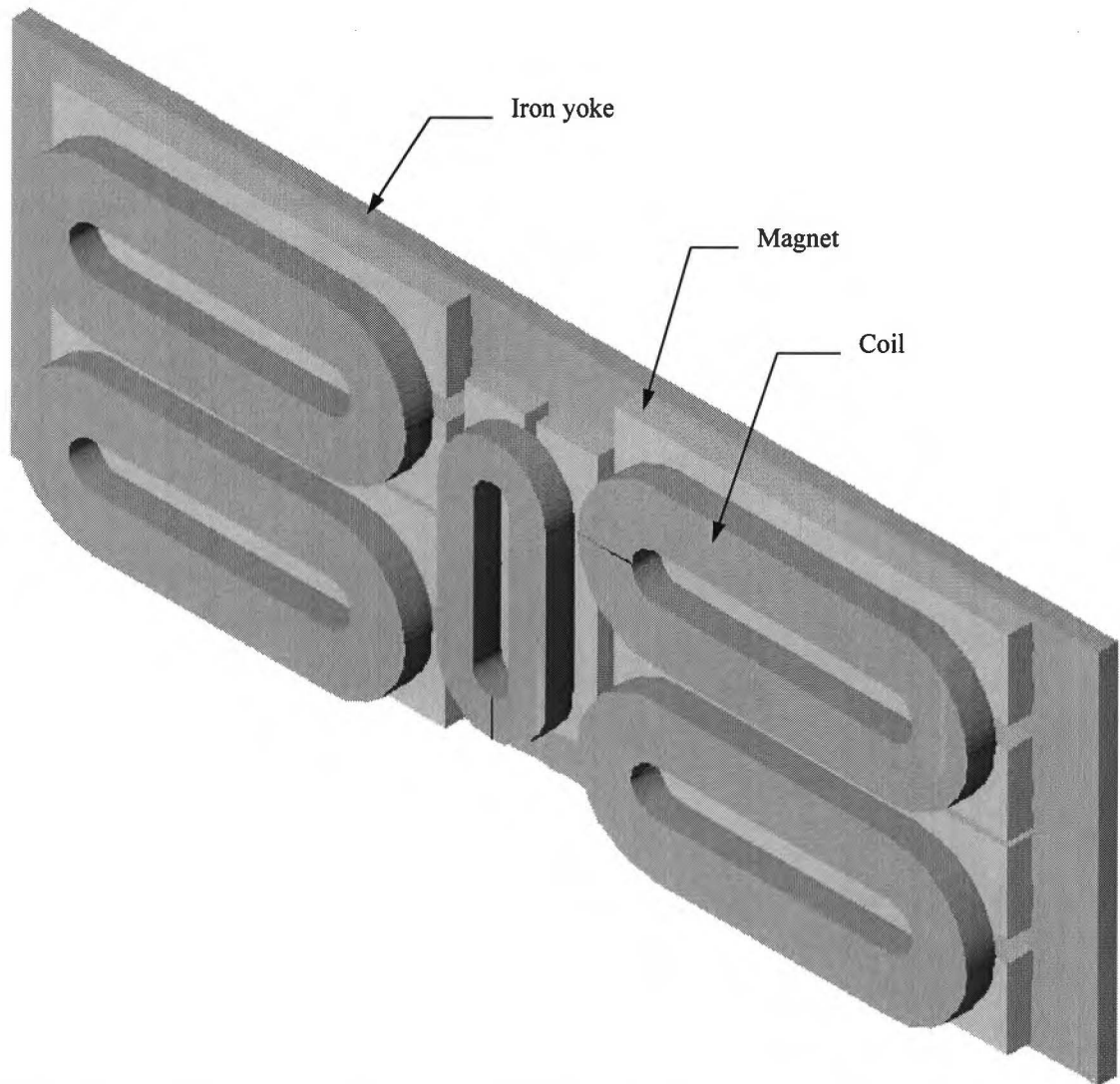


Figure A.1 Three dimensional view of the actuator, without an iron yoke.

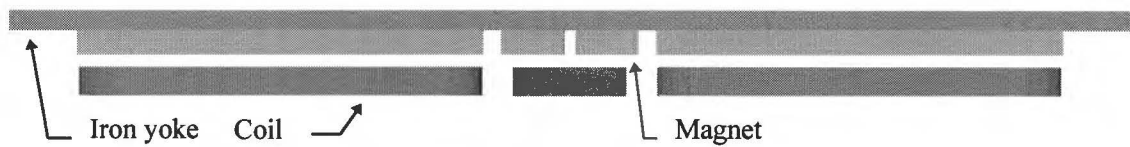


Figure A.2 Long side view of the actuator, without an iron yoke.

Appendix B Calculation figure of merit

The force which is generated by one coil can be calculated if the configuration of the coil and the magnetic field is known. Figure B.1 shows the applied configuration and the magnetic field. There are a few assumptions that have to be made. These assumptions are

that the magnetic field has a constant value to the left and right of the symmetry line, but they have different signs and the current density is uniform distributed over the coil volume. The coil has a height which is equal to h_c . The force generated in the coil is equal to:

$$\vec{F} = \int_V (\vec{J} \times \vec{B}) dV$$

In area I are J and B perpendicular, this means that the direction of the force is in the X-direction and is equal to:

$$F = JBV = JBl_o b_c h_c$$

In area II both the current density and the magnetic field have different directions, so the force doesn't change from direction. The contribution of area I and II is:

$$F_{I,II} = 2JBl_o b_c h_c$$

In the area's III and IV the calculation of the force has to be done in a different way. Both the current density and the magnetic field are vectors. The current density has an X- and Y-component and the magnetic field has only a Z-component. The vectors can be written as:

$$\vec{J} = (J_x, J_y, J_z) = (J_x, J_y, 0)$$

$$\vec{B} = (B_x, B_y, B_z) = (0, 0, B_z)$$

Figure B.2 displays the current density vector. With the use of the angle ϕ this vector can be written as:

$$\vec{J} = (J_x, J_y, J_z) = (-J \cdot \sin\phi, J \cdot \cos\phi, 0)$$

And the magnetic field vector is equal to:

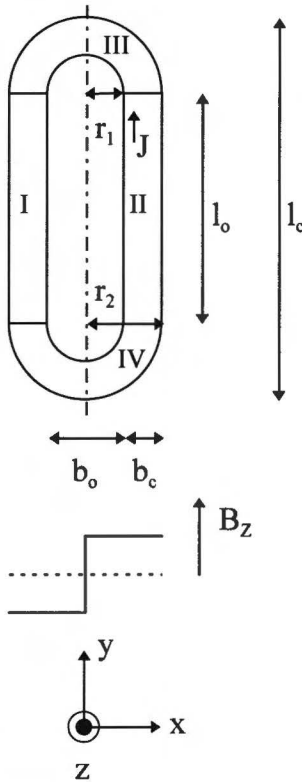


Figure B.1 Coil configuration

$$\vec{B} = (B_x, B_y, B_z) = (0, 0, \pm B)$$

With these descriptions the cross product of the vectors J and B can be calculated and is equal to:

$$\vec{J} \times \vec{B} = \begin{vmatrix} u_x & u_y & u_z \\ J_x & J_y & 0 \\ 0 & 0 & B_z \end{vmatrix} = (J_y B_z, J_x B_z, 0) = (\pm J \cdot B \cdot \cos\phi, \mp J \cdot B \cdot \sin\phi, 0)$$

The force in region III can be calculated by integrating the cross product over the volume of region III. The integral has to be split in two parts: one part varying ϕ from 0 to $\pi/2$ where B_z is $+B$ and the second part varying ϕ from $\pi/2$ to π where B_z is $-B$, the result is:

$$\vec{F} = h_c JB \int_{r_1}^{r_2} r dr \left[\int_0^{\pi/2} (\cos\phi, -\sin\phi, 0) d\phi + \int_{\pi/2}^{\pi} (-\cos\phi, \sin\phi, 0) d\phi \right]$$

$$\vec{F} = h_c JB (r_2^2 - r_1^2) (1, 0, 0)$$

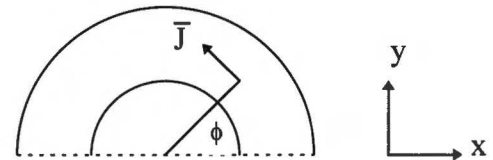


Figure B.2 Current density vector

The total force of areas III and IV works in the X-direction and equals:

$$F_{III,IV} = 2h_c JB(r_2^2 - r_1^2)$$

The total force generated by the coil is the sum of the forces generated by the areas I to IV and is equal to:

$$F = 2JBl_o b_c h_c + 2JBh_c (r_2^2 - r_1^2)$$

Substituting $l_o = l_c - 2b_c - b_o$, $r_1 = 0.5b_o$ and $r_2 = 0.5b_o + b_c$ leads to the total force generated in x-direction:

$$F = 2h_c b_c JB(l_c - b_c)$$

If the current density in the copper winding is substituted then the total force is equal to:

$$F = 2h_c b_c J_{Cu} f_{Cu} B(l_c - b_c) \quad (B.1)$$

There is a difference when the field doesn't have equal value's left and right from the symmetry line. The expression for the total force is then:

$$F = h_c b_c J_{Cu} f_{Cu} (B_l + B_r)(l_c - b_c) \quad (B.2)$$

The coil also dissipates, this dissipation is equal to the current squared times the resistance and can be written as:

$$P = \rho_{Cu} V_{Cu} J_{Cu}^2$$

The copper volume can be calculated using the geometry of the coil which can be seen in figure B.1, the expression for the dissipated power is:

$$P = f_{Cu} \rho_{Cu} h_c \left[2(l_c - 2b_c - b_o)b_c + \pi b_c b_o + \pi b_c^2 \right] J_{Cu}^2$$

The definition of the figure of merit is the force squared divided by the dissipated power. With the dissipated power and the generated force known, the figure of merit can be calculated and is equal to:

$$S = \frac{4(h_c b_c B)^2 (l_c - b_c)^2 f_{Cu}}{\rho_{Cu} h_c \left[2(l_c - 2b_c - b_o)b_c + \pi b_c b_o + \pi b_c^2 \right]} \quad (B.3)$$

If the fields aren't equal left and right from the symmetry line then the figure of merit can be written as:

$$S = \frac{(h_c b_c (B_l + B_r))^2 (l_c - b_c)^2 f_{Cu}}{\rho_{Cu} h_c \left[2(l_c - 2b_c - b_o)b_c + \pi b_c b_o + \pi b_c^2 \right]} \quad (B.4)$$

The term $h_c b_c (B_l + B_r)$ is equal to the surface integral $\iint B_z \cdot dA$ over the two cross sections of the coil, because this is the area where the force is generated. Substituting this into equation B.4 leads to:

$$S = \frac{\left(\iint B_z \cdot dA \right)^2 (l_c - b_c)^2 f_{Cu}}{\rho_{Cu} h_c \left[2(l_c - 2b_c - b_o)b_c + \pi b_c b_o + \pi b_c^2 \right]} \quad (B.5)$$

All the used variables have metric units.

Appendix C Opera2D simulation data

The data obtained by the 2D finite element simulations is displayed in table C.1 to table C.4. The figure of merit in these tables is calculated with formula B.5, which can be found in appendix B.

Table C.1 Simulation data of magnet height vs. Iron.

$h_c = 5 \text{ mm}$		$h = 44 \text{ mm}$		
$h_m \text{ [mm]}$	$h_y \text{ [mm]}$	$\iint B_z \text{ [Tmm}^2\text{]}$	$B_{y,\max} \text{ [T]}$	$S \text{ [Ns/m]}$
5	12	76.10	1.27	139.41
6	11	82.19	1.40	162.64
7	10	86.83	1.59	181.51
8	9	89.88	1.84	194.47
9	8	91.05	2.04	199.57
10	7	90.32	2.21	196.38
11	6	88.59	2.35	188.93
12	5	86.41	2.47	179.77
$h_c = 6 \text{ mm}$		$h = 45 \text{ mm}$		
$h_m \text{ [mm]}$	$h_y \text{ [mm]}$	$\iint B_z \text{ [Tmm}^2\text{]}$	$B_{y,\max} \text{ [T]}$	$S \text{ [Ns/m]}$
5	12	85.70	1.25	147.35
6	11	92.87	1.37	173.01
7	10	98.42	1.55	194.34
8	9	102.25	1.80	209.74
9	8	103.95	2.02	216.80
10	7	103.39	2.19	214.46
11	6	101.48	2.33	206.58
12	5	99.00	2.46	196.61
$h_c = 7 \text{ mm}$		$h = 44 \text{ mm}$		
$h_m \text{ [mm]}$	$h_y \text{ [mm]}$	$\iint B_z \text{ [Tmm}^2\text{]}$	$B_{y,\max} \text{ [T]}$	$S \text{ [Ns/m]}$
5	11	94.09	1.32	152.24
6	10	102.21	1.41	179.65
7	9	108.31	1.66	201.72
8	8	112.02	1.92	215.79
9	7	112.55	2.12	217.83
10	6	110.90	2.28	211.47
11	5	108.26	2.42	201.54
12	4	105.12	2.54	190.03

Table C.1 Continuation simulation data of magnet height vs. Iron.

$h_c = 8 \text{ mm}$		$h = 45 \text{ mm}$		
h_m [mm]	h_y [mm]	$\iint B_z$ [Tmm ²]	$B_{y,max}$ [T]	S [Ns/m]
5	11	101.48	1.25	154.94
6	10	110.52	1.39	183.79
7	9	117.47	1.62	207.62
8	8	121.89	1.88	223.54
9	7	122.91	2.10	227.31
10	6	121.26	2.27	221.26
11	5	118.41	2.41	210.98
12	4	114.96	2.53	198.84
$h_c = 9 \text{ mm}$		$h = 44 \text{ mm}$		
h_m [mm]	h_y [mm]	$\iint B_z$ [Tmm ²]	$B_{y,max}$ [T]	S [Ns/m]
4	11	95.57	1.18	122.16
5	10	107.97	1.28	155.91
6	9	117.78	1.47	185.35
7	8	124.86	1.76	208.52
8	7	128.25	2.02	219.97
9	6	127.58	2.21	217.67
10	5	124.77	2.36	208.21
11	4	121.07	2.50	196.04

Table C.2 Magnet width vs. coil width.

b_c [mm]	$\iint B_z$ [Tmm ²]	$B_{y,max}$ [T]	S [Ns/m]	F_x [N/mm]
14	122.91	2.15	227.31	0.123
16	138.07	2.13	242.67	0.138
18	151.61	2.12	251.27	0.152
20	165.52	2.12	260.17	0.166
22	175.34	2.12	255.99	0.175
24	183.31	2.11	247.11	0.183
26	189.65	2.11	235.02	0.190

Table C.3 Coil core width.

b_o [mm]	$\iint B_z$ [Tmm ²]	$B_{y,max}$ [T]	S [Ns/m]	F_x [N/mm]
8	118.15	2.26	216.53	0.118
10	121.18	2.21	225.46	0.121
12	123.11	2.18	230.36	0.123
14	124.33	2.21	232.58	0.124
16	125.10	2.14	229.17	0.125
18	125.55	2.13	224.78	0.126
20	125.78	2.12	219.84	0.126
22	125.86	2.12	214.66	0.126
24	125.84	2.11	209.41	0.126

Table C.4 Coil width.

$b_o = b_c$ [mm]	$\iint B_z$ [Tmm ²]	$B_{y,max}$ [T]	S [Ns/m]	F_x [N/mm]
11	92.82	2.08	175.91	0.093
12	103.69	2.13	197.02	0.104
13	114.21	2.17	215.98	0.114
14	124.33	2.21	232.58	0.124
15	134.01	2.24	246.75	0.134
16	143.23	2.27	258.53	0.143
17	151.97	2.30	267.93	0.152

Appendix D Analytical model

Table D.1 Comparison analytical data and simulation data.

hc=5								
h_m	h_y	$\iint B_Z \text{ sim}$	$\iint B_Z \text{ cal}$	KF	KF_{cal}	S_{sim}	S_{cal}	Err [%]
5	12	76.10	81.14	0.939	0.894	139.41	126.78	9.06
6	11	82.19	88.62	0.927	0.894	162.64	151.25	7.00
7	10	86.83	94.87	0.915	0.894	181.51	173.33	4.51
8	9	89.88	100.17	0.897	0.894	194.47	193.24	0.63
9	8	91.05	104.72	0.869	0.894	199.57	211.19	5.82
10	7	90.32	102.31	0.883	0.894	196.38	201.57	2.64
11	6	88.59	97.55	0.908	0.894	188.93	183.23	3.01
12	5	86.41	91.43	0.945	0.894	179.77	160.98	10.45
hc=6								
h_m	h_y	$\iint B_Z \text{ sim}$	$\iint B_Z \text{ cal}$	KF	KF_{cal}	S_{sim}	S_{cal}	Err [%]
5	12	85.70	92.41	0.927	0.885	147.35	134.10	8.99
6	11	92.87	101.32	0.917	0.885	173.01	161.22	6.81
7	10	98.42	108.82	0.905	0.885	194.34	185.97	4.31
8	9	102.25	115.21	0.888	0.885	209.74	208.46	0.61
9	8	103.95	120.73	0.861	0.885	216.80	228.90	5.58
10	7	103.39	119.74	0.864	0.885	214.46	225.17	4.99
11	6	101.48	114.35	0.887	0.885	206.58	205.37	0.59
12	5	99.00	107.36	0.922	0.885	196.61	181.08	7.93
hc=7								
h_m	h_y	$\iint B_Z \text{ sim}$	$\iint B_Z \text{ cal}$	KF	KF_{cal}	S_{sim}	S_{cal}	Err [%]
5	11	94.09	102.62	0.917	0.877	152.24	129.10	8.57
6	10	102.21	112.91	0.905	0.877	179.65	168.52	6.19
7	9	108.31	121.62	0.891	0.877	201.72	195.53	3.07
8	8	112.02	129.09	0.868	0.877	215.79	228.28	3.08
9	7	112.55	133.04	0.846	0.877	217.83	233.98	7.41
10	6	110.90	127.25	0.872	0.877	211.47	214.03	1.27
11	5	108.26	119.59	0.905	0.877	201.54	189.07	6.19
12	4	105.12	109.41	0.961	0.877	190.03	158.23	16.74
hc=8								
h_m	h_y	$\iint B_Z \text{ sim}$	$\iint B_Z \text{ cal}$	KF	KF_{cal}	S_{sim}	S_{cal}	Err [%]
5	11	101.48	111.93	0.907	0.870	154.94	142.67	7.92
6	10	110.52	123.54	0.895	0.870	183.79	173.82	5.42
7	9	117.47	133.43	0.880	0.870	207.62	202.76	2.34
8	8	121.89	141.95	0.859	0.870	223.54	229.49	2.66
9	7	122.91	148.46	0.828	0.870	227.31	251.06	10.42
10	6	121.26	142.21	0.853	0.870	221.26	230.33	4.10
11	5	118.41	133.88	0.885	0.870	210.98	204.12	3.25
12	4	114.96	122.68	0.937	0.870	198.84	171.40	13.80

Table D.1 Continuation comparison analytical data and simulation data.

hc=9								
h_m	h_y	$\iint B_Z \text{ sim}$	$\iint B_Z \text{ cal}$	KF	KF_{cal}	S_{sim}	S_{cal}	Err [%]
4	11	95.57	105.22	0.908	0.864	122.16	110.58	9.48
5	10	107.97	120.45	0.897	0.864	155.91	144.81	7.12
6	9	117.78	133.35	0.883	0.864	185.35	177.61	4.27
7	8	124.86	144.38	0.865	0.864	208.52	208.21	0.15
8	7	128.25	153.93	0.833	0.864	219.97	236.66	7.59
9	6	127.58	152.24	0.838	0.864	217.67	231.49	6.35
10	5	124.77	143.51	0.869	0.864	208.21	205.71	1.20
11	4	121.07	131.62	0.920	0.864	196.04	173.04	11.73

h_c , h_m and h_y have the dimension [mm];

$\iint B_Z \text{ sim} dA$ and $\iint B_Z \text{ cal} dA$ have the dimension [Tmm²];

S_{sim} and S_{cal} have the dimension [Ns/m].

Appendix E Example application of analytical model

Geometry in mm

$$b_m := 26 \quad h_c := 9 \quad b_c := 18 \quad h_g := 4 \quad l_c := 130 \quad b_o := 15 \quad h_y := 6 \quad h_m := 8$$

Constants

$$f_{cu} := 0.70 \quad \rho_{cu} := 1.75 \cdot 10^{-5} \quad H_{cb} := 900000 \quad \mu_0 := 4 \cdot \pi \cdot 10^{-7} \quad \mu_r := 1.1495$$

Effective iron path

$$l_y := \frac{b_o}{2}$$

Magnetic resistance

$$R_g := \frac{2 \cdot h_g + h_c}{b_m \cdot \mu_0} \quad R_b := \frac{\left(\frac{\pi}{2} + 1\right)^2 \cdot 2}{\pi \cdot \mu_0} \quad R_m := \frac{R_g \cdot R_b}{R_g + R_b}$$

Flux calculation

$$\Phi := 3$$

Given

$$\left[\left(\frac{-\Phi}{b_m \cdot \mu_0 \cdot \mu_r} + H_{cb} \right) \cdot 2 \cdot h_m - \begin{cases} 0 & \text{if } \Phi < 2.13 \cdot h_y \\ \frac{(\Phi - 2.13 \cdot h_y) \cdot l_y}{1.19398510^{-6} \cdot h_y} & \text{otherwise} \end{cases} \right] = R_m \cdot \Phi$$

$$ff := \text{Find}(\Phi)$$

Magnetic field in airgap

$$A := \frac{R_b}{R_b + R_m} \quad B_g := A \cdot \frac{ff}{b_m}$$

Integral Bz

$$B_z := 2 \cdot B_g \cdot b_c \cdot h_c \quad B_z = 158.655$$

Integral Bz after correction

$$KF = 1 - 0.3 \cdot \left[\frac{b_c \cdot h_c}{b_m \cdot (2 \cdot h_g + h_c)} \right] \quad BZ := KF \cdot B_z \quad BZ = 141.107$$

Figure of merit

$$S := \frac{[(BZ)^2] \cdot (l_c - b_c)^2 \cdot f_{cu} \cdot 10^{-6}}{\rho_{cu} \cdot h_c \cdot [2 \cdot (l_c - 2 \cdot b_c - b_o) \cdot b_c + \pi \cdot b_c \cdot b_o + \pi \cdot b_c^2]} \quad S = 235.677$$

Field in iron and force per mm

$$B_y := \frac{ff}{h_y} \quad F := \frac{BZ}{1000}$$

$$B_y = 2.407 \quad F = 0.1411$$

Appendix F Opera 3D simulation data

Table F.1 Opera 3D simulation data for total Y actuator.

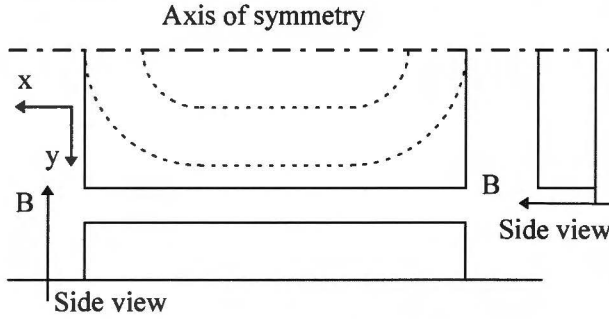
dz = 0.0 mm		j = 1 A/mm ²			
dx [mm]	dy [mm]	Fy [N]	Fz _{ED} [N]	Ky [N/A]	ΔK [%]
0.0	0.0	66.3545	0	0.4096	
0.0	0.5	33.3378	0	0.4095	-0.0252
0.0	1.0	66.2312	0	0.4088	-0.1858
0.5	0.0	66.3545	0	0.4096	0
0.5	0.5	66.3378	0	0.4095	-0.0252
0.5	1.0	66.2312	0	0.4088	-0.1858
1.0	0.0	66.3424	0	0.4095	-0.0182
1.0	0.5	66.3257	0	0.4094	-0.0434
1.0	1.0	66.2191	0	0.4088	-0.2641
dz = 0.5 mm		j = 1 A/mm ²			
dx [mm]	dy [mm]	Fy [N]	Fz _{ED} [N]	Ky [N/A]	ΔK [%]
0.0	0.0	66.4234	0	0.4100	0.1038
0.0	0.5	66.4067	0.0644	0.4099	0.0787
0.0	1.0	66.2997	0.1884	0.4093	-0.0826
0.5	0.0	66.4234	0	0.4100	0.1038
0.5	0.5	66.4067	0.0639	0.4099	0.0787
0.5	1.0	66.2997	0.1874	0.4093	-0.0826
1.0	0.0	66.4113	0	0.4099	0.0856
1.0	0.5	66.3946	0.0639	0.4098	0.0604
1.0	1.0	66.2876	0.1874	0.4092	-0.1008
dz = 1.0 mm		j = 1 A/mm ²			
dx [mm]	dy [mm]	Fy [N]	Fz _{ED} [N]	Ky [N/A]	ΔK [%]
0.0	0.0	66.7488	0	0.4120	0.5942
0.0	0.5	66.7320	0.1288	0.4119	0.5698
0.0	1.0	66.6233	0.3783	0.4113	0.4051
0.5	0.0	66.7488	0	0.4120	0.5942
0.5	0.5	66.7320	0.1279	0.4119	0.5698
0.5	1.0	66.6233	0.3762	0.4113	0.4051
1.0	0.0	66.7366	0	0.4120	0.5758
1.0	0.5	66.7197	0.1279	0.4119	0.5504
1.0	1.0	66.6111	0.3764	0.4112	0.3867
j = 1 A/mm ²					
dx [mm]	dy [mm]	dz [mm]	F _{REL} [· 10 ⁻³ N]		
0.5	0.5	0.0	0.0		
0.5	0.5	0.5	9.0437		
0.5	0.5	1.0	18.1440		

Table F.2 Opera 3D simulation data for X actuator.

dz = 0.0 mm		j = 1 A/mm ²			
dx [mm]	dy [mm]	F _x [N]	F _{Z_{ED}} [N]	K _x [N/A]	ΔK [%]
0.0	0.0	6.4030	0	0.0593	0
0.0	0.5	6.4020	0	0.0593	-0.0156
0.0	1.0	6.3993	0	0.0593	-0.0578
0.5	0.0	6.4004	0	0.0593	-0.0406
0.5	0.5	6.3994	0	0.0593	-0.0562
0.5	1.0	6.3968	0	0.0592	-0.0968
1.0	0.0	6.3929	0	0.0592	-0.1577
1.0	0.5	6.3919	0	0.0592	-0.1734
1.0	1.0	6.3893	0	0.0592	-0.2140
dz = 0.5 mm		j = 1 A/mm ²			
dx [mm]	dy [mm]	F _x [N]	F _{Z_{ED}} [N]	K _x [N/A]	ΔK [%]
0.0	0.0	6.4156	0	0.0594	0.1968
0.0	0.5	6.4146	0	0.0594	0.1812
0.0	1.0	6.4120	0	0.0594	0.1406
0.5	0.0	6.4131	0.0068	0.0594	0.1577
0.5	0.5	6.4121	0.0067	0.0594	0.1421
0.5	1.0	6.4095	0.0067	0.0593	0.1015
1.0	0.0	6.4055	0.0132	0.0593	0.0390
1.0	0.5	6.4045	0.0131	0.0593	0.0234
1.0	1.0	6.4015	0.0130	0.0593	-0.0172
dz = 1.0 mm		j = 1 A/mm ²			
dx [mm]	dy [mm]	F _x [N]	F _{Z_{ED}} [N]	K _x [N/A]	ΔK [%]
0.0	0.0	6.4753	0	0.0600	1.1292
0.0	0.5	6.4743	0	0.0599	1.1135
0.0	1.0	6.4717	0	0.0599	1.0729
0.5	0.0	6.4728	0.0135	0.0599	1.0901
0.5	0.5	6.4717	0.0135	0.0599	1.0729
0.5	1.0	6.4691	0.0134	0.0599	1.0323
1.0	0.0	6.4651	0.0264	0.0599	0.9699
1.0	0.5	6.4641	0.0263	0.0599	0.9542
1.0	1.0	6.4615	0.0261	0.0598	0.9136
j = 1 A/mm ²					
dx [mm]	dy [mm]	dz [mm]	F _{REL} [· 10 ⁻⁴ N]		
0.5	0.5	0.0	0.0		
0.5	0.5	0.5	4.2188		
0.5	0.5	1.0	8.4826		

Appendix G Effect of the magnet length

For the analytical calculations of the effect of the length of the magnet, an assumption for the magnetic field is taken into account and is displayed in figure G.1.



A current in the X-direction leads to a force in the Y-direction. The force in scan direction (Y-direction) is the most important one. This means that the next step is to calculate how much of the current in X-direction is present in the magnetic field. This can be done by calculation of the surface integral of the current in X-direction over an area which is equal to the shape of the coil. This has to be done for the straight parts and the round parts. The force

Figure G.1 Assumption magnetic field.

generated by the straight parts of the coil are equal to the magnetic flux density times the current times the length of the straight parts:

$$F_{ST} = 2 \cdot J \cdot B \cdot h_c \cdot l_o \tag{G.1}$$

The meaning of h_c and l_o can be found in figure B.1. Because of the symmetry of the coil, the force generated by the round parts of the coil can be calculated by multiplying the force generated by one quarter times four.

The left part of figure G.2 displays the value of the current density in the X-direction as a function of the place in one quarter. The generated force in one quarter is equal to the surface S of figure G.2 times the magnetic flux density. The line at x is A is the border of the magnet and is varied between zero and $x = R_2$.

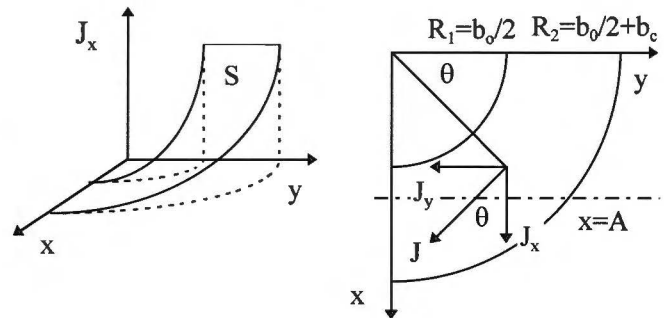


Figure G.2 Definition of the layout.

The current density in X-direction can be written as a function of the place (X,Y) and is:

$$J_x(x, y) = J \cdot \frac{y}{\sqrt{x^2 + y^2}}$$

Integrating the above equation over the area of one quarter leads to an equation for the integral of the current density if A is larger than R_1 and smaller than R_2 . This equation can be written as:

$$I = J \cdot \left\{ \int_0^A \int_0^{\sqrt{R_2^2 - x^2}} \frac{y}{\sqrt{x^2 + y^2}} dx dy - \int_0^{R_1} \int_0^{R_1} \frac{y}{\sqrt{x^2 + y^2}} dx dy \right\} \text{ if } R_1 \leq A \leq R_2$$

And if A is smaller than R₁, the following equation is valid:

$$I = J \cdot \left\{ \int_0^A \int_0^{\sqrt{R_2^2 - x^2}} \frac{y}{\sqrt{x^2 + y^2}} dx dy - \int_0^{R_1} \int_0^{\sqrt{R_1^2 - x^2}} \frac{y}{\sqrt{x^2 + y^2}} dx dy \right\} \text{ if } A < R_1$$

Solving these equations and multiplying them by the coil height and the magnetic field leads to the generated force due to one quarter. It results in:

$$F = \begin{cases} h_c \cdot J \cdot B \cdot \left(R_2 \cdot A - \frac{1}{2} \cdot (A^2 + R_1^2) \right) & \text{if } R_1 \leq A \leq R_2 \\ h_c \cdot J \cdot B \cdot (R_2 - R_1) \cdot A & \text{if } A < R_1 \end{cases} \tag{G.2}$$

Multiplying equation G.2 with four leads to the generated force for the round parts of the coil. When equation G.1 is multiplied by two and then added to four times equation G.2 then the total force generated by one Y-coil is obtained:

$$F_y = \begin{cases} 2 \cdot h_c \cdot J \cdot B \cdot \left(2 \cdot \left(R_2 \cdot A - \frac{1}{2} \cdot (A^2 + R_1^2) \right) + l_o \cdot b_c \right) & \text{if } A \geq R_1 \\ 2 \cdot h_c \cdot J \cdot B \cdot \left(2 \cdot (R_2 - R_1) \cdot A + l_o \cdot b_c \right) & \text{if } A < R_1 \end{cases} \tag{G.3}$$

To find the total force in Y-direction, equation G.3 has to be multiplied by four. The whole Y-actuator has been simulated with Opera3D for 2 cases, that is total overlap of the magnets and 90 % overlap of the magnets. The results of these cases are displayed in table G.1. The displacements dx and dy are in mm.

Table G.1 Opera 3D simulation data for Y actuator.

dz = 0.0 mm									
		Total overlap of magnets				90 % overlap of magnets			
dx	dy	F _y [N]	F _z [N]	K _y [N/A]	ΔK [%]	F _y [N]	F _z [N]	K _y [N/A]	ΔK [%]
0.0	0.0	46.00	0.0	0.2839	0.0	45.81	0.0	0.2828	0.0
0.0	1.0	45.85	0.0	0.2831	-0.2866	45.68	0.0	0.2820	-0.2799
1.0	0.0	45.98	0.0	0.2838	-0.0287	45.78	0.0	0.2826	-0.0489
1.0	1.0	45.84	0.0	0.2830	-0.3151	45.66	0.0	0.2818	-0.3283
dz = 0.5 mm									
		Total overlap of magnets				90 % overlap of magnets			
dx	dy	F _y [N]	F _z [N]	K _y [N/A]	ΔK [%]	F _y [N]	F _z [N]	K _y [N/A]	ΔK [%]
0.0	0.0	46.04	0.0070	0.2842	0.1102	45.86	0.0066	0.2831	0.1148
0.0	1.0	45.91	0.1799	0.2834	-0.1772	45.73	0.1868	0.2823	-0.1659
1.0	0.0	46.03	0.0070	0.2841	0.0851	45.84	0.0066	0.2829	0.0659
1.0	1.0	45.89	0.1799	0.2833	-0.2057	45.71	0.1861	0.2821	-0.2146
dz = 1.0 mm									
		Total overlap of magnets				90 % overlap of magnets			
dx	dy	F _y [N]	F _z [N]	K _y [N/A]	ΔK [%]	F _y [N]	F _z [N]	K _y [N/A]	ΔK [%]
0.0	0.0	46.19	0.0139	0.2851	0.4410	46.02	0.0132	0.2840	0.4593
0.0	1.0	46.06	0.3610	0.2843	0.1509	45.89	0.3750	0.2832	0.1760
1.0	0.0	46.18	0.0139	0.2850	0.4123	45.99	0.0132	0.2839	0.4100
1.0	1.0	46.04	0.3606	0.2842	0.1222	45.86	0.3736	0.2831	0.1268

Appendix H Opera 3D simulation data, new design for FUMO

Table H.1 Opera 3D simulation data for new Y actuator design.

dz = 0.0 mm		j = 1 A/mm ²			
dx [mm]	dy [mm]	Fy [N]	Fz _{ED} [N]	Ky [N/A]	ΔK [%]
0.0	0.0	45.8055	0	0.2828	0
0.5	0.0	45.7992	0	0.2827	-0.0138
1.0	0.0	45.7831	0	0.2826	-0.0489
0.0	0.5	45.7871	0	0.2826	-0.0402
0.5	0.5	45.7808	0	0.2826	-0.0539
1.0	0.5	45.7648	0	0.2825	-0.0889
0.0	1.0	45.6773	0	0.2820	-0.2799
0.5	1.0	45.6710	0	0.2819	-0.2936
1.0	1.0	45.6551	0	0.2818	-0.3283
dz = 0.5 mm		j = 1 A/mm ²			
dx [mm]	dy [mm]	Fy [N]	Fz _{ED} [N]	Ky [N/A]	ΔK [%]
0.0	0.0	45.8581	0.0066	0.2831	0.1148
0.5	0.0	45.8517	0.0066	0.2830	0.1009
1.0	0.0	45.8357	0.0066	0.2829	0.0659
0.0	0.5	45.8397	0.0445	0.2830	0.0747
0.5	0.5	45.8334	0.0444	0.2829	0.0609
1.0	0.5	45.8173	0.0441	0.2828	0.0258
0.0	1.0	45.7295	0.1868	0.2823	-0.1659
0.5	1.0	45.7232	0.1867	0.2822	-0.1797
1.0	1.0	45.7072	0.1861	0.2821	-0.2146
dz = 1.0 mm		j = 1 A/mm ²			
dx [mm]	dy [mm]	Fy [N]	Fz _{ED} [N]	Ky [N/A]	ΔK [%]
0.0	0.0	46.0159	0.0132	0.2840	0.4593
0.5	0.0	46.0096	0.0132	0.2840	0.4456
1.0	0.0	45.9933	0.0132	0.2839	0.4100
0.0	0.5	45.9975	0.0891	0.2839	0.4192
0.5	0.5	45.9912	0.0890	0.2839	0.4054
1.0	0.5	45.9749	0.0883	0.2838	0.3698
0.0	1.0	45.8861	0.3750	0.2832	0.1760
0.5	1.0	45.8798	0.3747	0.2832	0.1622
1.0	1.0	45.8636	0.3736	0.2831	0.1268
j = 1 A/mm ²					
dx [mm]	dy [mm]	dz [mm]	F _{REL} [· 10 ⁻³ N]		
0.5	0.5	0.0	0.0		
0.5	0.5	0.5	5.498		
0.5	0.5	1.0	11.044		

Table H.2 Opera 3D simulation data for new X actuator design.

dz = 0.0 mm		j = 1 A/mm ²			
dx [mm]	dy [mm]	F _x [N]	F _{Z_{ED}} [N]	K _x [N/A]	ΔK [%]
0.0	0.0	4.6872	0	0.0670	0
0.5	0.0	4.6798	0	0.0669	-0.1579
1.0	0.0	4.6544	0	0.0665	-0.6998
0.0	0.5	4.6844	0	0.0669	-0.0597
0.5	0.5	4.6770	0	0.0668	-0.2176
1.0	0.5	4.6516	0	0.0665	-0.7595
0.0	1.0	4.6780	0	0.0668	-0.1963
0.5	1.0	4.6706	0	0.0667	-0.3542
1.0	1.0	4.6452	0	0.0664	-0.8961
dz = 0.5 mm		j = 1 A/mm ²			
dx [mm]	dy [mm]	F _x [N]	F _{Z_{ED}} [N]	K _x [N/A]	ΔK [%]
0.0	0.0	4.6988	0.0010	0.0671	0.2475
0.5	0.0	4.6914	0.0240	0.0670	0.0896
1.0	0.0	4.6660	0.0520	0.0667	0.4523
0.0	0.5	4.6960	0.0010	0.0671	0.1877
0.5	0.5	4.6886	0.0238	0.0670	0.0299
1.0	0.5	4.6632	0.0518	0.0666	-0.5120
0.0	1.0	4.6894	0.0008	0.0670	0.0469
0.5	1.0	4.6820	0.0236	0.0669	-0.1109
1.0	1.0	4.6568	0.0516	0.0665	-0.6486
dz = 1.0 mm		j = 1 A/mm ²			
dx [mm]	dy [mm]	F _x [N]	F _{Z_{ED}} [N]	K _x [N/A]	ΔK [%]
0.0	0.0	4.7334	0.0018	0.0676	0.9857
0.5	0.0	4.7260	0.0478	0.0675	0.8278
1.0	0.0	4.7010	0.1036	0.0672	0.2944
0.0	0.5	4.7304	0.0018	0.0676	0.9217
0.5	0.5	4.7232	0.0476	0.0675	0.7680
1.0	0.5	4.6982	0.1032	0.0671	0.2347
0.0	1.0	4.7238	0.0018	0.0675	0.7808
0.5	1.0	4.7164	0.0472	0.0674	0.6230
1.0	1.0	4.6916	0.1028	0.0670	0.0939
j = 1 A/mm ²					
dx [mm]	dy [mm]	dz [mm]	F _{REL} [·10 ⁻³ N]		
0.5	0.5	0.0	0.0		
0.5	0.5	0.5	0.567		
0.5	0.5	1.0	1.146		

Appendix I Amplifier specification

The output voltage of the amplifier has to be equal to the voltage across the total resistance plus the linked flux change per time unit, so the voltage is equal to:

$$U = R_l \cdot i + \frac{d\phi_c}{dt} \quad (I.1)$$

The linked flux, ϕ_c , is a function of the current, i , and the displacement, say y . Knowing this equation I.1 becomes:

$$U = R_l \cdot i + \frac{\partial\phi_c}{\partial i} \cdot \frac{di}{dt} + \frac{\partial\phi_c}{\partial y} \cdot \frac{dy}{dt} \quad (I.2)$$

The second term on the right side of the equality sign is the contribution of the inductance, the third term is the motional voltage. Equation I.2 can be written as:

$$U = R_l \cdot i + (L + M) \cdot \frac{di}{dt} + K \cdot v_d \quad (I.3)$$

Where L is the self inductance, M the mutual inductance, K the motor constant and v_d the speed difference. When there is no speed difference between the long stroke actuator and the short stroke actuator (this means the long stroke is following the short stroke without lag) the third term on the right side of equation I.3 is zero. The generated force is equal to the moving mass times the acceleration and also has to be equal to the current times the motor constant, so:

$$K \cdot i = m \cdot a \quad (I.4)$$

Solving equation I.4 for the current i and substituting this current in equation I.3 leads to:

$$U = R_l \cdot \frac{m \cdot a}{K} + (L + M) \cdot \frac{m}{K} \cdot \frac{da}{dt} + K \cdot v_d \quad (I.5)$$

The derivative of the acceleration is called the jerk and has the symbol j_k . Also known is that the motor constant K is equal to the number of turns, N , times the initial motor constant, K_0 . The total resistance, R_t , is the sum of the cable resistance, R_{cable} , and the coil resistance, R_c . The cable resistance includes the resistance of the cable and the resistance of the connectors. Now equation I.5 becomes:

$$U = (R_{cable} + R_c) \cdot \frac{m \cdot a}{N \cdot K_0} + (L + M) \cdot \frac{m}{N \cdot K_0} \cdot j_k + N \cdot K_0 \cdot v_d \quad (I.6)$$

The flux in the coil with N turns is equal to:

$$\phi = N \cdot (L_0 + M_0) \cdot i \quad (I.7)$$

Where L_0 is the self inductance of the coil if the number of turns is equal to one. The linked flux is:

$$\phi_c = N \cdot \phi = (L + M) \cdot i \quad (I.8)$$

From equation I.7 and I.8 the inductance coefficient can be derived and is equal to:

$$L + M = N^2 \cdot (L_0 + M_0) \quad (I.9)$$

The figure of merit can be written as:

$$S = \frac{F^2}{P} = \frac{F^2}{I^2 \cdot R_c} \quad (\text{I.10})$$

Known is that the force is equal to the motor constant times the current. The motor constant can be written as the number of turns times the motor constant for one turn. If this is substituted in equation I.10, the figure of merit can be written as:

$$S = \frac{N^2 \cdot K_0^2}{R_c} \quad (\text{I.11})$$

The figure of merit can also be written as:

$$S = \frac{K_0^2}{R_0} \quad (\text{I.12})$$

Because the figure of merit is a constant equations I.11 and I.12 are equal. So for the coil resistance, the following expression can be written, assuming there is no dependency between f_{cu} and the number of turns:

$$R_c = N^2 \cdot R_0 \quad (\text{I.13})$$

In equation I.13 the term R_0 is the resistance of the coil when the winding number is one. Substituting equation I.9 and I.13 in I.5 leads to [3]:

$$U = R_{cable} \cdot \frac{m \cdot a}{K_0 \cdot N} + R_0 \cdot N \cdot \frac{m \cdot a}{K_0} + (L_0 + M_0) \cdot N \cdot \frac{m \cdot j_k}{K} + K_0 \cdot N \cdot v_d \quad (\text{I.14})$$

RS single Y-coil

Coil dimensions in mm

$$hc := 9.0 \quad lc := 99 \quad bc := 18 \quad bo := 10$$

Coil area in m^2

$$A_{cu} = hc \cdot bc \cdot 10^{-6} \cdot m^2 \quad A_{cu} = 1.62 \cdot 10^{-4} \cdot m^2$$

Coil volume in m^3

$$V_{cu} := hc \cdot [2 \cdot (lc - 2 \cdot bc - bo) \cdot bc + \pi \cdot bc \cdot bo + \pi \cdot bc^2] \cdot 10^{-9} \cdot m^3 \quad V_{cu} = 3.142 \cdot 10^{-5} \cdot m^3$$

Initial motor resistance in Ω

$$\rho := 17.5 \cdot 10^{-9} \cdot \Omega \cdot m \quad f_{cu} := 0.69 \quad R_0 := \frac{\rho \cdot V_{cu}}{A_{cu}^2 \cdot f_{cu}} \quad R_0 = 3.037 \cdot 10^{-5} \cdot \Omega$$

Correction in motor resistance, expected temperature rise 60 degrees

$$R_o := R_0 \cdot (1 + 60 \cdot 0.004) \quad R_o = 3.765 \cdot 10^{-5} \cdot \Omega$$

Motor inductance in H

$L_o := 61.114610^{-9} \cdot \text{henry}$ $M_o := 19.491410^{-9} \cdot \text{henry}$

Motor constant

$K_o := 0.0706875 \frac{\text{newton}}{\text{amp}}$

Requirements (maximum values)

acceleration	jerk	disturbance	mass/y-coil	Rcable	Voltage
$a := 48 \cdot \frac{\text{m}}{\text{sec}^2}$	$jk := 6000 \cdot \frac{\text{m}}{\text{sec}^3}$	$vd := 0.1 \cdot \frac{\text{m}}{\text{sec}}$	$m_o := 5.625 \text{ kg}$	$R_k := 0.5 \cdot \Omega$	$U := 81 \cdot \text{volt}$

$$N := \frac{U \cdot K_o + \sqrt{(U \cdot K_o)^2 - 4 \cdot R_k \cdot m_o \cdot a \cdot [R_o \cdot m_o \cdot a + (L_o + M_o) \cdot m_o \cdot jk + K_o^2 \cdot vd]}}{2 \cdot [R_o \cdot m_o \cdot a + (L_o + M_o) \cdot m_o \cdot jk + K_o^2 \cdot vd]}$$

N = 402.665

Calculation of parameters

$F := m_o \cdot a$ $K := N \cdot K_o$ $I := \frac{F}{K}$ $R := N^2 \cdot R_o$ $L := N^2 \cdot L_o$

$F = 270 \cdot \text{newton}$ $K = 28.463 \cdot \frac{\text{newton}}{\text{amp}}$ $I = 9.486 \cdot \text{amp}$ $R = 6.105 \cdot \Omega$ $L = 9.909 \cdot 10^{-3} \cdot \text{henry}$

$t := \frac{L}{R}$

$t = 1.623 \cdot 10^{-3} \cdot \text{sec}$

Appendix J Eddy current

From the ELEKTRA [2] reference manual the following equation for the eddy current density vector is obtained:

$$\vec{J} = \sigma \cdot (\vec{E} + \vec{v} \times \vec{B}) \tag{J.1}$$

Where σ is de conductivity in S/m, v is a constant speed in m/s, B is the flux density in T and E is de electric field strength in V/m. In one case the flux density of the eddy currents is neglected, so the flux density \vec{B} is due to the magnets only. From Maxwell's equations it follows that [9]:

$$\nabla \times \vec{E} = -\frac{\partial \vec{B}}{\partial t} \quad \text{and} \quad \nabla \cdot \vec{J} = 0 \tag{J.2}$$

as $\nabla \cdot \vec{B} = 0$, the flux density \vec{B} can be represented using a vector potential \vec{A} where:

$$\vec{B} = \nabla \times \vec{A} \tag{J.3}$$

Using the above equation and combining it with equation J.2 leads to the following expression for the field strength:

$$\begin{aligned} \nabla \times \vec{E} &= -\frac{\partial}{\partial t} \cdot (\nabla \times \vec{A}) \\ \nabla \times \vec{E} &= \nabla \times \left(-\frac{\partial \vec{A}}{\partial t} \right) \\ \nabla \times \left(\vec{E} + \frac{\partial \vec{A}}{\partial t} \right) &= 0 \end{aligned} \tag{J.4}$$

If the rotation of a vector is equal to zero, then the vector can be written as minus the gradient of a scalar potential function. This means for equation J.4, that:

$$\vec{E} + \frac{\partial \vec{A}}{\partial t} = -\nabla \Psi$$

The field strength can be written as:

$$\vec{E} = -\nabla \Psi - \frac{\partial \vec{A}}{\partial t} \tag{J.5}$$

Due to the effect that the vector potential is time independent, expression J.5 can be written as:

$$\vec{E} = -\nabla \Psi \tag{J.6}$$

Now the following simplification is introduced: the hatched areas in figure J.1 represent the areas were a permanent magnetic field exists. The areas one and two represents the areas with no magnetic field and an infinite conductivity is supposed, this gives the current a super conducting return path. In the areas where the conductivity is infinite the electric field strength is equal to zero, because: $\vec{E}' = 0$

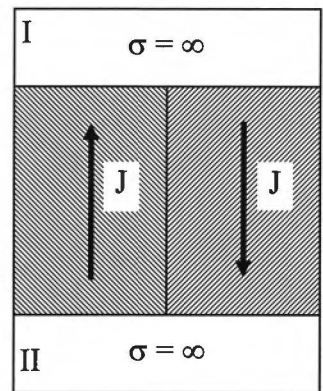


Figure J.1 Assumption.

At the boundary between the hatched areas and the areas with infinite conductivity the electric field strength must be continuous. This means that the electric field strength in the hatched areas is also equal to zero. Expression J.6 then becomes:

$$-\nabla\Psi = 0$$

The current density vector, equation J.1, can now be written as:

$$\vec{J} = \sigma \cdot \vec{v} \times \vec{B} \tag{J.7}$$

The field lines of the magnetic field are displayed in figure J.2. This picture is obtained by the Opera2D simulation results. The horizontal axes is the Y-direction and the vertical axis is the Z-direction.

The flux density vector can be written as:

$$\vec{B} = \begin{pmatrix} 0 \\ B_y \\ B_z \end{pmatrix}$$

There has been looked at two different cases: one case the coils have a velocity in the Y-direction and the other case has a velocity in the Z-direction. This means that velocity vectors can be defined, they can be written as:

$$\vec{v}_1 = \begin{pmatrix} 0 \\ v_y \\ 0 \end{pmatrix} \quad \text{and} \quad \vec{v}_2 = \begin{pmatrix} 0 \\ 0 \\ v_z \end{pmatrix}$$

Equation J.7 can be used to solve this problem for the 2D configuration. There is one assumption for the 2D configuration and that is that the third dimension is infinite large.

This means for the current density vector in case one:

$$\vec{J}_1 = \sigma \cdot \vec{v}_1 \times \vec{B}$$

$$\vec{J}_1 = \sigma \cdot v_y \cdot B_z \cdot \vec{u}_x$$

From this expression can be concluded that a velocity in Y-direction leads to a current density in the coil carrier where the flux density has a component in the Z-direction. For a velocity in Z-direction the current density vector is equal to:

$$\vec{J}_2 = \sigma \cdot \vec{v}_2 \times \vec{B} = -\sigma \cdot v_z \cdot B_y \cdot \vec{u}_x$$

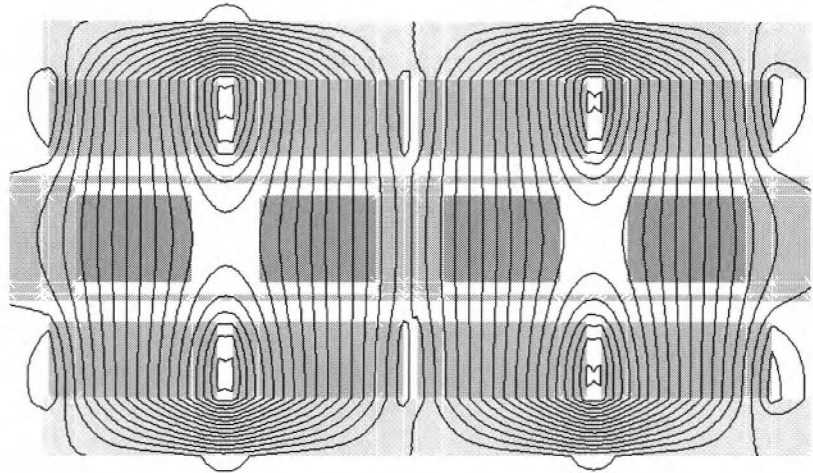


Figure J.2 Field lines of Y-actuator.

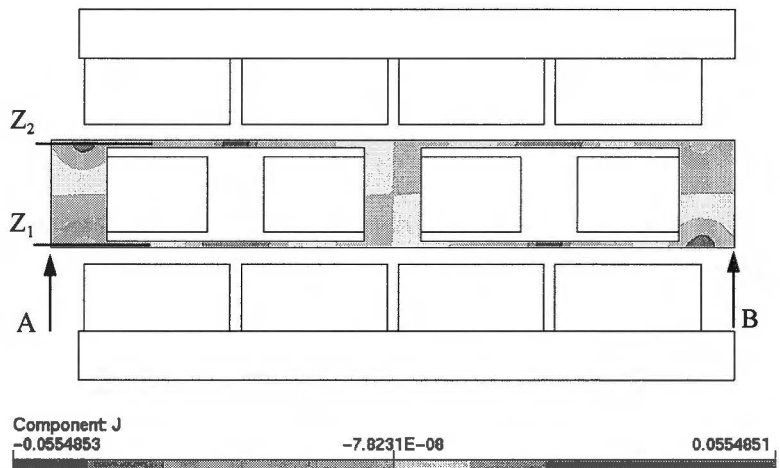


Figure J.3 Current density due to velocity in Z-direction.

A velocity in Z-direction leads to a current density in the X-direction where the flux density has a component in the Y-direction. The current density can be seen in figure J.3, the unit is A/mm². Figure J.4 displays the current density J_2 as a function of the Y-position, this has been done at 2 different Z-positions.

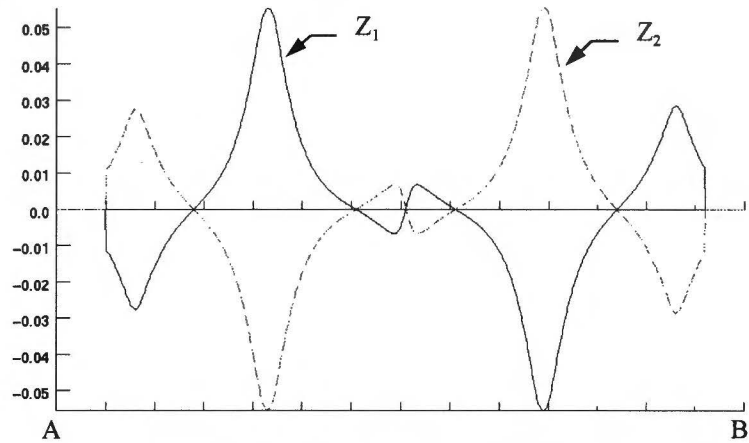


Figure J.4 Current density J_2 at different positions.

If figure J.2 is compared with figure J.4, then it can be seen that if the flux density has a Y-component a current density is present.

The sign of the current density depends on the direction of the flux density component, this can be in the positive or negative Y-direction.

As seen in appendix B, the force due to a current in a magnetic field is equal to:

$$\vec{F} = \int_V (\vec{J} \times \vec{B}) dV \tag{J.8}$$

Substituting the expression for the flux density vector and the current density vector for the two cases in equation J.8 leads to the force due to the velocity:

$$\vec{F}_1 = \int_V (\vec{J}_1 \times \vec{B}) dV = \int_V \begin{pmatrix} 0 & -\sigma \cdot v_y \cdot B_z^2 & \sigma \cdot v_y \cdot B_y \cdot B_z \end{pmatrix} \approx \int_V -\sigma \cdot v_y \cdot B_z^2 \cdot u_y \cdot dV$$

$$\vec{F}_2 = \int_V (\vec{J}_2 \times \vec{B}) dV = \int_V \begin{pmatrix} 0 & -\sigma \cdot v_y \cdot B_y \cdot B_z & \sigma \cdot v_y \cdot B_y^2 \end{pmatrix} \approx \int_V -\sigma \cdot v_z \cdot B_y^2 \cdot u_z \cdot dV$$

Conclusion from these forces is that they oppose their origin. This is completely in agreement with the law of Lenz.

Integrating over the volumes, using $1.1 \cdot 10^6$ S/m for the conductivity and using a velocity of 0.1 m/s leads to the following numerical values for the forces:

- $F_1 = 1.10$ N;
- $F_2 = 0.12$ N.

Dividing these force by the velocity leads to the damping:

- $D_1 = 11.0$ Ns/m;
- $D_2 = 1.20$ Ns/m.

Appendix K Damping due to control loop of amplifier

Due to movement of the coil carrier a voltage is induced in the coils. This voltage can be seen as a disturbance of the output voltage of the current controlled amplifier. Figure K.1 displays the block diagram of the amplifier.

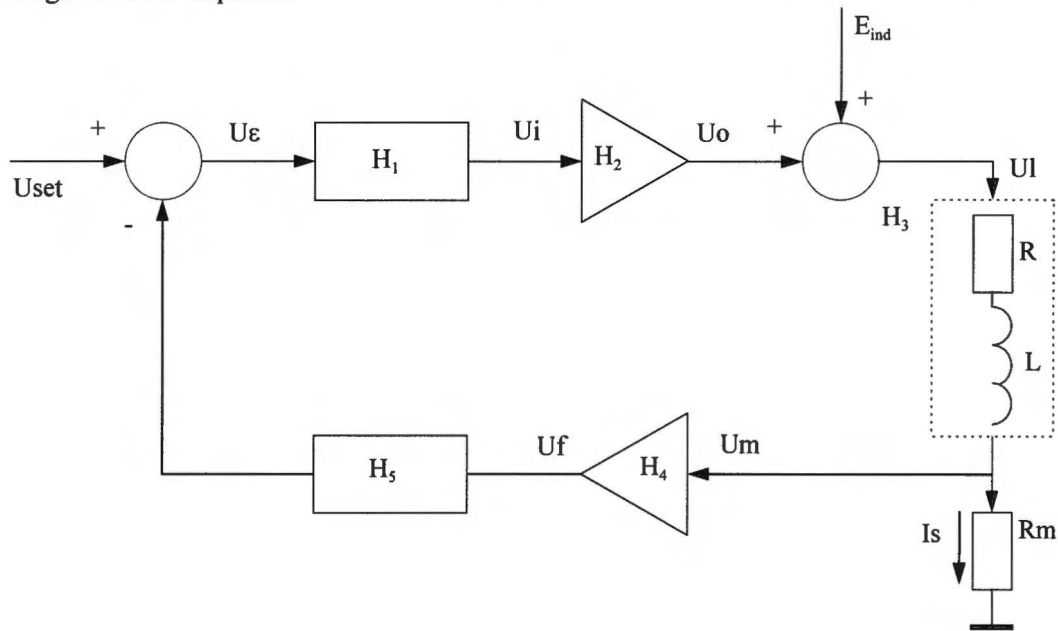


Figure K.1 Block diagram of the current controlled amplifier.

The transfer function H_1 has a gain of 35 dB, a zero at 16 Hz and a pole at 160 Hz. The bandwidth of the current control loop is equal to 10 kHz. This results in a transfer function of:

$$H_1(\omega) = \frac{56.23 \cdot \left(\frac{j\omega}{1000} + 1 \right)}{\frac{j\omega}{100} + 1}$$

The transfer functions H_2 and H_4 have only a gain and they are equal to:

$$H_2(\omega) = 100$$

$$H_4(\omega) = 10$$

There is an attenuation of -5 dB when the signal of U_f is transferred to the signal U_ϵ . This can be seen as a transfer function and is equal to:

$$H_5(\omega) = 0.56$$

The last transfer function which has to be determined is the one from signal U_1 to signal U_m and is equal to:

$$H_3(\omega) = \frac{U_m(\omega)}{U_1(\omega)} = \frac{R_m}{R_m + R + j \cdot \omega \cdot L} = \frac{\frac{R_m}{R_m + R}}{\frac{j \cdot \omega \cdot L}{R_m + R} + 1} = \frac{0.0259}{\frac{j \cdot \omega}{562.7} + 1}$$

The signal U_m is can be written as a function of the disturbance E_{ind} , and is equal to:

$$U_m(\omega) = \frac{H_3(\omega)}{1 + H_1(\omega) \cdot H_2(\omega) \cdot H_3(\omega) \cdot H_4(\omega) \cdot H_5(\omega)} \cdot E_{ind}(\omega)$$

Dividing the above expression by $E_{ind}(\omega)$ leads to the transfer function. Using the expressions of the transfer function H_1 to H_5 gives a expression for the transfer function that equals:

$$\frac{U_m(\omega)}{E_{ind}(\omega)} = \frac{0.0259 \cdot \left(\frac{j \cdot \omega}{100} + 1 \right)}{\left(\frac{j \cdot \omega}{562.7} + 1 \right) \cdot \left(\frac{j \cdot \omega}{100} + 1 \right) + 819 \cdot \left(\frac{j \cdot \omega}{1000} + 1 \right)}$$

Rewriting this expression leads to the following transfer function:

$$\frac{U_m(\omega)}{E_{ind}(\omega)} = \frac{3.16 \cdot 10^{-5} \cdot \left(\frac{j \cdot \omega}{100} + 1 \right)}{\left(\frac{j \cdot \omega}{1005} + 1 \right) \cdot \left(\frac{j \cdot \omega}{45886} + 1 \right)}$$

The voltage U_m is equal to the current I_s times the resistance R_m . This means that the transfer function from the current I_s to the voltage E_{ind} is equal to:

$$\frac{I_s(\omega)}{E_{ind}(\omega)} = \frac{3.16 \cdot 10^{-4} \cdot \left(\frac{j \cdot \omega}{100} + 1 \right)}{\left(\frac{j \cdot \omega}{1005} + 1 \right) \cdot \left(\frac{j \cdot \omega}{45886} + 1 \right)} \quad (\text{K.1})$$

Appendix L Prototype

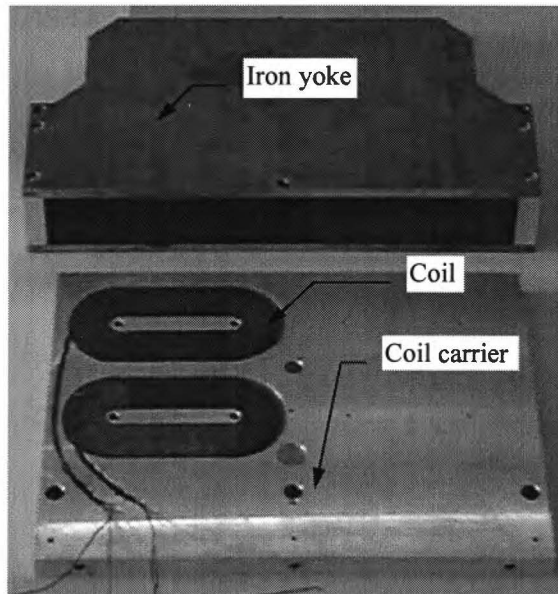


Figure L.1 Exploded view of prototype.

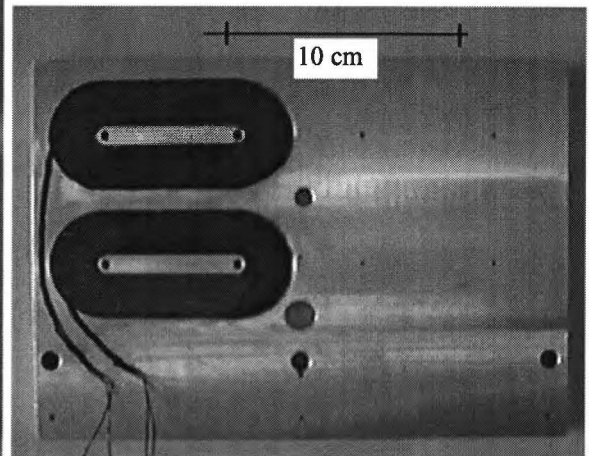


Figure L.2 Coil carrier.

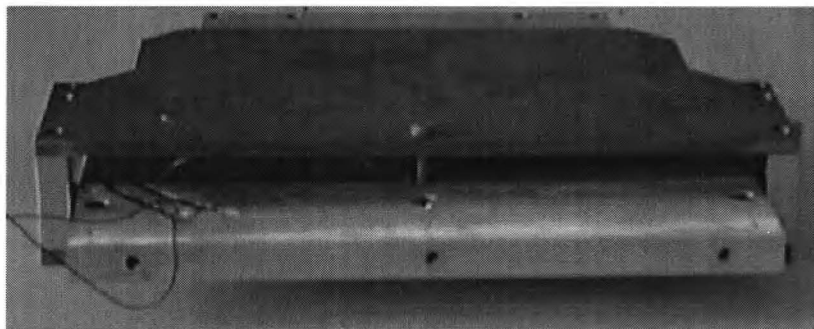


Figure L.3 Composition of coil carrier and iron yoke.

Appendix M Measured data

Table M.1 Measured data.

z [mm]	I+	F+	Fz+	I-	F-	Fz-	K+	K-	Kgem	Frel	Fed
Point A											
-1.0	1.24	55.6	0.8060	-1.24	-56.0	-0.8556	44.8387	45.1613	45.0000	-0.0161	0.6700
-0.5	1.28	56.0	0.5084	-1.22	-55.2	-0.5270	43.7500	45.2459	44.4980	-0.0139	0.4150
0.0	1.25	56.0	0.2635	-1.22	-54.8	-0.2573	44.8000	44.9180	44.8590	0.0000	0.2109
0.5	1.25	55.6	0.0620	-1.23	-55.6	-0.0558	44.4800	45.2033	44.8416	0.0017	0.0475
1.0	1.25	56.0	-0.2108	-1.22	-55.2	0.2728	44.8000	45.2459	45.0230	0.0223	-0.1965
Point B											
-1.0	1.26	56.4	0.3100	-1.26	-56.0	-0.3627	44.7619	44.4444	44.6032	-0.0166	0.2669
-0.5	1.26	55.6	0.2914	-1.24	-55.2	-0.3131	44.1270	44.5161	44.3216	-0.0085	0.2420
0.0	1.26	55.6	0.2635	-1.23	-56.8	-0.2604	44.1270	46.1789	45.1529	-0.0010	0.2104
0.5	1.25	55.6	0.2263	-1.23	-56.4	-0.2046	44.4800	45.8537	45.1668	0.0059	0.1736
1.0	1.25	56.0	0.2077	-1.23	-56.4	-0.1302	44.8000	45.8537	45.3268	0.0243	0.1358
Point C											
-1.0	1.22	54.8	-0.1147	-1.25	-55.6	0.0775	44.9180	44.4800	44.6990	-0.0130	-0.0782
-0.5	1.25	54.4	0.0806	-1.26	-56.0	-0.1302	43.5200	44.4444	43.9822	-0.0155	0.0838
0.0	1.24	54.8	0.2573	-1.27	-56.8	-0.2666	44.1935	44.7244	44.4590	-0.0010	0.2087
0.5	1.25	56.0	0.4402	-1.25	-56.4	-0.3937	44.8000	45.1200	44.9600	0.0149	0.3336
1.0	1.25	55.6	0.6200	-1.25	-56.0	-0.5456	44.4800	44.8000	44.6400	0.0238	0.4662

z [mm]	I+	F+	Fz+	I-	F-	Fz-	K+	K-	Kgem	Frel	Fed
Point D											
-1.0	1.21	55.6	0.7595	-1.24	-56.4	-0.8432	45.9504	45.4839	45.7171	-0.0214	0.6535
-0.5	1.21	55.6	0.5270	-1.24	-56.0	-0.5580	45.9504	45.1613	45.5559	-0.0059	0.4427
0.0	1.22	54.8	0.2635	-1.25	-56.8	-0.2666	44.9180	45.4400	45.1790	0.0011	0.2146
0.5	1.24	55.6	0.0372	-1.25	-56.0	-0.0248	44.8387	44.8000	44.8194	0.0041	0.0249
1.0	1.23	56.0	-0.2015	-1.25	-56.4	0.2759	45.5285	45.1200	45.3242	0.0229	-0.1920
Point E											
-1.0	1.23	56.0	0.3100	-1.25	-56.8	-0.3844	45.5285	45.4400	45.4842	-0.0224	0.2796
-0.5	1.23	56.4	0.2883	-1.26	-56.8	-0.3224	45.8537	45.0794	45.4665	-0.0086	0.2450
0.0	1.24	56.4	0.2790	-1.25	-56.8	-0.2635	45.4839	45.4400	45.4619	0.0057	0.2179
0.5	1.25	56.4	0.2480	-1.24	-56.0	-0.1891	45.1200	45.1613	45.1406	0.0184	0.1754
1.0	1.24	56.8	0.2263	-1.26	-56.4	-0.1488	45.8065	44.7619	45.2842	0.0258	0.1506
Point F											
-1.0	1.25	56.4	-0.1023	-1.25	-56.0	0.0434	45.1200	44.8000	44.9600	-0.0188	-0.0583
-0.5	1.25	56.8	0.0682	-1.23	-56.0	-0.1085	45.4400	45.5285	45.4842	-0.0136	0.0715
0.0	1.25	56.4	0.2573	-1.23	-55.6	-0.2635	45.1200	45.2033	45.1616	-0.0034	0.2101
0.5	1.24	56.8	0.4712	-1.24	-56.0	-0.4340	45.8065	45.1613	45.4839	0.0121	0.3650
1.0	1.25	56.4	0.6510	-1.25	-56.0	-0.5859	45.1200	44.8000	44.9600	0.0208	0.4948

Table M.1 Continuation measured data.

z [mm]	I+	F+	Fz+	I-	F-	Fz-	K+	K-	Kgem	Frel	Fed
Point G											
-1.0	1.26	55.6	0.8122	-1.24	-56.0	-0.8370	44.1270	45.1613	44.6441	-0.0122	0.6599
-0.5	1.26	56.0	0.5208	-1.24	-56.0	-0.5456	44.4444	45.1613	44.8029	-0.0107	0.4268
0.0	1.26	55.6	0.2666	-1.25	-56.0	-0.2759	44.1270	44.8000	44.4635	-0.0036	0.2162
0.5	1.25	56.0	0.0310	-1.24	-55.6	-0.0217	44.8000	44.8387	44.8194	0.0029	0.0211
1.0	1.25	55.6	-0.1984	-1.24	-56.0	0.2635	44.4800	45.1613	44.8206	0.0216	-0.1857
Point H											
-1.0	1.25	56.0	0.3410	-1.25	-56.4	-0.4061	44.8000	45.1200	44.9600	-0.0208	0.2988
-0.5	1.25	56.0	0.2945	-1.25	-56.0	-0.3317	44.8000	44.8000	44.8000	-0.0119	0.2505
0.0	1.25	56.0	0.2821	-1.24	-56.4	-0.279	44.8000	45.4839	45.1419	0.0003	0.2253
0.5	1.26	55.6	0.2728	-1.25	-56.4	-0.2015	44.1270	45.1200	44.6235	0.0220	0.1887
1.0	1.25	55.6	0.2325	-1.24	-56.4	-0.1457	44.4800	45.4839	44.9819	0.0275	0.1516
Point I											
-1.0	1.25	56.0	-0.1023	-1.26	-56.8	0.0465	44.8000	45.0794	44.9397	-0.0179	-0.0595
-0.5	1.24	56.0	0.0837	-1.26	-56.0	-0.1240	45.1613	44.4444	44.8029	-0.0124	0.0828
0.0	1.25	55.6	0.2542	-1.26	-56.4	-0.2759	44.4800	44.7619	44.6210	-0.0062	0.2111
0.5	1.25	55.6	0.4743	-1.25	-56.4	-0.4340	44.4800	45.1200	44.8000	0.0129	0.3633
1.0	1.25	56.0	0.6510	-1.25	-56.4	-0.5828	44.8000	45.1200	44.9600	0.0218	0.4935

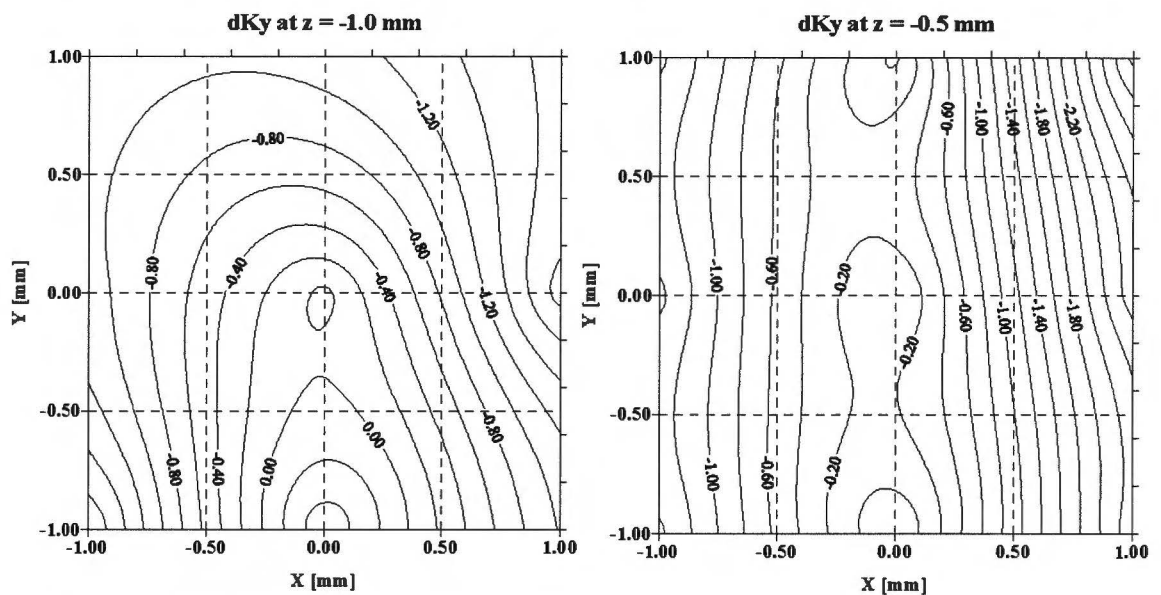


Figure M.1 Motor constant variation.

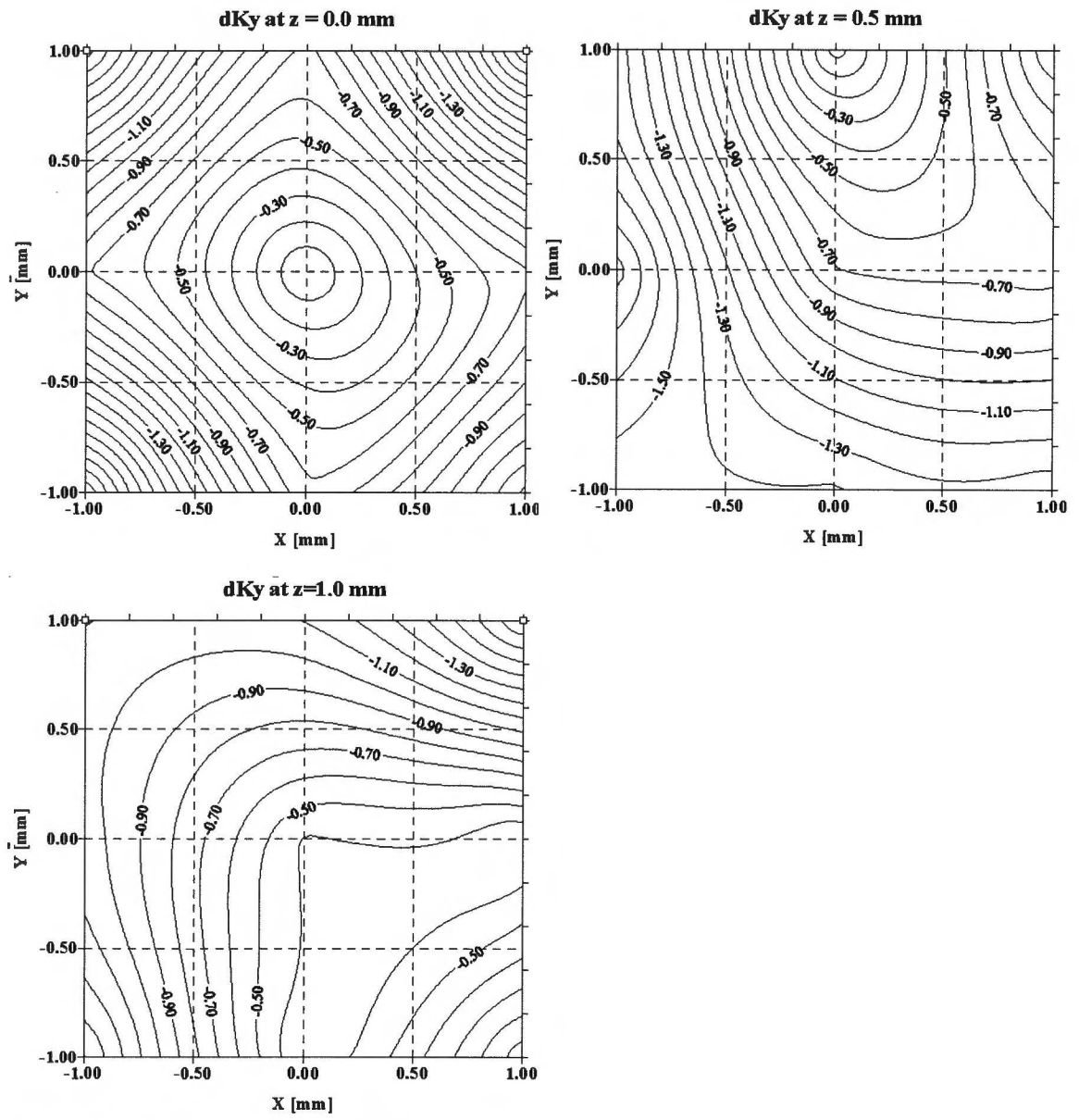


Figure M.1 Motor constant variation.

Appendix N Transfer functions

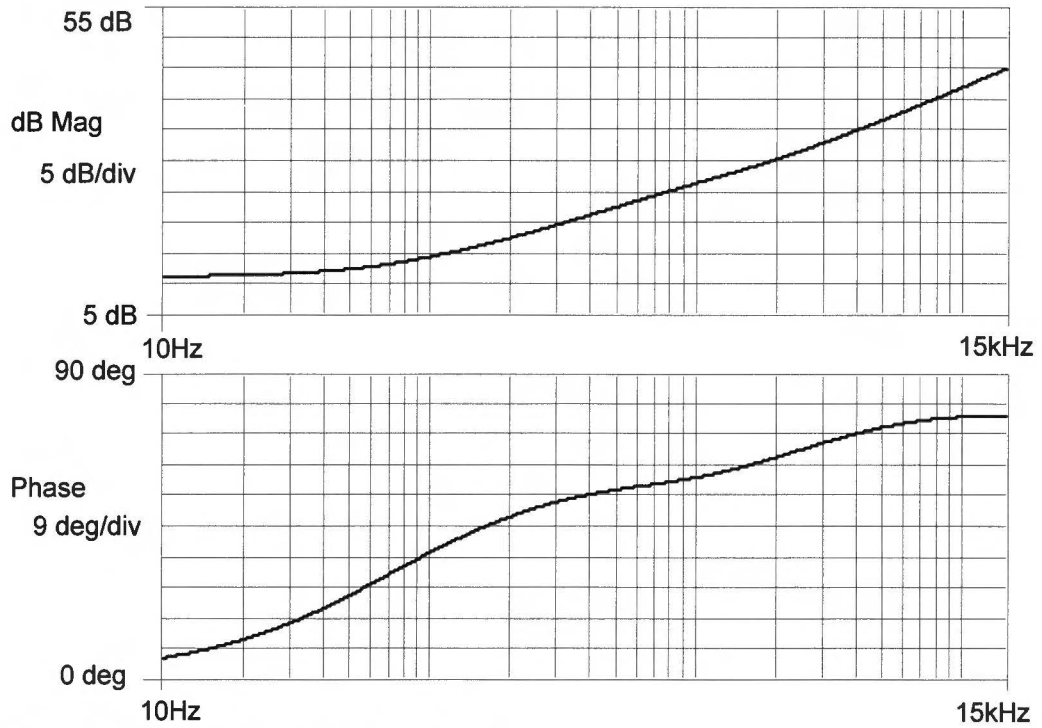


Figure N.1 Transfer function single coil in air.

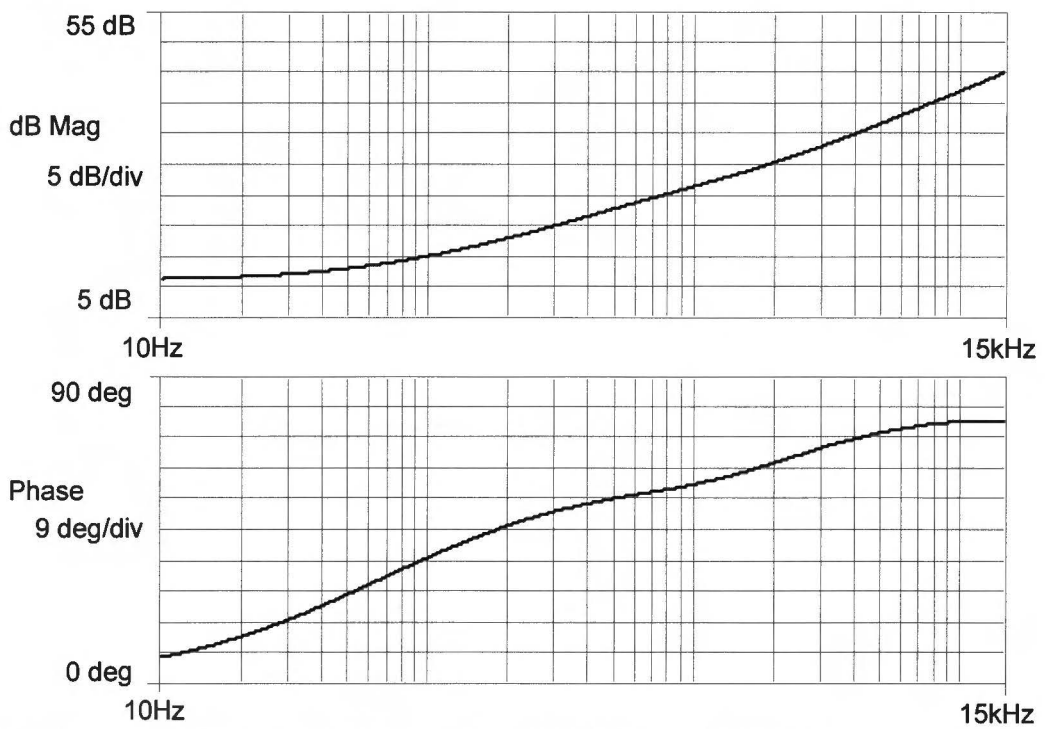


Figure N.2 Transfer function single coil between yokes without magnets.

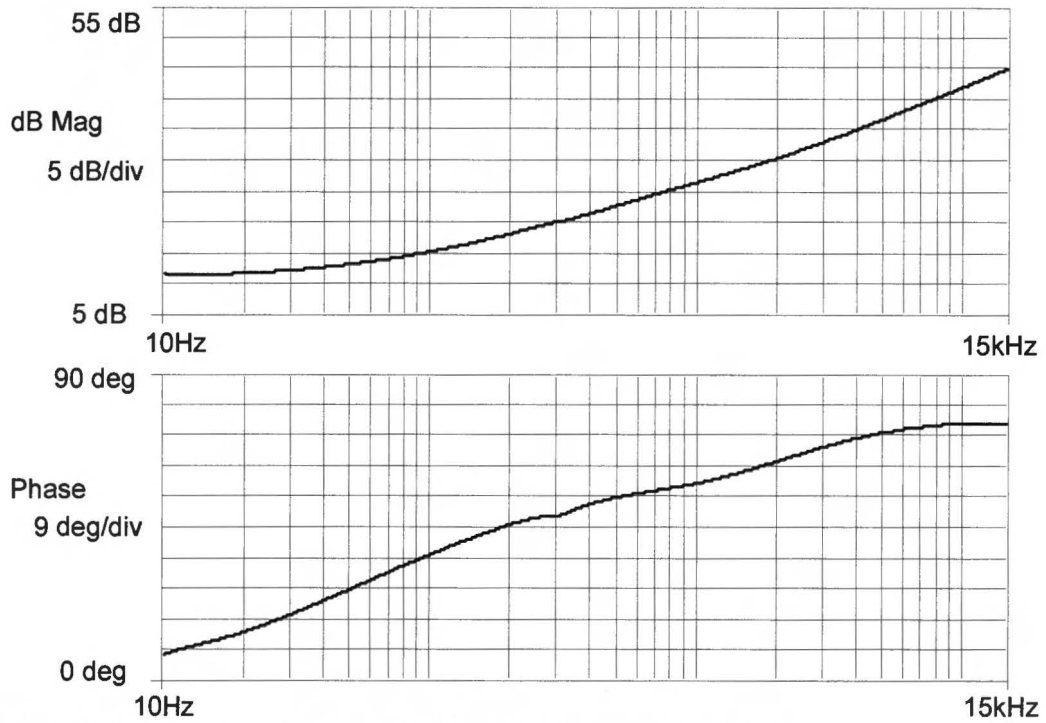


Figure N.3 Transfer function single coil between yokes with magnets.

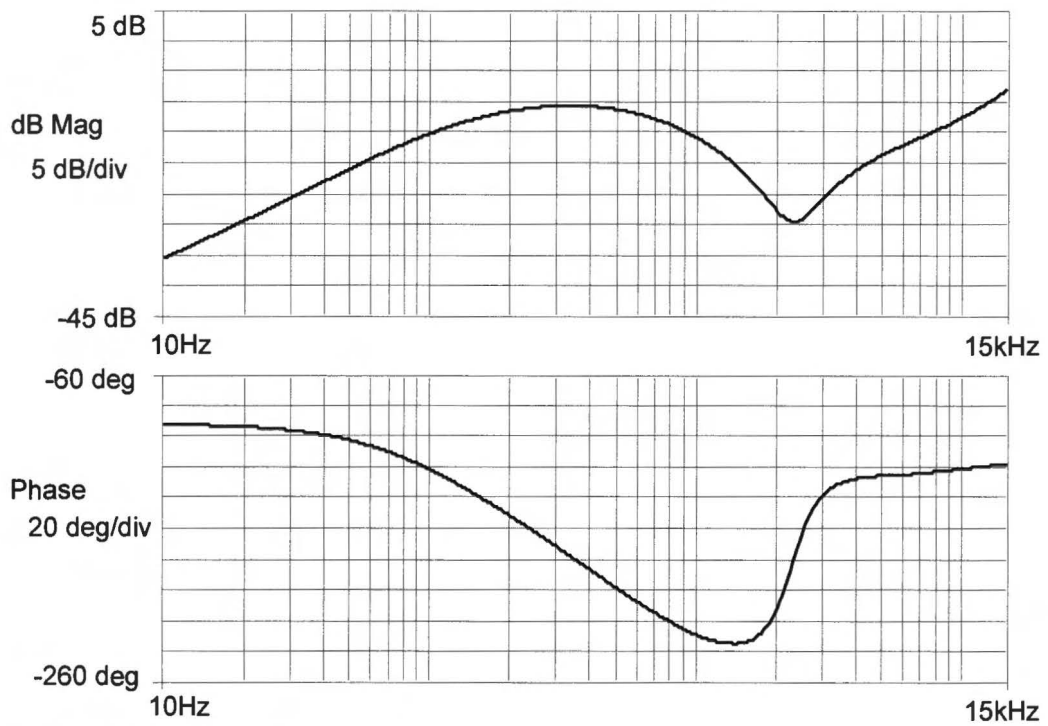


Figure N.4 Cross talk with coils in air.

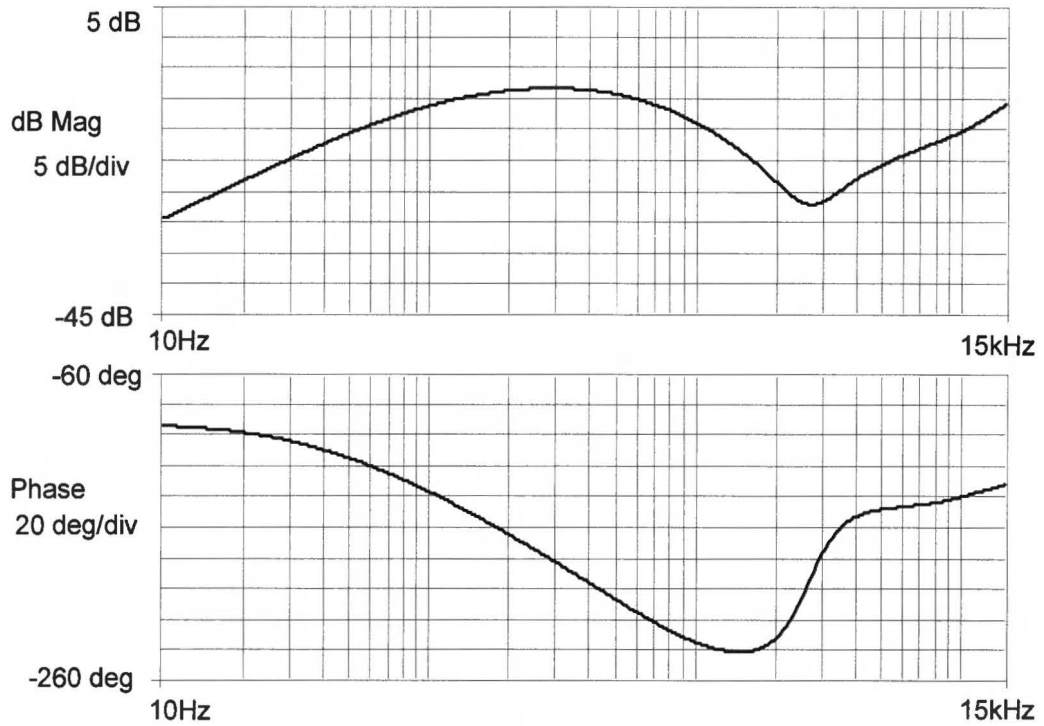


Figure N.5 Cross talk with coils between yokes without magnets.

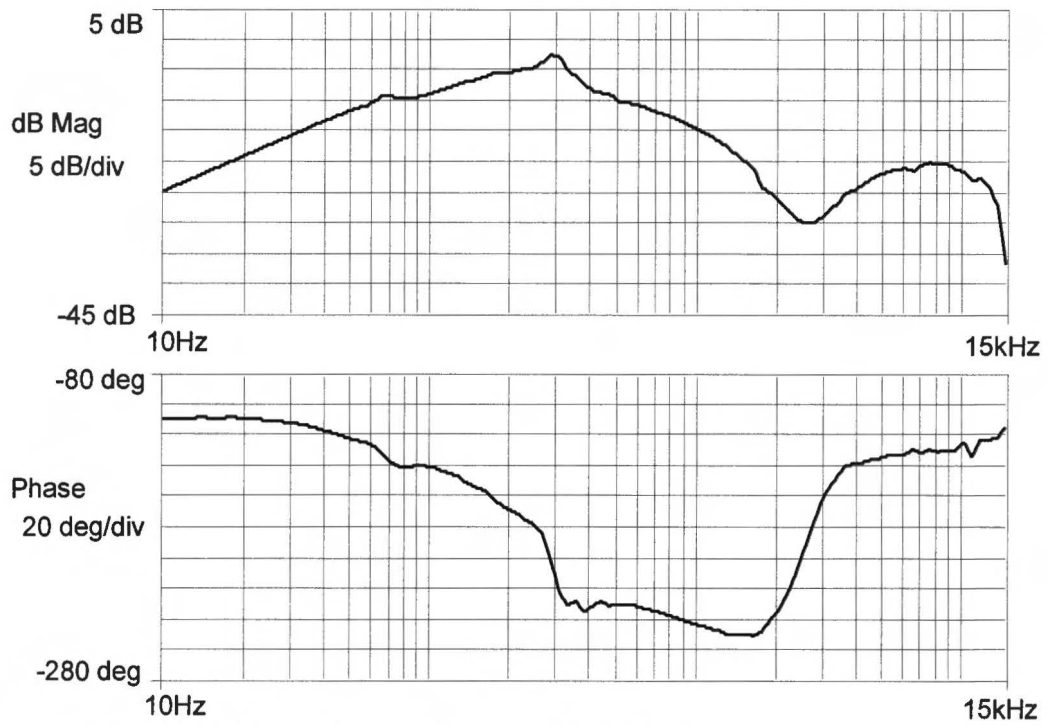


Figure N.6 Cross talk with coils between yokes with magnets.